SPECTRAL, SPATIAL AND TEMPORAL CONTROL OF HIGH-POWER DIODE LASERS THROUGH NONLINEAR OPTICAL FEEDBACK

Peter Danny van Voorst

Promotiecommissie:

Prof. dr. W. J. Briels	Universiteit Twente, Enschede
Prof. dr. K.- J. Boller	Universiteit Twente, Enschede
Dr. ir. H. L. Offerhaus	Universiteit Twente, Enschede
Prof. dr. J. L. Herek	Universiteit Twente, Enschede
Prof. dr. M. Pollnau	Universiteit Twente, Enschede
Prof. dr. C. Denz	Westfälische Wilhems-Universität, Münster
Prof. dr. R. W. Eason	University of Southampton, Southampton

The research presented in this thesis was carried out at the
Laser Physics and Nonlinear Optics Group, University of Twente
P.O. Box 217, 7500 AE Enschede, The Netherlands

This research was financially supported by the Dutch Technology Foundation STW TOE 5656

Printed by Koninklijke Wöhrmann, Zutphen

ISBN 978-90-365-2597-8

SPECTRAL, SPATIAL AND TEMPORAL CONTROL OF HIGH-POWER DIODE LASERS THROUGH NONLINEAR OPTICAL FEEDBACK

PROEFSCHRIFT

ter verkrijging van
de graad van doctor aan de Universiteit Twente,
op gezag van de rector magnificus,
prof. dr. W.H.M. Zijm,
volgens het besluit van het College voor Promoties
in het openbaar te verdedigen
op vrijdag 25 januari 2008 om 13.15 uur

door

Peter Danny van Voorst
geboren op 7 maart 1977
te Groningen

Dit proefschrift is goedgekeurd door de promotor

Prof. dr. K. J. Boller

en de assistent promotor

Dr. ir. H. L. Offerhaus

Publications and conferences

- P.D. van Voorst, R.M. Oldebeuving, H.L. Offerhaus and K.-J. Boller, *"Concept and modelling for a mode-locked laser with separated single-frequency gain sections"*, In preparation
- P.D. van Voorst, R.M. Oldebeuving, H.L. Offerhaus and K.-J. Boller, *"Spectral combining of elements in a diode array with modelocking possibility"*, Physics@Veldhoven meeting Veldhoven, poster contribution, 2008
- P.D. van Voorst, M.R. de Wit, H.L. Offerhaus, S. Tay, J. Thomas, N. Peyghambarian and K.-J. Boller, *"Holographic injection locking of a broad area laser diode via a photorefractive thin-film device"*, Optics Express 15 page 17587, 2007
- P.D. van Voorst, M.R. de Wit, H.L. Offerhaus, S. Tay, J. Thomas, N. Peyghambarian and K.-J. Boller, *"Injection locking of a broad area laser diode by use of holographic four-wave mixing in a photorefractive polymer"*, Conference on Lasers and Electro-Optics (CLEO), Baltimore USA, May 2007, oral presentation, 2007
- P.D. van Voorst, H.L. Offerhaus, K.-J. Boller, *"Injection locking of a broad area laser diode by dynamic fourwave mixing in a photorefractive polymer"*, Physics@Veldhoven meeting Veldhoven, poster contribution, 2007
- P.D. van Voorst, H.L. Offerhaus, K.-J. Boller, *"Single frequency operation of a broad area laser diode by injection locking of a complex spatial mode via a double phase conjugate mirror"*, Optics Letters 31 page 1061, 2006
- P.D. van Voorst, H.L. Offerhaus, K.-J. Boller, *"Holographic transformation of multi-mode output from a broad area diode into a TEM_{00} beam with a*

double phase conjugate mirror", Conference on Lasers and Electro-Optics (CLEO), Long Beach, USA, May 2006, oral presentation.

- P.D. van Voorst, H.L. Offerhaus, K.-J. Boller, *"Spatial performance of a broad area laser diode injection locked to a single frequency by a double phase conjugate mirror"* NNV-AMO meeting Lunteren, poster contribution, 2005

- P.D. van Voorst, H.L. Offerhaus, K.-J. Boller, *"Holographic single frequency injection locking of a broad area diode"*, NNV-AMO meeting Lunteren, poster contribution, 2004

- P.D. van Voorst, H.L. Offerhaus, K.-J. Boller, *"High brightness diode lasers with holographic feedback"*, NNV-AMO meeting Lunteren, poster contribution, 2003

Abstract

A high-power diode laser offers multi-Watt output power from a small and efficient device, which makes them an interesting source for numerous applications. The spatial and spectral output however, are of reduced quality which limits the applicability. This limited quality is connected to the design aiming at high power. The optical power limit achievable by a single-mode element is approximately 100 mW, limited by damage to the end-face of the diode. Scaling to higher power often is usually achieved by increasing the transverse size of the diode laser waveguide. These lasers are called Broad Area diode Lasers (BAL). The broad amplification region supports a number of transverse modes while the broad spectral gain supports oscillation at many longitudinal frequencies. The output therefore consists of many modes in space and frequency. These modes compete for gain and connect through nonlinear effects. The exact superposition of modes emitted at any time depends on many parameters such as the precise dimensions of the waveguide, temperature distribution in the gain region, spatial profile of pump current. The output profile is therefore hard to predict, unstable and changes as the diode ages.

The first part of this work concerns holographic injection locking, a technique that allows to address both the spectral and spatial complexity for improving the beam quality and obtaining single-frequency operation. In this approach a low-power, high-quality primary laser is injected into the broad area laser diode via a hologram written by both the primary laser and the diode laser. In this way the spatial mode of the primary laser can be converted into a mode fitting the complex superposition of modes preferred by the diode laser, while the diode laser will adapt the single frequency of the primary laser. We examine different photorefractive materials, used to

record the holograms, and different configuration. In the first experiment we use a photorefractive crystal and the configuration for a double phase conjugate mirror (DPCM). A previously reported limitation of such a setup (2k-gratings) is circumvented by the introduction of mirrors that vibrate in a controlled manner. Holographic locking of the BAL to the single frequency of the primary laser is achieved for extended periods (30 minutes). Furthermore we demonstrate that the spatially complex output mode pattern of the high-power broad area laser is converted (diffracted) back into a single spatial mode of high quality.

In a second experiment we introduce photorefractive polymers as an alternative to the photorefractive crystal. We want to replace the crystal because they are sensitive to mechanical stress and temperature and suffer from a slow response time (up to minutes at 800 nm) and limited diffraction efficiency. In the polymers, the various physical processes involved to provide photorefractive process can be individually tailored by mixing different chemicals, which allows a greater freedom to design a material. We use the polymer in a four-wave-mixing (FWM) setup. Response times of mseconds are observed and, with careful wavelength tuning, holographic injection locking to the single frequency of the primary laser has been maintained for several minutes.

An alternative approach to achieve high-power output from diode lasers is not to increase the output of a single emitter, but instead to overlap the output of many emitters. This approach is used for the last experiment. A grating is used to overlap the output of different elements of an array of single-mode diode lasers towards a common reflector. Instead of single-frequency operation, a comb-like emission spectrum is generated and an attempt is made to lock the phases at these frequencies to produce pulses. In contrast to conventional modelocked lasers, the pulse parameters in this approach are no longer directly related the cavity parameters, but they can be adjusted via the dispersion parameters of the grating. For instance it should be possible to access different locking regimes, such as the generation of ultra-high repetition rates I the range of hundreds of GHz. Also the requirements for modelocking differ from conventionally modelocked lasers. A Semi conductor Saturable Absorber Mirror (SESAM) is used to induce modelocking, and several configurations are explored. Although no stable pulsing was observed yet, clear

signs of mode-locking were observed. The spectral amplitude profile flattened and broadened, the emission levels between the locked modes reduced. Also increasing spiking was observed in autocorrelation traces indicating the increased appearance of pulses. Research will continue in collaboration with a research group specialising in advanced SESAMs.

Samenvatting

Diode lasers kunnen een vermogen emitteren oplopend tot een aantal Watt. Bovendien zijn diode lasers klein en efficiënt en daarmee interessant voor vele toepassingen. Echter, bij hoog vermogen zijn de spatiële en spectrale eigenschappen van de bundel, bepalend voor de bundelkwaliteit, vaak slecht. Deze lage bundelkwaliteit is niet inherent aan diode lasers maar houdt verband met het vermogen. Diode lasers met een laag vermogen kunnen wel een goede bundelkwaliteit leveren. De grens tussen hoog- en laag vermogen ligt ongeveer op 100 mW. Boven dit vermogen moet de uitkoppelspiegel vergroot worden om schade ten gevolge van de hoge intensiteit te voorkomen. Door het vergroten (meestal in de transversale richting), in het Engels aangeduid als broad area lasers (BAL), gaan z.g. hogere-orde modes resoneren naast de laagste orde mode en deze combinatie verlaagt de ruimtelijke bundelkwaliteit naarmate een hoger vermogen wordt gewenst. Bovendien kan elke van de genoemde ruimtelijke modes met een hoger aantal frequenties resoneren omdat diodelasers over een grote spectrale bandbreedte van het versterkingsspectrum beschikken. De precieze superpositie van al deze spatiële modes en spectrale modes, is een functie van meerdere fabricage- en operationele parameters, zoals de precieze maten van de resonator, de, van de pompstroom afhankelijke, temperatuurverdeling in de diode en de ruimtelijke dichtheidsverdeling van de pompstroom. Verder treedt competitie tussen de verschillende modes om de versterking op en niet-lineaire processen kunnen een rol spelen. Het hoge aantal van resonerende modes leidt tot een toevallige ruimte-tijdelijke fluctuaties van de intensiteit. Samengevat is het moeilijk te voorspellen welk ruimtelijke bundelprofiel optreedt, welk emissiespectrum of tijdelijke gedrag optreedt. Dit proefschrift behandelt een aantal experimenten gericht op het verbeteren van de ruimtelijke, spectrale

en tijdelijke kwaliteit van de bundel uit hoog vermogen diode lasers.

Het eerste deel van dit proefschrift behandelt holografische oscillator synchronisatie (in het Engels holographic injection locking): het schijnen van licht van een enkele frequentie in een complex spatiëel patroon in de diode laser. Door extern licht in de diode laser te schijnen wordt deze ertoe aangezet om de frequentie en fase van dat licht over te nemen. Echter, deze overname levert alleen een stabiel spatiëel patroon als het ruimtelijke patroon van het externe licht overeenkomt met het patroon (ruimtelijke mode-superpositie) van de diode zelf. Door gebruik te maken van *holografische* oscillator synchronisatie kunnen zowel de spectrale als spatiële complexiteit gereduceerd worden zodat de bundelkwaliteit verbetert: Een primaire laser met een zwakke laserbundel met een hoge bundelkwaliteit wordt via een hologram in de diode laser geschenen. Dat hologram wordt gevormd uit het interferentie patroon tussen de bundels van de primaire laser en de diode laser. Op deze manier wordt de spatiële mode van de primaire laser geconverteerd naar een complexe, passende mode van de diode laser, en zal de diode laser de frequentie en fase van de externe laser overnemen. De daardoor bereikte stabiele complexe mode kan via het hologram weer worden omgezet naar de spatiële mode de primaire laser (van hoge kwaliteit).

Het fotorefractieve materiaal waar de hologrammen in worden gevormd, en de soort opstelling zijn de twee meest kritische parameters voor een experimentele demonstratie. In het eerste experiment gebruiken we een fotorefractief kristal in een opstelling voor een 'dubbele faseconjugerende spiegel' (double phase conjugate mirror, DPCM). Een beperking van deze opstelling (2k-hologrammen) die werd gerapporteerd in de literatuur is omzeild door het gebruik van speciale vibrerende spiegels in de opstelling. We zijn er in geslaagd om het spectrum van een BAL te reduceren tot een enkele frequentie en het patroon van de geëmitteerde bundel te controleren voor langere tijd (30 minuten). Bovendien hebben we het hologram kunnen gebruiken om de spatiëel complexe bundel van de diode te converteren naar de enkele spatiële mode van de primaire laser.

In het tweede experiment vervangen we het fotorefractieve kristal door een fotorefractief polymeer. We doen dat omdat kristallen een aantal nadelen hebben: zij zijn erg gevoelig voor mechanische schokken en temperatuurverschillen, de reactietijd is erg lang (meerdere minuten bij een golflengte van

800 nm) en de diffractie efficiëntie is beperkt. Een fotorefractief polymeer bestaat uit een mix van chemische componenten, waardoor er vrijheid is om de mix voor de verschillende fysische processen te optimaliseren die aan het fotorefractieve effect bijdragen. Wij gebruiken een fotorefractief polymeer dat gemaakt wordt door een groep in Arizona met een reactietijd in in de orde milliseconden. We gebruiken een opstelling waarin vier bundels gekoppeld worden, die in het Engels aangeduid wordt als fourwave mixing (FWM). De bundel van de diode kan voor enkele minuten gecontroleerd worden maar om dit te bereiken moet de frequentie van de primaire laser nauwkeurig worden afgesteld.

In plaats van het vermogen uit een enkele diode te vergroten kan ook een hoog vermogen verkregen worden door bundels uit vele individuele laser diodes te combineren. Een goede bundelkwaliteit kan worden behaald als al die bundels een goede bundelkwaliteit hebben. En een hoge tijdelijke kwaliteit in de combineerde bundel zou bereikbaar worden door terugkoppeling met een optisch nietlineaire element, bvb een verzadigbare absorber. Deze benadering is gekozen voor het laatste experiment en gedetailleerd onderzocht via een numerieke modellering. De verschillende diode lasers maken deel uit van een array en de bundels worden via een tralie gecombineerd tot een enkele bundel. Deze bundel heeft dezelfde, hoge, spatiële kwaliteit als een enkele diode laser, maar bevat de frequenties van alle diodes in het array en is daardoor opgebouwd als een frequentiekam. Een dergelijke frequentiekam leidt doorgaans tot een toevallig patroon in de tijd maar door de spectrale fases van de verschillende frequenties te controleren kan modesynchronisatie (mode-locking) bereikt worden en ontstaat een regelmatig patroon van korte pulsen. Modelocking op deze manier is nog niet eerder onderzocht. De parameters van de puls zijn af te leiden uit de dispersie parameters zoals die gegeven worden door de tralie. Dit is in tegenstelling tot de conventionele lasers waarin modes zijn gesynchroniseerd, waarbij de resonator lengte de belangrijkste rol speelt. De randvoorwaarden om tot mode-synchronisatie te komen zijn ook anders dan bij conventionele lasers. Hierdoor kan onze laser in een ander bereik pulsen produceren, bijvoorbeeld pulstreinen met een extreem hoge herhalingsfrequentie van tientallen GHz. Om tot mode synchronisatie te komen wordt een SESAM (semiconductor saturable absorber mirror, halfgeleider verzadigbare absorptiespiegel) ge-

bruikt, waarbij verschillende opstellingen worden onderzocht. Spectraal zijn er duidelijke tekenen van modelocking en in autocorrelatie metingen zijn kortstondige pulstreinen gemeten, maar stabiele pulsen nog niet. Het is waarschijnlijk dat dit veroorzaakt wordt door onvoldoende verzadiging van de SESAM of omdat de vervaltijd (relaxation time) van de SESAM te lang is. Het onderzoek zal in die richting worden voortgezet in samenwerking met een groep die ultrasnelle SESAMs kan leveren. De gemeten veranderingen in het spectrum en het tijdelijk gedrag tonen dat het concept een duidelijke kans van slagen heeft.

Contents

Chapter 1

Introduction

Although there exist many different kind of light sources, a certain class of them, lasers, is unique because of the special properties of the emitted light. The properties lasers are most associated with is the emission of a well-defined beam in a single, distinct direction (a spatial property), and the emission at a single, distinct light frequency (a spectral property). The spectral properties of a laser, however, comprise more than a well-controlled power spectrum, namely, also the phase of the emitted light can be controlled in lasers. For example, if laser oscillation occurs at an entire set of evenly separated light frequencies, rather than at a single frequency, it is the phase spectrum that determines whether the light is emitted as short pulses or as quasi-random fluctuations (a temporal property). When the named properties are near their theoretical optimum, the output of a lasers is termed to be of high spatial quality meaning a diffraction limited output beam, of high spectral quality which usually means a power spectrum with narrow bandwidth, and of high temporal quality meaning the generation of pulses with a short duration.

When lasers are scaled to higher powers, as is required for most industrial and scientific applications, usually the spectral, spatial and temporal quality of the output degrades significantly. A typical example for this are diode lasers where a trade-off is routinely required between the quality of the output beam and the output power. On the other hand, diode lasers are highly attractive for applications, which is due to their small physical size and their high efficiency in light generation. In view of this, in this thesis, I will fo-

cus on quality improvements for the output of high-power diode lasers. In standard operation, such high-power diode lasers show a spatially and spectrally rather low output quality. The former is seen as an output beam with complexly-structured (apparently multi-lobed) spatial beam profile, and the latter can be seen as a multi-frequency complexly-structured output spectrum of significant bandwidth. Temporally, this corresponds to a rapid fluctuation output power.

To improve the spatial and spectral quality of high-power diode lasers, or to improve the spatial and temporal quality, we chose two approaches where the diode laser is subject to optical feedback via an optically nonlinear process.

The first approach, to obtain a high beam quality and single-frequency output, is based on the injection of light with a single frequency into the complex spatial mode of a high-power broad area laser (BAL) diode. The injected light originates from an external source, a single-frequency laser, with a beam of high spatial quality, operating at low power. Dynamic holograms, recorded via the nonlinear optical response of photorefractive materials, are used to diffract the high-quality beam of the external laser into a specific, spatially complex pattern which matches the preferred, spatially complex beam pattern of the high-power diode laser. The injected frequency imposes its oscillation frequency and phase on the high-power diode, such that the hologram provides an optical feedback to the beam pattern preferred by the diode. Simultaneously, the same hologram diffracts the complex beam pattern emitted from the high-power diode back into to a beam of high spatial quality.

The second approach aims on improving the spatial and temporal quality from diode lasers with high power. It is based on a diode array of single-stripe emitters that receive nonlinear optical feedback from a saturable absorber. For this, the emission frequencies of the individual emitters are brought into an evenly spaced (comb-like) spectrum and spatially superimposed into a single, common beam with a diffraction grating. The nonlinear feedback from the saturable absorber in this common beam should then control the relative phase of emission for each emitter, to arrive at modelocking for the generation of a train of ultrashort pulses from the diode array.

Both approaches attempt to circumvent the usual limits of high-power

diode lasers by harnessing the complexity that comes with high-power operation and convert the beam of a high-power diode back to the high quality as found usually only in low power operation.

1.1 A very brief history

The concept of stimulated emission of light, introduced by Einstein in 1917 [1], can be considered the most essential step towards the realisation of lasers. The first working device, the maser, albeit at a rather low frequency (in the microwave range), was demonstrated by Gordon and Zeiger in the group of Townes [2] in 1954, with important contributions from Basov and Prokhorov. Gordon, Basov and Prokhorov shared the Nobel Prize in 1964 for the invention of the maser. Maiman realised the first laser, a Ruby-laser emitting at 694.3 nm in 1960 [3]. Also in 1960, the first light emission from a semiconductor material was demonstrated by Lowen [4], followed by the first diode laser in 1962 by Hall [5]. The high quality of the light that could be generated by lasers and the high degree of control concerning its spatial, spectral and temporal properties initiated a huge wealth of laser-based optical research as well as numerous developments towards applications.

For the research presented here, the spectral, spatial and temporal properties of diode lasers form a central issue, but also other development are being made use of. These are, in particular, the invention of holography in 1948 by Gabor [6], and the frequency and phase control of oscillators via injection locking, as reported for mechanical oscillators by Huygens in 1665 [7].

1.2 Scope of this work

This work describes three experiments, all aiming at improving the spatial beam quality in combination with an improved spectral or temporal quality. The first two experiments demonstrate holographic injection locking of a single high-power diode, either via a photorefractive crystal or via a photorefractive polymer. In the third experiment a new type of high-power modelocked laser is investigated.

The thesis is organised as follows. The motivation and background for the holographic locking experiments are described in chapter 2. The causes

of degradiation of the beam quality of high-power diode lasers are examined in order to evaluate techniques that may improve the beam quality and narrow the spectral bandwidth, such as injection locking and holographic injection locking. Different materials with photorefractive properties, crystals and polymers, are introduced and their properties and differences analysed in comparison. The experiments follow in chapter 3 and 4. The first experiment uses a photorefractive crystal in a double phase conjugate mirror (DPCM) configuration. It extends previous work, by achieving some significant improvements such as a first-time single-frequency locking of a BAL diode while the long-term stability of the locking is maintained. The second experiment using photorefractive materials is described in chapter 4. Here, for the first time in the context of laser injection locking, a photorefractive polymer is employed for a successfull locking of a high-power diode laser.

In chapter 5, the concept of a new type of modelocked laser is proposed, where the amplification of light is spectrally distributed over a larger number of separate gain elements. An implementation is suggested as based on an array of single-stripe diode lasers with feedback from a saturable absorber mirror. The spectro-temporal properties of this implementation are analysed with a numerical model in order to identify ranges of experimental parameters where modelocking might be feasible.

Chapter 6 describes the first experimental investigations of such a type of laser, with the goal to achieve modelocking. So far, the results reveal that the generation of a stable train of output pulses would require an improved performance of, particularly, the saturable absorber. However, some first indications of modelocking were observed.

In the last chapter 7 conclusions and an outlook are presented.

Chapter 2

Motivation and overview on holographic injection locking

Abstract

Some of the problems of high-power diode lasers are described with possible solutions to these problems proposed and evaluated. Reasons for the deterioration of the beam quality of a laser diode at higher output power are given. Holographic injection locking, direct injection locking and phase conjugation are introduced. The photorefractive effect, a nonlinear effect critical to the creation of adaptive holograms, is discussed. Photorefractive mechanisms in inorganic crystals and organic polymers, together with a set of configurations for photorefractive experiments are introduced.

Low-power diode lasers are efficient, small, low-cost laser sources available with up to a few tens of mW output power over a wide range of wavelengths. Such low-power diode lasers are the preferred source of light in many existing applications, e.g. in CD/DVD-technology and optic telecommunications. However, where it is possible to scale the output power to the high-power regime ($\geq$100 mW and up to the kW scale), without any loss of coherence, it would be possible to use diode lasers in new applications, or to replace the much more expensive and bulky gas or solid state lasers. Examples of applications that would benefit from high beam quality and high

power include the efficient nonlinear conversion, holographic recording, or laser-display like applications. The classification "high-power", for diode lasers with an output of already more than 100 mW, seems suprising on a first view. However, this limit arises from a purely physical border, namely the output power of a single mode laser diode is limited by the catastrophic optical damage which occurs at the front output facet due to extremely high intensities with a single-stripe laser emitting a single spatial mode with more than 100 mW output power [8], due to the microscopically small area from which the light is emitted, these intensities easily lie in the order of several tens of MW/cm^2. Engineering of laser diodes has extended the current single-mode power limits up to 150 mW at 808 nm (Sanyo DL8142-201) and 300 mW single mode output for a more advanced waveguide structure at 980 nm (Thorlabs L980P300J) [9]. These approaches are based on increasing the emitting area and transverse size of the internal light field, where care has to be taken in order to maintain the single spatial mode operation or and to maintain a sufficiently high rate of stimulated emission. For further improvements, different approaches have been devised to increase the output power significantly beyond this borders.

Diode lasers have been scaled into the high-power regime in two ways. In the first approach, the output of several independent single mode emitters are combined into an array for a coherently combined single beam output. A recent overview of progress in coherent beam combining can be found in the review paper of Fan [10]. However, despite the numerous experimental configurations explored since 1968 [11–15] offering increased output powers while avoiding a degrading beam quality. Major disadvantages are a lack of scalability of the number of elements, limited efficiency and undesired nonlinear effects which degrade the beam quality.

A second approach is to scale diode lasers into the high-power regime by increasing the transverse size of the gain medium in a single emitter, a so-called broad area laser (BAL), allowing a higher output power from a single element. It can be expected that the holographic feedback method we investigate here to improve the spatial and spectral output quality of a single BAL can also be applied to an array of BALs which should increase the output power further.

As a major part of this thesis will focus on improvements of the spectral

and spatial quality of light emitted by BALs, we will in the following review some important properties of such high-power diodes lasers. BALs typically offer multi-Watt power levels with a high efficiency from a single emitter. However, this high power is achieved with a transverse increase of size of the active laser volume, the spectral and spatial beam quality is much below that of a low-power single mode laser. Typically, a BAL emits a broad spectrum ($\geq$450 GHz) and a complex spatial pattern (M^2 >100) and not a single spatial mode (M^2=1) in a small spectral band ($\leq$10 MHz) as possible with a low-power diode laser.

To force a BAL to maintain single-frequency operation, injection locking can be applied. This is achieved by the injection of the radiation of a low-power, single frequency laser, called primary oscillator, into the BAL [16–18]. In order to achieve successful injection locking, strict spatial and spectral requirements have to be fulfilled. Spectrally, some detuning between the primary oscillator and the secondary oscillator (in our case the BAL) is allowed, as long as the amplitude of the primary oscillator is sufficient to compensate the losses in the secondary laser. These losses in the secondary laser are introduced by the detuning. Spatially, the transverse mode pattern of the primary laser should overlap the mode pattern of the secondary laser at the facet. For injection locking of a BAL this means that the primary laser should be aligned in such a way that its radiation matches within the microscopically small (typically several μm in size) facet of the BAL. Sometimes the use of an additional oscillator can be avoided. Here one takes advantage of the, generally, two-lobed output of the BAL, and uses feedback of one of the lobes via a wavelength-selecting element, e.g. with a grating [19]. However, this approach has turned out to be only partially successful (see below).

The basic properties of injection locking are extensively studied in single-mode emitters, in which a wide range of dynamically unstable behaviour is observed [20–22], even when the named tight alignment restrictions are met. Due to spatial and spectral multi-mode oscillation of a BAL, injection locking of a BAL is much more difficult and much less successful than locking of a single-mode diode. Frequency-selective feedback or injection of single-frequency light into a BAL easily narrows the spectrum of the BAL, however, this does not improve the spatial beam quality much. This is due to the fact the simple (high-quality) spatial pattern from the injected radiation

of the primary oscillator cannot match the preferred, internal spatial intensity distribution (pattern of superimposed transverse modes) of the BAL. On the other hand, it shows that the spatial beam quality of a BAL improves to a near-diffraction limited beam by feedback from an external cavity (also called self-injection locking), but this does not narrow the broad spectrum [23–25]. It turns out that an external cavity cannot be constructed in such a way that it only supports a single frequency within the emitted bandwidth of the BAL, feeds back only a single spatial mode, and simultaneously provides a sufficiently high feedback efficiency. For successful spatial and spectral beam improvement, a single-frequency emission from the BAL needs to be selected while avoiding any spatial filtering. For injection locking this means that the primary laser input beam shape has to be given a rather complex beam shape such that it matches the preferred output pattern of the BAL.

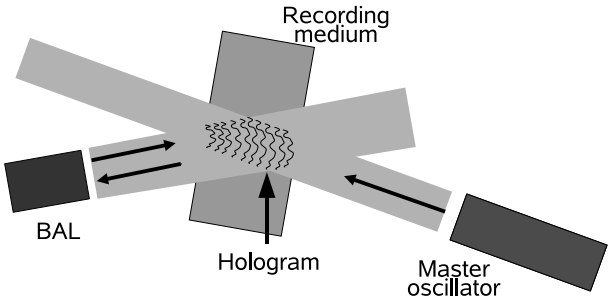

Figure 2.1: *Principle scheme of a holographic locking setup.*

Therefore a method is required which converts the simple spatial mode of the primary oscillator into the spatial mode of the BAL before its radiation is injected into the BAL. To solve this problem, an interesting possibility is to provide a suitable hologram which converts the spatial pattern of the primary oscillator into the pattern preferred by the BAL. It is impossible, however, to pre-determine the fitting hologram due to the highly complex and unpredictable mode pattern emitted (and thus preferred) by the BAL. To solve this problem as well, we propose a method to dynamically record the proper hologram in a suitable medium using the primary oscillator and the BAL as the recording beams, see figure 2.1 [18]. This method will be referred to as holographic injection locking. In this method the spatial properties of the BAL diode pattern will be copied, by diffraction in a suitable hologram, onto

the injected single-frequency beam. This way the BAL is offered the possibility to spectrally lock to the primary oscillator frequency, however, without the primary oscillator imposing a pre-defined spatial mode pattern on to the BAL. A successful locking should then become apparent as a complex spatial pattern which is stable in time. It is important to note that, in this state, the hologram used to diffract the spatial mode of the primary oscillator into the spatial mode of the BAL should convert the complex, preferred spatial beam pattern of the BAL into the simple, high-quality mode of the primary oscillator. In summary, holographic injection locking should allow to lock a BAL to a single-frequency in a matching spatial mode without actually knowing the particular shape of this complex spatial mode and, simultaneously, to obtain high-quality spatial output pattern from the BAL.

In this thesis we will report on two experiments where two different photorefractive materials were used to successfully achieve holographic injection locking. In the first experiment described in chapter 3, a standard, inorganic photorefractive $BaTiO_3$-crystal is used. Related experiments with $BaTiO_3$-crystals to injection-lock BALs have been reported before [26–34]. A problem in these experiments so far is to maintain injection locking of the BAL once the BAL and the primary laser become mutually coherent, and we will show, for the first time, that the stability of the locking is maintained even after the single-frequency laser and the BAL become mutually coherent by the injection locking. Further, we demonstrate that the spatial mode of the single frequency oscillator beam is not only converted into the complex BAL mode, but also converts the spectrally locked, complex mode pattern of the BAL beam back into the spatial beam profile of the single-frequency primary oscillator.

In a second experiment, described in chapter 4, we replace the inorganic photorefractive crystal by an organic photorefractive polymer, with the motivation to avoid a number of disadvantages associated with photorefractive crystals. In this chapter, the first holographic injection locking using a photorefractive polymer is demonstrated. The optical properties of the locked BAL are comparable to the optical properties of the BAL in the experiment using the inorganic crystal.

To prepare the presentation of the described results, in the remainder of this chapter more background on the optical properties of diode lasers is

given, the properties of photorefractive crystals and polymers are reviewed, and the concept of phase conjugation is described.

2.1 Diode lasers

In its most elementary form, a conventional laser diode can schematically be depicted as in figure 2.2 [35,36]. When a current is applied, light amplification is provided in an active layer formed by the pn-junction. The front and back facets are cleaved parallel to each other and the backfacet is coated to provide a mirror with a reflectivity close to unity. Due to the high small-signal gain in such diodes, laser oscillation can be achieved without a reflective coating on the front (output) facet. The reason for this is that the high refractive index n of semiconductor materials (AlGaAs in our case, with a n around 3.5 at 800 nm, depending on the concentration on Al) leads to a sufficiently high feedback via Fresnel reflection. Thus a cavity is formed between the front and the back facet, light can be amplified in the medium and coupled out at the front facet.

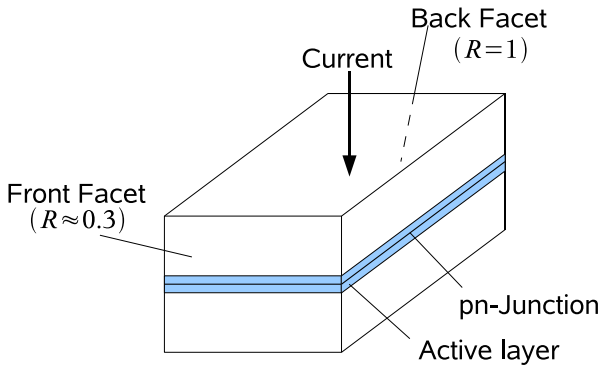

Figure 2.2: *Schematic of the basic principle of a diode laser*

The Fresnel reflectivity of the output coupler (typically 0.3) is actually a very low value compared to most other lasers, such as in a HeNe-laser where the reflectivity of the output coupler is typically 0.99. Laser operation with much lower reflectivities in a diode laser is possible because of the extremely high roundtrip gain; the roundtrip gain in a half roundtrip (small-signal gain) typically amounts to a factor of 10^2 to 10^3. The gain bandwidth is typically

tens of nanometres due to the energetically wide distribution of levels in the conduction and the valence band of the semiconductor material. This high density of states usually allows for light amplification at all light frequencies within this bandwidth.

Like any cavity, a laser diode cavity can allow oscillation at a multitude of longitudinal and transverse modes, depending on the cavity parameters , such as the cavity length, the mirror curvature and the transverse width of the active volume. In this thesis I will refer to a single-mode diode if the cavity selects only a single transverse mode, usually the fundamental transverse mode, also called the longitudinal mode.

Within this thesis, certain coordinate axes are defined which relate to the typical divergence properties of the emitted light, as seen in figure 2.3. The axis along which the light propagates up and down the cavity, is called the cavity axis. The two axes perpendicular to the cavity axis are referred to as the fast axis and the slow axis. This is derived from the diffraction angles observed once the light has left the cavity. Along the fast axis the divergence is stronger than along the slow axis, because along the fast axis the emitting aperture is small ($\approx 1\mu$m) compared to the aperture along the slow axis ($\approx 3\mu$m for a single-mode diode, up to tens to hundreds of μm for BALs), also see figure 2.3.

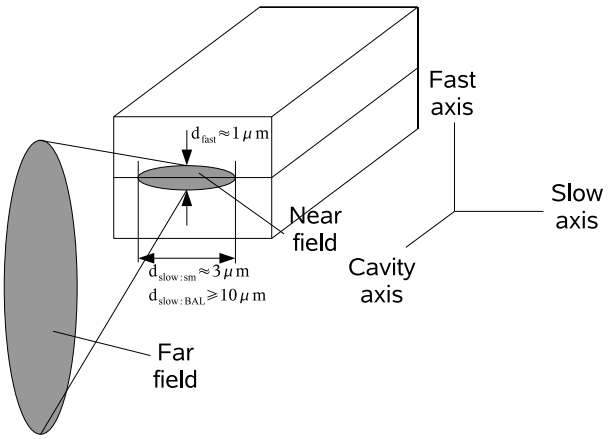

Figure 2.3: *The standard labelling of axes for a laser diode, the near field due to different diverging angles along the slow and fast axis, and the shape of the far field.*

In a cavity, different modes can occur, i.e. ways light can propagate in the cavity with minimum loss and, if a gain medium is present, can be amplified. When it is relevant whether light is present or not in such modes, the term cold cavity modes will be used to indicate no light is present, and the term oscillating, or emitting mode, to indicate light is present in a mode.

Longitudinal modes, (also named wavelength modes as defined by Numai in [36]) occur when the fundamental transverse mode supports the oscillation of light at several different wavelengths. The condition which needs to be fulfilled for such a wavelength is that an integer number N of wavelengths fits a full cavity roundtrip:

$$N\lambda = l_{cavity} \tag{2.1}$$

with λ the wavelength and l_{cavity} the optical length of a full roundtrip in the cavity. If a wavelength fits this condition and resides within the gain band of the diode laser oscillation can occur at this wavelength. A laser diode in which several longitudinal modes are excited simultaneously can show an emission spectrum such as depicted in figure 2.4.

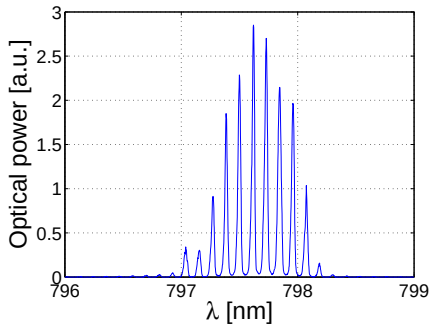

Figure 2.4: *Several longitudinal modes emitting in a spectrum.*

The longitudinal mode, i.e. the lowest-order transverse mode, is associated with light propagating on-axis. In single-mode diodes only this lowest-order transverse mode can be excited along both the slow and fast axes. However, in BALs higher-order transverse modes are allowed to oscillate along the slow axis. Along the fast axis light can only oscillate in the lowest-order transverse mode. The larger the emitter size and width of the active volume is along the slow axis, the more transverse modes can start to oscillate in the cavity. As in all lasers, the presence of multiple higher-order transverse

modes is manifested in a degraded spatial beam quality. The cold cavity modes are orthogonal, so a that light contained in a first transverse mode does not influence the amount of light in another transverse mode, although the two modes show a high spatial overlap. When a gain medium is introduced in the cavity, the light in different transverse cavity modes becomes coupled via the gain medium. In the gain medium where the modes partially overlap and light in the modes will compete for the available population inversion, which is called gain (or mode) competition. Because the gain in a diode laser is, to a good approximation, homogeneously broadened, all the available gain can, in principle, be depleted by a single frequency in a single transverse mode. However in a BAL, where a high number of different transverse modes at numerous frequencies experiences gain, this will rarely be the case. Instead, due to insufficient competition (due to a limited overlap of all modes at all locations in the active volume), many modes will oscillate simultaneously in a BAL. This is then seen as a highly complex spatial output pattern which contains the superposition of all oscillating modes. Due to the multiple-frequency character of this superposition, this leads, in the time domain, to rapid fluctuations of the output intensity, with times in the order of the roundtrip time (nanoseconds). However, when a specific transverse mode superposition is given an advantage, such a via injection of a particular, single light frequency, this spatial pattern could deplete the other transverse modes. In this case, although he mode superposition selected thereby is certainly not a single spatial mode, its single-frequency character is of advantage because it extinguishes the named rapid fluctuations. This temporal stabilisation of the BAL's spatial output pattern can then be used to obtain a suitable photorefractive hologram, even when the photorefractive material shows a slow photorefractive response (see the following sections).

2.1.1 Single mode and broad area diode laser

In figure 2.5 the front viewed structure of a single-mode diode is compared to that of a BAL. In a single-mode diode the light is confined not only along the fast axis by waveguiding such as in the active layer, but also along the slow axis by two electrically insulating layers with a wider bandgap. The light is confined between these layers, along the slow axis, for two reasons. Firstly,

no gain is generated there, because no current is present in the insulating layers. Rather, the absence of pump current renders the semiconductor material strongly absorbing in these regions. The resulting, gain-related transverse restriction of the light field is also called gain guiding. Secondly, the wider bandgap of the insulating layers is associated with a lower refractive index than the refractive index of the gain (p-n junction) layer. This confines propagating light along the slow axis to the gain layer by waveguiding, also called index guiding. The geometrical width of the gap between the insulating layers in the direction of the slow axis is chosen in such a way that it only supports the fundamental transverse mode, i.e. longitudinal propagation in the laser cavity, much like in single-mode optical fibres which support only the fundamental mode as well. For realising a single-mode diode at 800 nm, the named guiding mechanisms lead to a choice of a size for the active area along the slow axis of approximately 3 μm . In contrast to this, the width of the active volume in the direction of the fast axis is determined by the natural thickness of the p-n-junction, i.e. the typical diffusion distance of carriers (about 1 μm). The resulting maximum area of the emitting facet (1x3 μm) for single-transverse mode oscillation, together with the typical damage threshold of 10 MW/cm^2 the semiconductor material its constructed of, limits the output power to approximately 100 mW. The named or similar constructions of laser diodes, where the laser gain is restricted to a narrow (3mum wide) stripe to obtain fundamental transverse mode emission, is often named single-stripe laser.

In contrast to single-stripe lasers, in a BAL light propagation along the slow axis is usually defined only by gain guiding and not by index guiding, as can be seen in figure 2.5(b) . In a BAL, the width of the gain area is deliberately chosen much wider than the gain area in a single-mode laser. The purpose of this approach is to achieve a much higher output power, up to several Watts for a single emitter. However, the larger gain area also implies that a broad area diode is no longer restricted to oscillation at a single spatial mode, rendering the named reduction in spatial and spectral quality of the output.

The aim of our experiments was to be able to access the high-power output of a BAL and improve the spatial and spectral beam quality comparable to the beam quality of a single mode emitter.

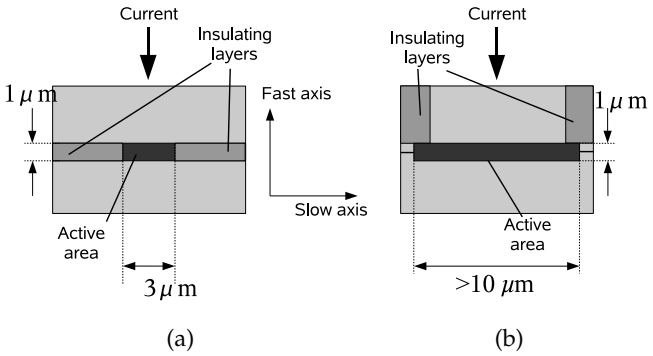

Figure 2.5: *The front facet of a single-mode diode (a) compared to a broad area laser(b). The light is confined in a small cavity in the single-mode case by two insulating areas with a lower refractive index n. In the broad area laser insulating areas do confine the area where the current can flow, but the cavity is not confined at the sides. The effective cavity size is determined by gain guiding.*

2.1.2 Injection Locking

The discovery of the phenomenon of injection locking is often credited to the Dutch scientist Christiaan Huygens [7] who lived in the 17th century. In his work on pendulum clocks he discovered that, if two clocks were positioned on a wall close enough together, after some time the clocks would run synchronous [7,37]. Synchronous means that, the both clocks both oscillate at the same frequency and with a fixed phase relation. Many similarities between the injection locking of mechanical oscillators and optical injection locking of laser oscillator have been discovered since. If two similar lasers are used (see figure 2.6), instead of two similar clocks, and light from one laser is injected into the other laser, under appropriate conditions both lasers will oscillate at exactly the same frequency and maintain a constant phase relation. An optical spectrum analyser (OSA) can be used to verify oscillation at the same frequency, while the disappearance of a temporal beat can also prove a constant phase relation. In this thesis the two lasers will be termed the primary and secondary lasers, where the primary locks the secondary one. An undesired locking of the primary by the secondary laser is usually excluded by introducing an optical (Faraday) isolator in the connecting beam path.

The first successful injection locking experiments with lasers was demon-

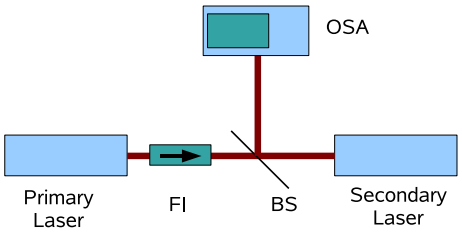

Figure 2.6: *A simple scheme for injection locking of lasers. FI=Faraday Isolator, BS=Beam-splitter, OSA=Optical Spectrum Analyser.*

strated by Stover and Streier in 1966, using HeNe-lasers [38]. In 1980 Kobayashi and Kimura [16] demonstrated the first locking of a diode laser, a GaAlAs laser. In their experiment, both the primary and the secondary laser were single mode lasers.

In the context of this thesis we used the technique of injection locking to lock a high-power (secondary) diode which, in free-running operation, emitted many wavelengths in many transverse modes, to the single frequency of a primary laser with a low optical output power. In figure 2.6 a simple scheme of an injection locking setup is shown. Due to the injection of light from the primary laser, stimulated emission in the secondary laser leads to amplification at that same wavelength (or frequency). Stimulated emission also preserves the phase of the incident light such that the secondary laser oscillation is also driven into a fixed phase relation with regard to the injected phase.

Injection locking in diode lasers is much more complex than with other lasers. Even if just single mode diodes are used, the nonlinear locking dynamics can only be understood using extensive theoretical modelling [21, 22, 39] and experiments [40, 41]. With diode lasers, there is a wide range of types of behaviour. In particular, there exist various regimes, some of which do not correspond to stable injection locking, but produce a spectral and spatial chaotic output pattern of the secondary laser instead, as we also observed in our experiments. Typically, regimes are characterised by the amount of detuning between the primary and secondary laser (explained below), and the amount of optical power injected into the secondary laser. The much more complex behaviour of diode lasers can be largely explained by the fact that a diode laser does not obtain its gain from a a single laser transition, unlike

most other lasers, but from a multitude of levels located in a valence and conduction band. The high density of energy levels in both these bands allows many additional transitions, such as intraband transitions, which gives rise to additional intraband electron and hole dynamics not present in 2-level systems. Because in our experiments we did not use single mode laser diodes but BALs we made no attempt to model the locking dynamics, but restricted ourselves to experimental observations and improvements, with only their qualitative explanations.

Although the multi-level nature of gain in diode lasers is complicating a thorough understanding, it provides also some important practical advantages. The same band structure, namely, allows to provide a high value for high small-signal gain and also a broad spectral bandwith of the gain. Both are advantageous for injection locking, making laser diodes, despite their complexity, amenable sources for injection locking. To explain the latter statement, it is important to realise that the extent to which injection locking can control the oscillation of a secondary laser grows with the locking range. This range, $\Delta\nu_{locking}$, is the maximum frequency detuning between the primary laser frequency, ν_{in}, and the frequency of the free-running mode of the secondary laser to be locked, ν_{fr}. The locking range is, in a simple picture, e.g. described by Siegman [37] given by equation 2.2, where P_{in} and P_l are the respective powers of the injected and locked lasers, and where $\Delta\nu_{cavity}$ is the spectral linewidth of the respective cold cavity mode in the secondary laser.

Qualitatively, as long as the detuned injected beam injects a sufficiently strong field to compensate for the extra cavity losses induced by the detuning, injection locking will occur. In a more quantitative way, the locking range $\Delta\nu_{locking}$ (FWHM) can be defined as [42]:

$$\Delta\nu_{locking} = \Delta\nu_{cavity}\sqrt{\frac{P_{in}}{P_l}} \tag{2.2}$$

Why diode lasers are particularly suitable for injection locking can be explained by a more detailed discussion of equation 2.2, and here, in particular, by considering the linewidth of cold cavity modes in diode lasers. This linewidth, $\Delta\nu_{cavity}$ (FWHM) is associated with Q (quality) factor of the secondary laser cavity modes, which is given by [43]:

$$Q = \frac{\nu_c}{\Delta\nu_{cavity}} \tag{2.3}$$

where ν_c is the centre frequency of a cold cavity mode. Most lasers(e.g. HeNe lasers), have a cavity with a high Q-factor. However, from equations 2.2 and 2.3 it can be seen, a low Q-factor is favourable in for injection locking, since $\Delta\nu_{cavity}$ is larger for such a cavity, as illustrated in figure 2.7 where a low Q and a high Q cavity are compared

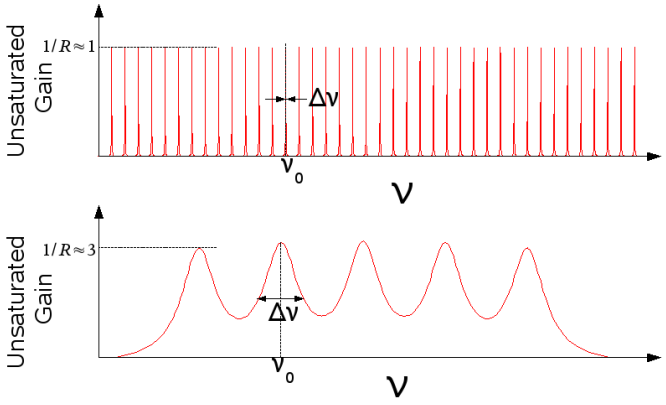

Figure 2.7: *The selectivity of a HeNe-laser (top) compared to the mode selectivity of a diode laser (bottom).*

When looking at equation 2.2 and 2.3 a wide locking requires to use a cavity with a low Q. Furthermore, when ν_c is fixed, a large $\Delta\nu_{cavity}$ (lossy cavity) is the only way to reduce Q. The cavity linewidth $\Delta\nu_{cavity}$ is inversely proportional to the photon lifetime τ_{photon}, which is the average time a photon is contained in the cavity:

$$\Delta\nu_{cavity} = \frac{1}{2\pi\tau_{photon}} \tag{2.4}$$

The photon lifetime τ_{photon}, which obviously is to be made as short as possible for a large locking bandwidth, is determined by two factors, as can be seen from equation 2.5. First, the optical effective length of the cavity is important, L_{eff}, the physical length multiplied by the refractive index. The

second factor is the average number of roundtrips a photon makes in the cavity before it is coupled out by losses.

$$\tau_{photon} = \frac{N_{rt} * L_{eff}}{c} \tag{2.5}$$

In a standard laser, e.g., a HeNe laser, the number of roundtrips is mostly given by the reflectivity of the output coupler. Here, typically, the reflectivity of the output coupler is close to unity and a photon can make hundreds of roundtrips on average before being coupled out. This is in sharp contrast to the circumstances in a diode laser. In a diode laser, with a typical reflectivity of 0.3, the number of roundtrips (N_{rt}) is only 1.5. Furthermore, the cavity length of a HeNe is typically about 30 cm. With the diode lasers we used, the cavity length is only 0.7 mm times a refractive index of 3.5, giving a L_{eff} of 2.45 mm.

In conclusion from this comparison it can be seen that, the high output coupling and short cavity of a diode laser results in a short photon lifetime τ_{photon}, a wide spectral cavity linewidth $\Delta\nu_{cavity}$, a low Q-factor and thus also in a wide locking range $\Delta\nu_{locking}$. To make a more quantitative comparison, some typical numbers can be calculated for the HeNe and the diode laser. For the diode we assume the a reflectivity 0.3 and set the centre frequency at 375 THz (corresponding with the 800 nm light used), the length of the cavity 0.7 mm and the refractive index n=3.5. For the HeNe the reflectivity is taken at 0.99 and the centre frequency 474 THz (633 nm), the length of the cavity 30 cm and the refractive index of the HeNe gas 1. To estimate a $\Delta\nu_{locking}$, the injected power from the primary laser is taken to be 1% of the output power of the secondary laser. The results of this comparsion can be found in table 2.1.

Table 2.1: *Compare cavity parameters HeNe and diode laser*

Parmeter	units	HeNe laser	Diode laser
τ_{photon}	s	2*10^{-7}	2.5*10^{-11}
$\Delta\nu_{cavity}$	Hz	8.0*10^{5}	6.5*10^{9}
Q-factor	-	6.0*10^{8}	5.8*10^{4}
$\Delta\nu_{locking}$	Hz	8.0*10^{4}	6.5*10^{8}

From the table we can see, for example, the locking range of a diode laser

is four orders of magnitude larger than that of a HeNe laser, in the order of hundreds of MHz instead of only tens of KHz. Correspondingly, the injection locking ranges of a diode laser tolerates about four orders of magnitude larger detunings. Another way of interpreting this is that a diode laser can be injection locked also with light of significant spectral bandwidth, such as hundreds of MHz when looking at the example in table 2.1. This makes diode lasers very suitable for an external control by light injection.

As illustrated with Huygens' clocks at the beginning of this section, the establishment of a fixed phase relation between the two mechanical oscillators is observed. This is also the case in injection locking of lasers. However, there is an important difference. The oscillation present in the primary oscillator has to propagate, in the form of an emitted light beam, a substantial distance to reach the location of the secondary laser (propagational distance). This distance has to be compared to the coherence length of the primary laser used, which is given by its spectral bandwidth, $\Delta\nu$, as $L_c = c/\Delta\nu$. When the coherence length is shorter than the propagational distance this means that the oscillation in the locked secondary laser is not temporally coherent with that of the primary laser. As a result, when the output beam from the locked laser is superimposed with that of the primary laser, this does not yield a temporally stable interference pattern, although the secondary laser is locked by the primary one. This lack of mutual coherence will be termed as incoherent locking. Only when the propagational distance is shorter than the coherence length of the primary laser, the superposition of their beams yields a temporally stable interference pattern. This case of mutual coherence between the two lasers will be termed as coherent locking.

As will be explained below, the build-up of a phase hologram in a photorefractive material requires that a stable interference pattern of light is to be generated in the material for time intervals longer than the materials response time. This means that coherent locking is required, when the interference pattern is generated by the primary and the secondary lasers beams, i.e., a hologram will only be generated when the coherence length of the primary laser is longer than, approximately, the physical separation between the primary and secondary lasers. This issue has to be taken into account when realising a corresponding experimental setup.

Besides these spectral considerations, the spatial aspects of injection lock-

ing are important as was already found in the first locking experiments. In these, the incoming transverse mode or modes from the primary laser were precisely matched to the transverse modes of the secondary laser in beamsize and polarisation with exactly the opposite direction and divergence in order to achieve stable locking [38]. This can be understood because at optimum overlap there is a maximum competition of the injected field with the (undesired) free running field. In the case of single-mode lasers this is a matter of properly aligning the primary and secondary laser, with respect to the mentioned properties, so that they emit light in exactly the opposite directions, as depicted in figure 2.6.

In broad area lasers however, it is impossible to attempt injection locking in such a straightforward way, because the spatial output pattern from a BAL is of hard to predict and complex shape and is not stable in time. As was explained above, this results from the simultaneous oscillation of many transverse and longitudinal modes in the presence of internal coupling mechanisms. However, when the diode can be forced to a emit a single frequency, the complex spatial pattern would become stable in time, since the mode superposition containing modes of the same frequency, with a constant relative phase relation. If the wavefront injected from the primary laser had the same complex shape only that it propagated in the opposite direction, this would be the perfect wave for injection locking the BAL into single-frequency emission. A wave with this property, i.e. having the exact same wavefront, beamsize, frequency and polarisation, but propagating in the opposite direction, is called the phase-conjugate wave of the incoming wave. The next section will recall the concept of a phase-conjugate wave in more detail.

2.2 Phase conjugation

Phase conjugation is a well-known concept from nonlinear optics that has received a lot of attention due to its property to correct wavefront aberrations. Such abberations occur when light is propagating through a medium in which the refractive index is spatially inhomogeneous. This applies also to deliberately realised inhomogeneities, such as in a hologram. Here, when diffracting a beam of high spatial quality in a hologram into a complex pattern, phase conjugation can revert (convert) this pattern back into a high spa-

tial quality beam. Here we will show the use of phase conjugated beams to solve the above named problem of the spatial mismatch between the primary and secondary laser in a direct injection locking scheme for a BAL (with its highly complex spatial mode pattern).

In this section first the concept of phase conjugation is recalled and followed by some examples of nonlinear optical effects used to create phase conjugated beams of light.

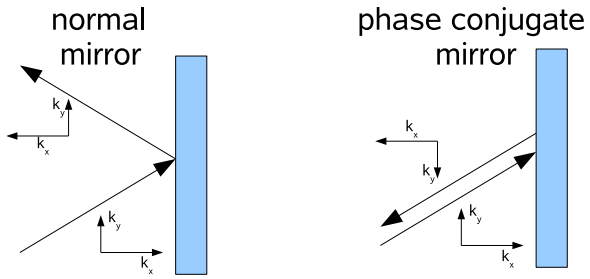

Figure 2.8: *Normal mirror and phase conjugate mirror.*

Upon reflection on a standard mirror, only the k-vector perpendicular to the mirror surface ($\vec{k_x}$) is reversed in direction. This is illustrated in the left hand side of figure 2.8 in which the incoming beam is decomposed in a wavevector $\vec{k_y}$ parallel to the mirror and a component $\vec{k_x}$ perpendicular to the mirror. The difference made by a phase conjugate reflection is that also $\vec{k_y}$ is reversed resulting in a beam travelling in exactly the opposite direction of the incoming beam, independent of the angle of incidence, as is depicted in the right hand side of figure 2.8. In this sense a photorefractive mirror can be seen as a "perfect" mirror.

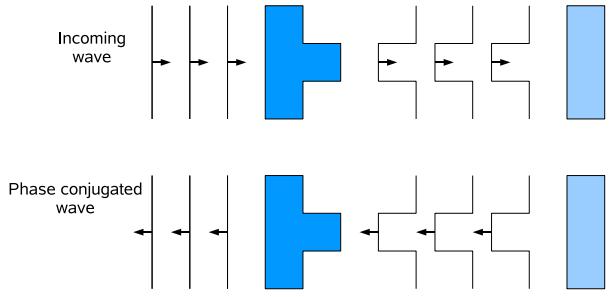

Figure 2.9: *Wavefront correction by a phase conjugate mirror.*

It is this property of reversing all k-vectors which implies that a phase conjugate mirror can correct an arbitrary distortion on a wave by reflecting the wave on a phase conjugate mirror and letting it pass through the distorting medium again, if propagating a pre-distorted wave through the medium results in cancelling of the initial distortion, see figure 2.9. That also arbitrary distortions can be corrected is explained by the consideration that any distorted wavefront can be seen as a superposition of plane waves, and where each of these plane wave components will be reflected the way figure 2.8. The superposition of all the phase conjugated waves will then add up as the same wavefront before it was reflected by the phase conjugate (PC) mirror , however, that now it propagates in exactly the opposite direction. The PC mirror has the property to reflect a distorted wave in as a 'pre-distorted' wave so that passing the medium again will exactly nullify the changes in the wavefront.

Mathematically, it is thus sufficient to model a monochromatic plane wave. A plane wave, E_{signal}, propagating in the +z direction can be written as:

$$\begin{aligned} E_{signal}(x,y,z,t) &= A(x,y,z)e^{-ikz}e^{i\omega t} \\ &= A(x,y,z)\Psi_s(z)\Psi_t(t) \end{aligned} \tag{2.6}$$

with A being the real-valued field amplitude and $\Psi_s(z)$ and $\Psi_t(t)$ being complex-valued phase factors,:

$$\Psi_s(z) = e^{-ikz} \tag{2.7}$$

$$\Psi_t(t) = e^{i\omega t} \tag{2.8}$$

In order to obtain from this the complex conjugate wave, E_{pc}, of E_{signal}, one has to convert either $\Psi_s(z)$ or $\Psi_s(t)$ into its complex conjugate value. First, the complex conjugate of E_{signal} is taken by conjugating $\Psi_s(z)$.

$$\begin{aligned} E_{pc} &= E^*_{signal} \\ &= A(x,y,z)\Psi^*_s(z)\Psi_t(t) \\ &= A(x,y,z)e^{+ikz}e^{i\omega t} \end{aligned} \tag{2.9}$$

Note that this indeed inverts the sign of k as described from phase conjugate reflection. the second alternative, E_{pc} can also be calculated by inverting

$\Psi_s(t)$ instead of $\Psi_s(z)$:

$$\begin{aligned} E_{pc} &= E^*_{signal} \\ &= A(x,y,z)\Psi_s(z)\Psi^*_t(t) \\ &= A(x,y,z)e^{-ikz}e^{-i\omega t} \end{aligned} \tag{2.10}$$

Here, not the k-vector, but the time appears as inverted, hence the notion of a phase conjugated beam as a 'time-reversed' wave, as illustrated in figure 2.9.

Physically, phase conjugation is achieved by letting a signal wave and possibly other waves to write index gratings into a medium using a nonlinear effect such that the wave diffracted from this grating is the phase conjugate signal. One of the nonlinear effects suitable to achieve phase conjugation is stimulated Brillouin scattering (SBS) with which phase conjugation of optical waves was initially discovered by Zeldovich [44]. Here, an optical wave entering a suitable nonlinear medium creates a phonon wave, spatially modulates the refractive index of the medium with the period of the phonon wave. This effectively creates a moving index grating in the medium with its period fitting the optical wave such that the optical wave can diffract from this grating in the exact opposite direction that it came from.

Another nonlinear optical effect used to create a phase conjugate wave is photorefraction. However, for making use of photorefraction, an additional beam is required from another laser source, the so-called pump beam. When spatially overlapping the incident beams form an interference pattern and the photorefractive response converts this into a refractive index pattern of the same shape. The diffraction of the pump at this pattern then generates an additional wave being phase conjugate with regard to the incident signal wave.

We have used the latter approach based on photorefraction to holographically injection lock the BAL. For these experiments we used two different types of photorefractive materials, the properties of which will be discussed in the section 2.5. However, before we discuss an general property of optically generated holograms that has been made use of for the conversion of an incident beam into a beam of a desired shape.

2.3 Holographic beam conversion

To illustrate the working principle of holographic beam conversion we refer to a well-know and simple example as is depicted in figure 2.10. Consider that the goal is to diffractively convert an incident monochromatic wave of given shape (e.g., the plane wave represented by beam1) into a desired monochromatic wave of different shape, which is here, e.g., the converging (focused) wave represented by beam 2. Also assume that the frequency of the two waves is the same and that the the waves are mutually coherent, i.e., that they possess a constant phase relation with regard to each other. The problem to be solved then is to find and to generate a suitable index pattern, i.e., a suitable diffractive optical element, that converts beam 1 into beam 2.

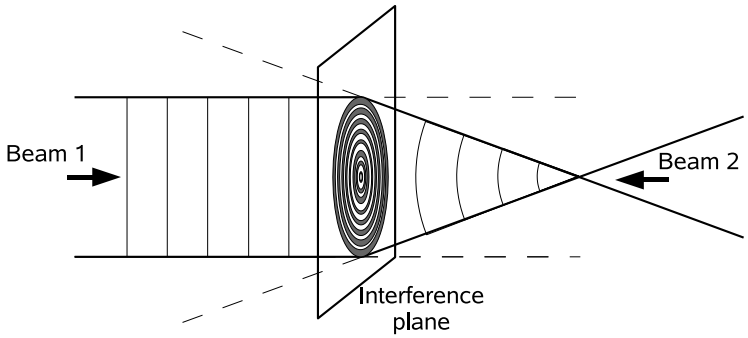

Figure 2.10: *The interference pattern between a plane wave and a focusing wave.*

The experimental solution to this problem is the following: One first provides the desired beam 2 by some other means and lets it counter-propagate with regard to beam 1. At some plane, chosen for convenience, here labelled 'interference plane', the waves are superimposed such that they form an interference pattern. This pattern then contains the information of both wavefronts. In the given example, where we have chosen an interference plane normal to the beam axis, this pattern would consist of a set of concentric rings generated by alternating constructive and destructive interference, a so-called Fresnel ring pattern. In a next step, to turn this diffraction pattern into a diffractive optical element, i.e., to record the ring pattern, one places a light-sensitive material in the selected plane, e.g., a photorefractive material, in which the refractive index changes in proportion with the local light

intensity. In the considered case this results in concentric rings with alternating low and high index, which is also know as a Fresnel zone plate or Fresnel lens [45, 46]. After this recording, when the Fresnel lens remains to persist over some certain life-time (depending on the choice of material), even when beam 2 is turned off, the Fresnel lens found and realised is precisely the diffractive element that converts, as was the goal, the incident plane wave (beam 1) into the desired focused wave (beam 2). Note that this Fresnel lens also fulfils a second function: when letting the diverging beam 2 fall on the recorded pattern, diffraction generates a plane wave (beam 1).

In the given example the beam shapes are rather simple and result in a hologram with well-known shape. The importance of this holographic beam conversion principle, within the scope of the present thesis, is based, however, on two issues that can be concluded from the example as well. 1) The shown principle is not limited to particularly shaped beams. For instance, in place of the converging beam 2, one could inject a beam of any other arbitrary shape, e.g. a highly complex beam pattern. In this case, of course, the shape of the recorded index pattern would change and become some highly complex pattern as well. Nevertheless, when sending only beam 1 through this pattern, diffraction of the plane wave would generated precisely the complex pattern of beam 2, only with a reverted direction of propagation. 2) In the described holographic beam conversion it is neither required to know the particular shape of a complex beam 2 injected from the left for recording, nor is it required to know the complex shape of recorded index pattern (hologram). The working principle of the methods ensures that, after recording, the plane wave (beam 1) will be diffracted into the original complex pattern of beam 2, and, the complex pattern (beam 2) will be diffracted by the hologram into a plane wave. In the holographic locking experiments described in this thesis, we will make use of the named properties of holographic beam conversion as follows: By superimposing the (unknown) complexly-shaped beam pattern from an injection locked, single-frequency BAL with the simple beam from a single-transverse mode, single-frequency Ti:Sa-laser in a photorefractive material, we record a (unknown) hologram. This hologram diffracts the simple-shaped beam from the Ti:Sa laser into whatever complex beam the BAL emits. At the same time, the hologram diffracts whatever complex pattern is emitted by the BAL into the high-quality beam shape provided by the

Ti:Sa laser.

2.4 Nonlinearity in holographic injection locking

After having discussed injection locking, phase conjugation, and holographic beam conversion, the fundamental nonlinear optical nature of the concept of holographic injection locking can be reviewed. A schematic of a corresponding setup is shown in figure 2.11. In this figure it is indicated that, essentially, two processes which are mutually dependent because the power generated by one of the processes determines the power generated in the other process.

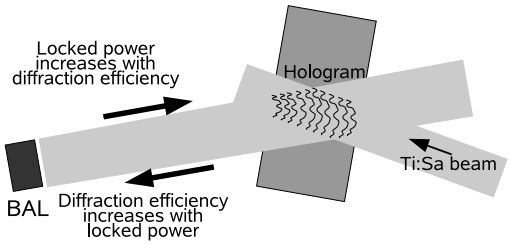

Figure 2.11: *The two mutually dependent processes in holographic injection locking*

The two processes which are then strongly interdependent are the following. First, the (injection locking) response of the BAL to the injected light from the primary Ti:Sa laser is dependent on the power that arrives from the hologram at the BAL in the form of a matching spatial beam pattern. An injected power which is too weak will not induce a change in the emitted spectrum of the BAL. Also too strong a power initiates an strong nonlinear and unstable response from the BAL , as was described in the section on injection locking of diode lasers, section 2.1.2. Only if the optical power of the injected light is in a certain range, stable injection locking to a single-frequency can be achieved. This power is, however, depending on the diffraction efficiency of the recorded of the hologram which is, in turn, is also dependent on the optical power locked to single-frequency emission of the BAL. This interplay and feedback between the diffraction efficiency of the hologram and the injection locking of the BAL is summarised in figure 2.11 as the two arrows labelled as ”Diffraction efficiency increases with locked power” and as ”Locked power

increases with diffraction efficiency". It is expected that the two mechanisms form a nonlinear feedback loop which starts off as follows. Initially, when the BAL is in its free-running mode, there is only a very weak portion of its emitted power accidentally coincident with the frequency of the Ti:Sa laser. However, this small portion, in superposition with the beam from the Ti:Sa laser, generates a photorefractive hologram with a certain, low contrast that was not present without the Ti:Sa laser. Next, this hologram diffracts some extra power from the Ti:Sa laser into the BAL, thereby increasing also the portion of single-frequency emission from the BAL, via the onset of weak injection locking. This then increases the diffraction efficiency of the hologram further, letting the injected power from the Ti:Sa laser grow, resulting in a stronger injection locking of the BAL. If the system, in this nonlinear feedback loop, reaches a steady state, this would indicate that the total diffraction efficiency of the hologram has increased such that it diffracts sufficient light back into the BAL to injection-lock it to a single-frequency, while, at the same time, the diffraction efficiency remained low enough to avoid chaotic behaviour of the BAL.

The next section will focus on the photorefractive effect, the effect we will use to record (or 'write') holograms in order to create the phase-conjugate beam required for stable injection-locking of the BAL.

2.5 Photorefractive effect

The photorefractive effect was discovered by F.S. Chen in 1967 [47] and, following the use of $LiNbO_3$, many types of crystals have been shown to be photorefractive [48,49]. A lot of potentially interesting applications have been suggested which take advantage of the holograms (index patterns) the photorefractive effect allows to be written in such materials: Holographic data storage, optical image processing an real time holography are some examples [50–56]. In the context of this thesis, the photorefractive effect is relevant because of its ability to improve injection locking of high-power diode lasers in spite of their spatially complex output beam pattern, via a suitably optically written holograms.

Following the class of inorganic crystals, in 1991, the first photorefractive polymers were discovered (S. Ducharme et al. [57]), adding a new class of

photorefractive materials. In this chapter both classes of materials are discussed, particularly, with regard to their behaviour in an experimental setup for holographic injection locking. For this purpose, a qualitative description of the basic working of the photorefractive effect in both of these materials will be given, and the material properties are compared. Before photorefractive polymers are introduced, an experimental setup used to determine the photorefractive properties of a material, the two-beam gain configuration, is introduced.

In the second part of this section, two further configurations, both used as setups to achieve holographic injection locking and both capable of generating phase conjugate beams, will be discussed: nondegenerate Four-Wave Mixing (FWM) and the Double Phase Conjugate Mirror (DPCM).

2.5.1 Optical axis

In anisotropic materials the refractive indices n_x, n_y and n_z can all be different. In isotropic materials they are all the same, and, therefore a perfect sphere of the refractive index as a function of the direction in a crystal can be drawn, as in 2.12(a) . In uniaxial crystals, n_x, n_y and n_z are not all different, two are still the same. So $n_x = n_y = n_o$ and $n_z = n_e$. If the curve of the refractive index as a function of the direction in the crystal is drawn again an ellipse for n_e will appear and n_o is still circular. There are two possibilities, a negative and a positive uniaxial one, both depicted in 2.12(b) and 2.12(c) . Now there are two points on the z-axis on which $n_o = n_e$ making the z-axis the optic axis, referred to as c-axis.

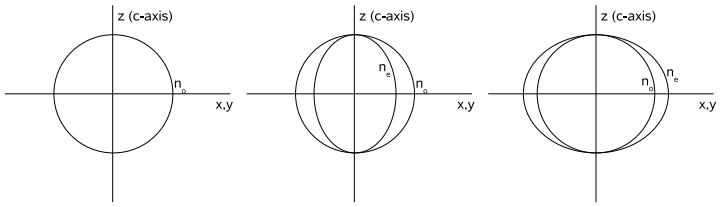

(a) (b) (c)

Figure 2.12: *A 2d representation of (a) an isotropic material, (b) a negative uniaxial crystal ($n_e \leq n_o$), (c) a positive uniaxial crystal($n_e \geq n_o$).*

Normally, not only the direction of the optical axis is relevant, but also

the sign. There is a c+ and c- direction along the axis if the material is ferroelectric. This means that, due to the structure of the material, an ion in a unit cell has an offset and the unit-cell acts as permanent dipole. If the dipoles in a crystal are all oriented in the same way, a macroscopic effect occurs. This is comparable to magnets in which all the magnetic dipole moments of electrons are oriented the same way creating a macroscopic effect, hence the name ferroelectric derived from ferromagnetic [48]. In models and experimental configurations relying on photorefraction, the direction of the c+ axis is often given as a reference point. Furthermore, the direction of this axis (labelled as the 'c+ direction' of this axis) is relevant since, as will be explained below, it determines the spatial phase shift that arises between an illuminating interference pattern and the resulting index grating. The direction of this phase shift, as determined by the direction of the c+ axis, is important to judge the two-beam gain setup.

2.5.2 Photorefractive effect in crystals

Here we recall the generally accepted model to describe photorefraction in crystals, which is the so-called bandtransport model.

For an extensive and quantitative treatise we refer to the work of Yeh [49] or Nolte [48]. Here the goal is to focus only on certain issues that are essential for the understanding of the experimental configurations investigated in this thesis. Specific differences found with photorefractive polymers, used in our experiments as well, is presented hereafter.

First, a short overview of photorefraction will be given to provide a general understanding of photorefraction, which also apply to crystals as well as to polymers.

The photorefractive effect is schematically depicted in figure 2.13. The origin of photorefraction is understood easiest when seen as four separate steps as illustrated in the figure. The first step is to illuminate the medium by two beams of mutual temporal coherence, but different k-vectors, which imposes an interference pattern on the intensity distribution in the crystal. In the second step, in the bright regions of this pattern, free charge is generated by the illumination. The free charge diffuses to other regions and becomes trapped in darker regions. This light-induced charge separation can be ex-

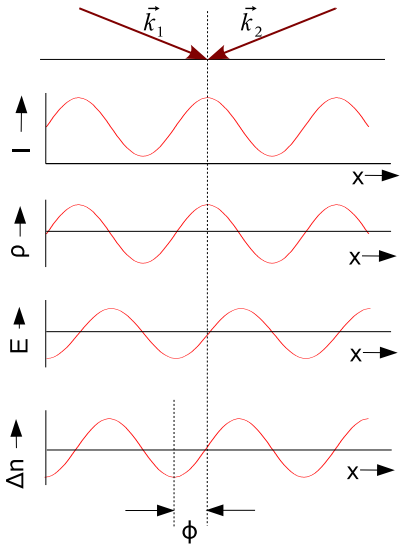

Figure 2.13: *Irradiation of a photorefractive material: an interference pattern (I) causes a spatially modulated charge density (ρ) and the associated electric field $\vec{E}$ causes the desired refractive index modulation Δn.*

pressed as spatially inhomogeneous charge density, $\rho(x)$ in figure 2.13 In the third step, the charge inhomogeneities induce a spatially patterned electric field, the space-charge field $\vec{E}(x)$. In the last step, this electric field introduces a modulation in the refractive index $\Delta n(x)$, due to the electro-optic effect, which is proportional to the electric field $\vec{E}(x)$. The result is a spatially patterned index distribution, also called index grating. This contains a single period if the two incident light waves contain only a single k-vector each, as can be seen in figure 2.13. However, in the more general case, when two beams with a wider distribution of k-vectors (i.e. non-plane waves) are superimposed in the material, a more complexly-shaped index pattern is called a (volume) phase hologram. Note that there occurs some spatial phase-shift between the intensity modulation function and the index modulation, ϕ on the horizontal axis.

For inorganic crystals, the charge transport, mentioned in the second step above is based on the transport of electrons. Once the electrons have been excited into the conduction band and they become mobile, while the corresponding ions remain rigidly fixed in the crystal lattice. This is described to

further detail in the band transportmodel [49]. A corresponding sketch of the typical configuration of the band structure and energy levels in a photorefractive crystal is given in figure 2.14

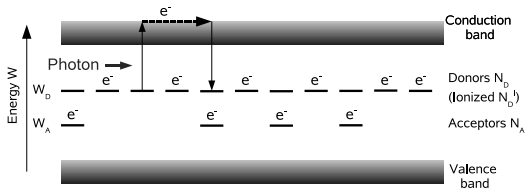

Figure 2.14: *Banddiagram of a photorefractive crystal*

As can be seen in the figure, in addition to the valence and conduction band, two extra types of levels are involved. These are donor levels and acceptor levels, introduced by imperfections in the crystal lattice and/or by impurities due to doping. A feature of acceptors is their lower position in the energy diagram compared to those of the donors, as indicated schematically $W_A < W_D$.

The donor levels are found either occupied with an electron (thus neutralising the total charge at that location), or, when they are not occupied , they can accept electrons, from which these levels have a positive net charge. In a photorefractive crystal, the electron is, actually, removed from an appreciable fraction of donors, even when no incident light is present. This is the result of the simultaneous presence of acceptors at an even lower energy. The internal equilibrium in the crystal is thus found in an occupational state as shown in figure 2.14, where essentially all acceptor levels have bound an electron, thus creating an equal number of donor levels where the electron is lacking. However, as usually the number density of available acceptors, N_A, is chosen to be lower than the density of donors, N_D, there will still be a substantial number of electrons present at the donor level.

Now suppose that a photon with a sufficient energy excites an electron from the donor level to the conduction band. The excited electron will then be able to diffuse freely through the material, which can be expressed as an effective diffusion current, $\vec{j_{diff}}$. Due to the anisotropy of the material, expressed by the existence and orientation of a c-axis, this current will have a preference for a certain direction. However, due to the existence of many un-

occupied donors, which can be referred to as electron-traps, the excited electron will recombine in an electron trap after some time, and this will likely be at another location than where it was optically excited.

When a medium is illuminated in such a way with an interference pattern that is sufficiently stable in time, initially many electrons become excited and start to diffuse in the described way. Since the excitation of these electrons is based on the absorption of light, it is much more likely electrons are excited in the bright fringes of the interference pattern. Also, it is likely electrons diffuse into a dark region, where they remain trapped due to the lack of light in the dark regions.

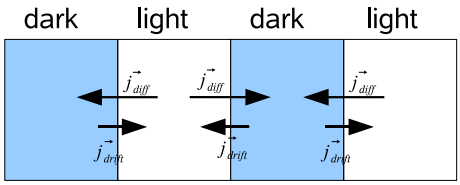

Figure 2.15: *The two competing currents $\vec{j_{diff}}$ and $\vec{j_{drift}}$. In the depicted case the grating is still growing because $\vec{j_{diff}} > \vec{j_{drift}}$.*

After irradiating the crystal for some time with a temporally stable interference pattern, a dynamical equilibrium between optical excitation, diffusion, and trapping of electrons is established, thereby creating an inhomogeneous charge distribution (i.e. a charge separation) ρ, in the material. The charge separation then builds up a space-charge field $\vec{E}$, which causes a second type of (directed) current called drift current $\vec{j_{drift}}$. This current starts to counteract the diffusion by causing drift into the bright regions. This is shown in figure 2.15. Once these two currents are equal, the contrast of the charge separation grating will, when looking at this as a macroscopic effect, stop increasing. At this moment, the maximum spatial modulation in $\vec{E}$ is reached, and the maximum contrast in the associated electro-optically induced index grating ($\Delta n(x)$ in figure 2.14) is reached as well.

For obtaining a high diffraction efficiency, the length of the period of the photorefractively induced grating, and, therefore, the length of the period of the illuminating interference pattern used, is important. If this spatial period becomes too small, diffusion results in a weak charge separation field and thus also in a weak modulation of $\Delta n(x)$, i.e., in a low index contrast of the

hologram to be generated. Also, if the spacing becomes too wide, the light in the illuminating interference pattern does not provide sufficient energy to separate the charges over the large distances. This means that $\vec{j_{drift}}$ becomes dominant before charge separation is achieved, thereby reducing the index contrast as well. To adjust for the optimum period of the illuminating interference pattern (i.e., the maximum contrast of the resulting index) the angle between the incident beams, can be adjusted

From these physical processes on which the photorefractive effect is based, it can be seen that the photorefractive response of a specific crystal depends, in a rather complex manner, on a set of different crystal properties. It depends particularly on the mobility tensor ($\vec{j_{diff}}, \vec{j_{drift}}$), the dielectric tensor ($\vec{E}$) and the electro-optic tensor (Δn). In view of this, the quantitative modelling of the photorefractive response of a specific crystal sample is extremely difficult, and unreliable because named material properties are usually not well known. For instance, there is a lack of information on the mobility tensor and the electro-optic tensor for the cobalt-doped $BaTiO_3$ crystals that were used in our experiments. The main reason for this is that the density of donors and acceptors cannot be well-controlled during crystal growth, as well as the density and type of residual irregularities in the crystal structure. Therefore we have restricted ourselves on the demonstration of the use of photorefractive crystals for controlling injection locking in high-power diode lasers, rather than attempting to understand the specific quantitative response of our individual crystal samples.

2.5.3 Two beam gain

The two-beam gain (TBG) setup, as depicted in figure 2.16, can be used to characterise the response of a photorefractive material on two incident light beams. As was mentioned in the previous section, the phase angle ϕ is the phase shift between the illuminating pattern of light, ($I(x)$) and the resulting pattern of the refractive index, $\Delta n(x)$. In crystals, where the charge separation is achieved by electrons only, one obtains $\phi = 90^o$, but this is not the case with photorefractive polymers. Instead, when any nonzero value for the phase angle is obtained with a polymer, the polymer is classified as a photorefractive polymer. As will be explained, the importance of the TBG setup

is that it can be used to measure whether a certain material shows a nonzero phase angle and thus whether how suitable it is for a use in photorefractive experiments.

Before introducing the working principle of the TBG setup, it is useful to recall the meaning of the term "thick hologram" [58]. A volume grating, or volume hologram, recorded by the interference pattern of two beams ('written') in a photorefractive material, can typically be considered as a thick hologram. This means that the spatial extent of the hologram is much larger than the wavelength used for writing the hologram, and thus also much larger than the wavelength of the beam that is to be diffracted by the hologram (the latter is called the 'reading' beam). In such holograms, light can only diffract efficiently if the incoming light enters very near the Bragg angle with respect to the grating vector defined by the writing beams. In this case, the diffraction efficiency as can be derived from coupled wave theory, can be as high as 1, hence the name 'thick hologram'. A high efficiency is important to achieve holographic injection locking in our experiments, and also to be able to measure two-beam gain as explained below.

In figure 2.16, a typical setup for realising two-beam gain coupling is depicted. Assume, for simplicity, that two plane waves (of the same wavelength forming a stable interference pattern) are incident as both beams are incident, indicated by their wavevectors $\vec{k_1}$ and $\vec{k_2}$ and overlap in a photorefractive medium (grey area). The overlapping beams then form an interference pattern characterised by the following grating vector,

$$\vec{k_g} = \vec{k_1} - \vec{k_2}, \tag{2.11}$$

as is also depicted in figure 2.16.

This grating vector points in the direction along which the grating period is shortest, and possesses a length inversely proportional to the grating period Λ_g:

$$|\vec{k_g}| = \frac{2\pi}{\Lambda_g} \tag{2.12}$$

The direction of the phase-shift between the interference pattern of the beams and the periodically changing refractive index, θ, is determined by the direction of the optical axis $c+$, also depicted in figure 2.16. It is important to note that, due to the nonzero-value of the phase-shift, light is not diffracted

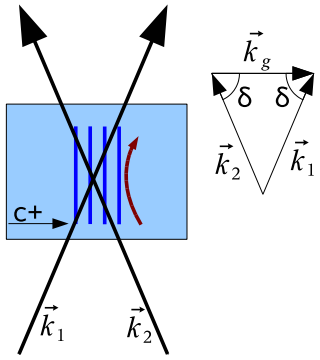

Figure 2.16: *A two-beam gain setup and the corresponding k-vectors to build the grating. The angles marked by δ are the relevant Bragg angles in this configuration.*

in equal amounts to the output directions $\vec{k_1}$ and $\vec{k_2}$. Instead, as shown in figure 2.16, more light is diffracted into one of the directions, here in the direction $\vec{k_1}$, such that less light is diffracted into the other direction, of $\vec{k_2}$. This asymmetry in power flow, with more power flowing into the direction of the optical axis, is indicated by the curved arrow. Another way to express this asymmetry is to speak of the flow into direction $\vec{k_1}$ as being "amplified" by the flow of another incident light (direction $\vec{k_2}$), hence the name two-beam gain. In the optimal case, if $\theta = 90^o$, and if the diffraction efficiency is 1, all the light will be diffracted to output beam $\vec{k_1}$. For photorefractive polymers, however, the phase angle is typically, smaller than 90^o, and the asymmetry of power flow measured in a TBG experiment can be used to quantify the photorefractive properties of a material.

2.5.4 Photorefractive polymers

Inorganic crystals possess some distinct disadvantages. An important disadvantage is that a low sensitivity to light at wavelengths around 800 nm. This lack of sensitivity results in a long response time, a low diffraction efficiency of the hologram and a lack of reproducibility of crystals. Inorganic crystals typically also have to be handled with great care, in order to avoid a depoling of the crystal due to mechanical stress or due to temperature changes. These properties make inorganic crystals quite unsuitable for a use in 'real-world'

applications. In the following we recall the properties of organic photorefractive polymers because it appears that the named disadvantages of crystals can be avoided with such polymers.

A first and simple point of interest in photorefractive polymers is that the physical appearance in which polymers can be brought can be widely selected because it is not related to crystal growth, cutting an polishing techniques. The named polymers are available in liquid state and thus can be easily used in the form of a thin film (thin film devices). In this case, the liquid polymer can be contained between two glass plates to form a layer of, in our case 105 μm thick. In this case, the glass plates are coated with an ITO-layer so that an electric field may be applied throughout the polymer. The purpose of this is to orientate the molecules to obtain a macroscopic photorefractive effect, similar to the case of a crystal with an optical axis. The direction of the applied field then defines direction of anisotropy in the material, such that an electro-optic effect can occur [61].

The mechanisms required for photorefraction in such a polymer are of somewhat different form those explained in the previous paragraph for inorganic crystals. Here we restrict ourselves to a qualitative description, particularly with regard to use in diode locking experiments, while a more detailed treatise can be found in the references 48, 59, 60.

Although the four basic steps (nonuniform illumination, charge transport and trapping, electric field build-up, and electric field induced change in the refractive index) remain the same in polymers, as depicted in figure 2.13, however, there are some fundamental differences.

Photorefraction is, again, initiated in the first step by illuminating the polymer with an interference pattern of incident light. The second step is to achieve a photoinduced charge separation, $\rho(x)$. Without the externally applied electric field, recombination would be dominant and little charge separation would be seen. However, in with an electric field applied, freed charges move a certain distance through the material before they are trapped. While in crystals the process of free charges moving though the material is entirely due to diffusion, in polymers the drift due to the external field also plays a critical role. Another difference is that, typically, in polymers the holes (created by freeing an electron from a certain location within a molecule) are more mobile than the electrons so that charge transport in polymers is mainly

based on hole transport. For crystals, we recall that the donor and acceptor sites are fixed within the crystal lattice and only the electrons become mobile. As in polymers both carriers are involved in charge transport one obtains here an index grating which is phase-shifted in space by a non-ninety-degree value from the illuminating interference pattern, and that this phase angle grows with the applied electric field.

A further difference with charge transport in polymers is found in the non-periodic arrangement and physical separation of molecules. Here, transport happens in a hopping-like manner and is not comparable to electrons diffusing through the conduction band. As a result, the electrical resistance encountered by charges in polymers is much higher and reduces the charge mobility. However, to increase the mobility, certain chemical components can be added to the photorefractive polymer. This facilitates the charge-transport by supplying a dense network across which holes can hop from one molecule to the other. Besides changing the mobility, unlike in crystals, the charge mobility in polymers is found to increase with the field ($\mu \sim e^{\sqrt{E}}$, for many known photorefractive polymers [48]). Because the charge separation process and the charge transport are both dependent on the applied external electrical field, the TBG (measure of ϕ) of a photorefractive polymer is also dependent on the applied external field [62–64]

Also, the trapping times of charges found in a polymer are different from the ones in a crystal. Longer trapping corresponds to a more persistent grating. A high density of traps increases the growth rate (i.e. response time of photorefraction) and it also increases the index contrast in equilibrium (i.e. the diffraction efficiency for incident light). A qualification of the trapping time can be achieved via defining so-called trapping areas in the material in which charges are kept from participation in the transport for some given period of time. In the charge-hopping scenario named above, longer trapping can be achieved with a lower energy for the holes, where the depth of a trap is determined by the local energy-gap.

When inspecting the various types of photorefractive polymers that have been fabricated, a general classification of the depth of traps can be made by considering whether a charge can escape from a trap only via the absorption of a photon (called a deep trap) or whether it can also escape by absorbing thermal energy from its environment (shallow trap). If deep traps are domi-

nant in a polymer, the response time increases, but also the phase shift ϕ increases (i.e. the two-beam gain increases). Shallow traps, on the other hand, provide a faster photorefractive response, however, this is associated with a smaller ϕ and thus less TBG coupling.

As the last step, an electric field pattern, resulting from charge transport and inducing a modulation in the refractive index, $\Delta n(x)$ has to be induced. For this purpose chromophores, i.e., molecules with a strong electro-optic response, are used. Besides this, the so-called 'orientation enhancement effect' improves the nonlinear response of the material, discovered by Moerner [65] and also explained in reference 59.

Having discussed the physical processes that enable and control the photorefractive effect in polymers and standard photorefractive crystals we will, in the following section, compare the various characteristics of crystals and polymers with regards to how these would affect their potential use in our holographic locking experiments.

2.5.5 Crystals compared to polymers

In polymers, to optimise all the different processes that contribute to a photorefractive effect, a variety of chemicals is added to the polymeric liquid. Chemicals can be added to modify each one of the involved properties, such as charge generation, carrier mobility, trapping and recombination, thereby determining the photoconductive behaviour of a polymer over wide ranges. Alltogether, one can enable an easier separation of electrons and holes, sensitisers can be used to increase the absorption of photons and to reduce the required photon energy for charge separation, plasticisers can improve the orientational enhancement provided by the chromophores and, sometimes, dopings can be used to change the trapping properties. Because for each of these individual functions a number of different chemicals have been identified, a wide variety of photorefractive polymers can be designed to fit a certain purpose in an experiment. In our case, this includes adding sensitisers to improve the response to 800 nm light, in which range we performed our experiments.

In, for comparison, a crystal the photorefractive effect is largely inherent to the crystal structure which is responsible for all of the involved physical

processes at once. The only way to alter the response of a crystal is to add dopings at various concentrations in order to modify the density and energy of the donor and acceptors levels. This is done, for example, to improve the photorefractive response to near-infrared light, in our case with cobalt. However, this is technically hard to control because during crystal growth crystallisation tends to drive the doping out of the crystal to an extent that is difficult to predict.

A clear disadvantage of crystals is that they are very sensitive to mechanical stress and also should be stored at controlled temperatures between 10 and 60 degrees to avoid a depolarisation of the crystal. Polymers are not very sensitive to mechanical stress and temperature changes, however, as an organic material they are more sensitive to optical damage.

An clear advantage of polymers is their fast response time which is in the order of milliseconds, while crystals typically show a rather slow response. It can take several minutes to build up a photorefractive grating, even with comparatively high light powers of tens of mW, collimated to a few mm^2, particularly when using near infrared light with its low photon energy. Furthermore, due to the different mechanisms managing the photorefractive effect, the maximum achievable refractive index modulation, Δn, can differ by up to two orders of magnitude. For instance, for $BaTiO_3$, Δn is as low as 10^{-5}. In polymers, Δn can be as high as 10^{-3}. This means that less periods are required in a grating or hologram to achieve a given efficiency. The slow response time of crystals also initiates a memory-effect. For example, after an experiment is conducted, it takes a rather long time (several hours) for the electrons to diffuse through the crystal and restore a homogenic distribution of electrons. Although the diffusion can be speeded up by illuminating the crystal with an intense white-light source, or with a laser of a different wavelength, practice shows that a second experiment performed on the same day was almost always hampered by some residual gratings in the crystal.

With a polymer these problems were not encountered, which can be attributed to the much faster response times. Additionally, because the generation of a photorefractive effect requires the application of a voltage across the polymer, all gratings in the material are almost immediately erased by turning the voltage off.

A relatively high refractive index, such as in $BaTiO_3$ (n=2.4) can cause par-

asitic effects. This is because a high refractive index leads to strong internal Fresnel reflections ($R \approx 0.17$ for $BaTiO_3$ at normal incidence). This allows undesired internal roundtrips of the involved light beams through the crystal, thereby creating undesired gratings at all beam crossings. In contrast to this, the refractive index of a polymer is comparatively low, only about 1.5. This, especially when a polymer is used in the shape of a thin film as described above, reduces parasitic gratings drastically.

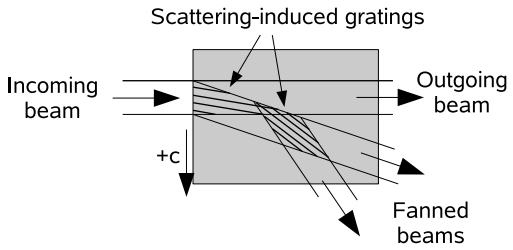

Figure 2.17: *The mechanism of beam fanning in a photorefractive medium (grey block). Due to scattering, a new beam is formed which, in turn, can write a TBG grating with the original beam. Depending on the orientation of this grating, light can be diffracted in to a greater or lesser degree from the original beam into the scattered beam. This process can repeat itself, i.e., the scattered beam can scatter again, and a next grating will be formed to diffract light to this second scattered beam. As the overall effect, spatially well-defined, incoming beam becomes a wide (fanned) beam after propagating through the photorefractive medium.*

Another difference between crystals and polymers is the expected amount of so-called beam fanning. This is, in most cases, an undesired effect occurring because a beam entering a photorefractive material is scattered (by e.g. a rough air-crystal interface, an inhomogeneous refractive index, impurities in the material, Rayleigh scattering, etc.). Suppose that a beam enters the crystal with an angle with regard to the optical axis. Then, between a scattered beam and the incident beam a photorefractive index grating will be recorded (or 'written') as well, as is indicated in figure 2.17. This grating is essentially a TBG grating, and optical power from the originally incoming beam is coupled towards the optical axis, as discussed in the section on TBG, i.e., parts of the incoming beam are slight bent (or fanned) more in the direction of the

optical axis (see details in figure caption 2.17). The amount of such beam fanning grows with the distance a beam propagates through the medium. Since crystals haves typical sizes in the order of a few mm and the thickness of an a photorefractive polymer is in the order of hundreds of μm, beam fanning is likely to be much stronger in crystals.

When looking at the described differences between the photorefractive crystals and polymers, it becomes clear that for our goal, to achieve injection locking via photorefractive feedback, one has to take into account the differences between the materials to be able to achieve injection locking in both cases.

2.5.6 Nondegenerate four-wave mixing

In order to generate a phase-conjugate beam in a photorefractive configuration, the nondegenerate four-wave mixing (FWM) setup is the most simple and straightforward setup (at least from a theoretical point of view), see also chapter 19 in [61]. In a FWM setup, one beam becomes phase-conjugated by using two additional pump beams in opposing directions such that the three beams overlap in the photorefractive medium. In our experiments we used the beam from the BAL as the beam we intend to phase-conjugate, and the beam from a single-frequency continuous-wave Ti:Sapphire (Ti:Sa) laser, retroreflected by a mirror after a single passing of the medium, as the two pump beams. The phase conjugated beam possesses the spatial pattern preferred by the BAL, while at the same time, the phase conjugated beam has the spectral linewidth (e.g. single frequency) of the Ti:Sa laser.

Geometrically, the typical setup for FWM looks like figure 2.18 where, for simplicity, we have assumed again that all waves are plane, monochromatic waves with a fixed relative phase relation (mutually coherent). It can be seen that there are two index holograms that can be considered for the generation of a phase-conjugate output, $\vec{k_4}$, from the signal input, $\vec{k_1}$, as depicted.

To achieve the gratings shown in figure 2.18 two pump beams are present, which propagate in opposite direction, $\vec{k_2}$ and $\vec{k_3}$. In this case $\vec{k_2}$ and $\vec{k_3}$ are each others phase conjugates: $\vec{k_2^*} = \vec{k_3}$ and $\vec{k_3^*} = \vec{k_2}$, as is expressed in the following equation:

$$\vec{k_1} + \vec{k_2} + \vec{k_3} + \vec{k_4} = 0. \tag{2.13}$$

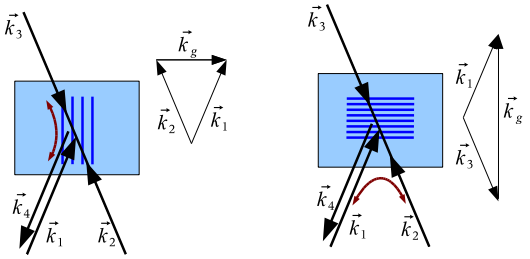

Figure 2.18: *The two possibilities for a four-wave mixing setup. The red arrows indicate which beams are coupled by gain.*

In the configuration depicted and the using the fact $\vec{k_2}$ and $\vec{k_3}$ are each others' phase conjugates, and cancel each other out in the equation, it can be seen, the equation can only be fulfilled with $\vec{k_4}$ the conjugate beam of $\vec{k_1}$, i.e. $\vec{k_4} = \vec{k_1^*}$. This shows that injecting a wave with $\vec{k_1}$, independent of the pump beam wave vectors, the setup always generates a beam which is phase conjugate to$\vec{k_1}$, ($\vec{k_4}$).

The next step is to discuss the two ways to achieve the desired beam $\vec{k_4}$. In the first way, depicted on the left hand side in figure 2.18, $\vec{k_1}$ and $\vec{k_2}$ illuminate the medium and the resulting interference pattern, through the photorefractive effect, is converted to an index grating. This will be briefly referred to as 'writing' a hologram or grating. Then, $\vec{k_3}$ diffracts from the written grating ($\vec{k_3}$ 'reads' the hologram), and this results in a diffracted wave, $\vec{k_4}$. So, the two gratings that possibly generate a phase conjugate beam, $\vec{k_4}$, can be written as:

$$\vec{k_g} = \vec{k_1} - \vec{k_2}$$

or

$$\vec{k_g} = \vec{k_1} - \vec{k_3} \tag{2.14}$$

Because of symmetry considerations, light from the grating will not only diffract from $\vec{k_3}$ to $\vec{k_4}$, but also from the opposite direction $\vec{k_1}$ into the direction of $\vec{k_3}$, as depicted by the double headed curved arrow in the figure. The second case is also shown on the right hand side of figure 2.18.

The orientation of the charge grating with regard to the anisotropy direction of the photorefractive material determines the resulting index contrast,

i.e., which of the two alternative gratings competes favourably in its build-up. For example, when $\vec{k_g}$ points parallel to the direction of the electro-optic coefficient, this provides the highest index contrast, leading to a stronger diffraction from that grating. Similarly, a charge density pattern with a small period shows a lower contrast, as was explained above, due to a higher value of the drift field.

The described competition of gratings is a general property of photorefractive materials, however, for a particular experiment it is sometimes not possible to discover beforehand which of the allowed gratings will dominate and how strong the competition will be. Thus, in the general case, one expects that a grating builds up which is a superposition of the two possible gratings. In most experimental situations, however, only one of the gratings will be present because, simply, one of the gratings is dominating. In this case, the resulting grating superposition can be accurately approximated by only the dominating grating. A way to deliberately let a particular grating dominate is to rotate the the polarisation of the intended read beam is rotated 90°. In the experimental section we will discuss a scenario in which the grating superposition is important and must be treated in detail.

2.5.7 Double phase conjugate mirror

An alternative way to generate a phase-conjugated beam is by using the setup of a double phase conjugated mirror (DPCM). In our experiments, the DPCM setup had, in comparison, offered some advantages over the FWM setup in achieving holographic injection locking, while from a theoretic point of view the FWM setup is easier to understand. Our experiments will show using a DPCM is possible when employing a photorefractive crystal, while this is not possible when employing the photorefractive polymer. Besides recalling the DPCM setup, the differences between a DPCM and a FWM for employment in a holographic injection locking schemes will be discussed.

In figure 2.19 the typical beam configuration to realise a DPCM is depicted. Four wave vectors are involved, two that correspond to the incoming beams, $\vec{k_1}$ and $\vec{k_2}$, and two that correspond to diffracted (outgoing) beams, $\vec{k_3}$ and $\vec{k_4}$. In the context of holographic locking, one of the incoming beams will be the beam from the BAL, and the other will be the beam from the Ti:Sa

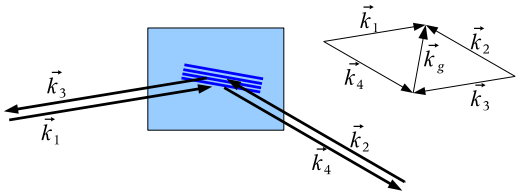

Figure 2.19: *A double phase conjugate mirror setup and the corresponding k-vectors to build the grating.*

laser. The diffracted beams have the exact opposite direction to the incoming beams. In this configuration, the grating vector is found as the difference between k-vectors, however, in this case, the grating vector is determined by the difference between the incoming beam and its correspondingly diffracted beam, again, via the phase matching condition:

$$\vec{k_g} = \vec{k_1} - \vec{k_4} = \vec{k_2} - \vec{k_3}, \tag{2.15}$$

and not as the difference between incoming beams. The DPCM configuration can be selected via a corresponding choice of the direction of the anisotropy of the material as follows. The anisotropy is directed such that the contrast of the grating in equation 2.15 is higher than that of the competing grating formed by $\vec{k_1}$ and k_2. The DPCM shows an important difference with respect to the FWM configuration. This difference is that, in the DPCM configuration, an initial coherence between the incoming beams is is not required because a grating is written between a beam, and its own, diffracted beam, e.g. between the pairs $\vec{k_1}$ and $\vec{k_4}$, or the pair $\vec{k_2}$ and $\vec{k_3}$. Note that each of these pairs originates from the same source and can thus be expected to be mutually coherent. The FWM-setup, on the other hand, does require initial coherence between the incoming beams to start the writing process.

In more detail, in a DPCM, the incoming beam $\vec{k_1}$ is diffracted by the grating vector $\vec{k_g}$ in such a way that $\vec{k_4}$ is the phase conjugated beam of $\vec{k_2}$. This also holds for $\vec{k_2}$, making $\vec{k_3}$ the phase conjugated of $\vec{k_1}$. This double sequence (cascading) of phase conjugation explains the name "double phase conjugated mirror".

The advantage that phase matching is fullfilled for all pairs of $\vec{k_1}$ and $\vec{k_3}$ in a DPCM, independent of the actual choice of $\vec{k_1}$, can also be seen as some technical disadvantage for the proper realisation of a DPCM. Namely, the

described tolerance with regard to the actual choice of $\vec{k_1}$ allows that, besides the desired grating, many other gratings may build up as well. These gratings can occur due to scattering and beam fanning (section 2.5.5), such that beams other than $\vec{k_3}$ and $\vec{k_4}$ emerge [26].

The gratings that fullfill the phase matching condition and are oriented such that they have a significant diffraction efficiency will form (a part of) an ellipse on the plane perpendicular to vector $\vec{k_1}$ (This plane is also perpendicular to the page). In this ellipse the phase conjugated beam, $\vec{k_3}$, is the brightest spot. This desired grating has the best diffraction efficiency and is written with the most light [66–68]. The same is true for the other pair of vectors, $\vec{k_2}$ and $\vec{k_4}$, on the plane perpendicular to $\vec{k_2}$ [69]. Eventually the ellipse disappears due to competition and only the grating corresponding to the phase conjugates of the original beams remains.

Due to the rather complex principle of working of a DCPM, it has long been doubted if a DPCM could be realised at all [70]. This can also be summarised as the following controversy. A grating is built up between the incoming wave vector ($\vec{k_1}$ or $\vec{k_2}$) and its phase conjugated wave ($\vec{k_3}$ for $\vec{k_1}$ and $\vec{k_4}$ for $\vec{k_2}$) but, intially, when only $\vec{k_1}$ and $\vec{k_2}$ are present, there is no phase conjugated wave yet ($\vec{k_3} = \vec{k_1^*}$ or $\vec{k_4} = \vec{k_2^*}$). Thus, the grating would not build up, and therefore, also the wave with $\vec{k_3}$ (and $\vec{k_4}$) would not build up. Nevertheless, a working DPCM setup was first demonstrated by Weiss and Sternklar of the group of Fischer in 1986 and 1987 [71, 72] and almost simultaneously by Eason and Smout [73], thereby proving the experimental possibility of a DPCM while the precise building process is still under debate. The build-up may be contributed to random scattering processes and beam fanning, followed by competition processes as described in the previous paragraph. In summary, the named controversy in the build-up phase and the additional complexity introduced by the required anisotropy of the photorefractive material is probably the reason why a detailed and generally accepted model of the best way to realise a DPCM is still lacking.

For any DPCM there are two parameters that can essentially be chosen freely. These are the angle δ between the beams with $\vec{k_1}$ and $\vec{k_2}$ ($\vec{k_3}$ and $\vec{k_4}$, respectively) and the angle β between the optical axis and the grating vector $\vec{k_g}$, of the grating between $\vec{k_1}$ and $\vec{k_4}$ (or $\vec{k_2}$ and $\vec{k_3}$), as depicted also in figure 2.20. Based on this freedom of choice, there are many different configurations

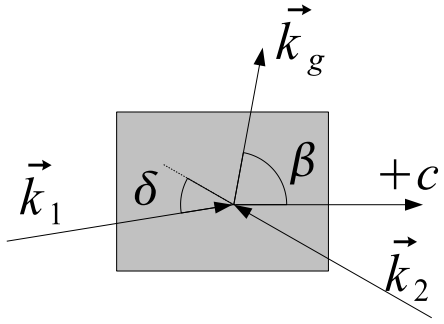

Figure 2.20: *The degrees of freedom in a DPCM.*

possible with the result that almost all experiments involving a DPCM so far have used a different configuration [27,28,67]. The motivation to use a variety of configurations with different values for ϕ and β are manifold. A number of considerations are now explained in more detail, due to their importance for choosing an appropriate configuration that would enable a holographic injection locking via a DPCM.

In some experiments, the goal was to attempt a modelling of the DPCM [67,69,74]. Other work were meant to explore more of the phenomenological aspects of DCPM's, such as: an optimisation of the coupling of light beams into the crystal by using Brewster's-angle, an optimisation of the beam overlap by anticipating the beam-fanning, or the avoiding of parasitically amplified roundtrips in the crystal [75, 76]. In the realisation of DCPM's, beam scattering and resulting beam fanning is generally considered an undesired effect because this removes light from the paths originally intended. On the other hand, beam scattering is sometimes considered to form initial, spontaneous gratings that initiate the desired growth of the grating for forming a DPCM.

Parasitic roundtrips of light in a photorefractive crystal occur because, after a few internal Fresnel reflections in the crystal (minimum 3 for a rectangular crystal), a beam overlaps itself again and a grating in this overlapping region can be formed (see figure 2.21). Depending on the orientation of this grating, two-beam gain coupling can occur. The requirements for parasitic roundtrips are: an angle of incidence that is is sufficiently big to reduce the number of required internal reflections, a coherence length of the light suffi-

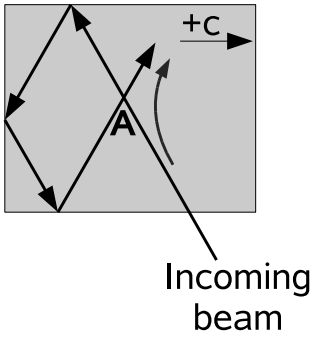

Figure 2.21: *An example of a parasitic roundtrip. Due to crystal-internal Fresnel reflection of an incoming beam, the beam can overlap with itself and a TBG grating is formed at location A. Due to the direction of the c+-axis in this case, light will be coupled away from the original incoming beam and may assist to form the grating for a DCPM.*

ciently long (at least a few times the depth of the crystal, which is typically a few millimetres), to be able to form a temporally stable interference pattern at the overlapping area, and a high refractive index of the crystal for providing a high Fresnel reflectivity at the crystal-air interfaces. A last requirement is a beam with a small divergence angle, i.e. a beam that is not strongly focused into the crystal. When a focused beam is injected which diverges too strongly, the power density in the beam drastically decreases with propagation and this reduces the temporal rate at which gratings can be written. Unfortunately, these requirements are often easily fullfilled in DPCM experiments with typical photorefractive crystals. For example, the refractive index of $BaTiO_3$ is relatively high, 2.4, and the roundtrip length in a crystal is of typical size of a few millimetres. These conditions would easily lead to the build-up of undesired gratings via parasitic roundtrips, which was found also in our initial experiments.

The described phenomena, such as beam fanning and parasitic roundtrips, can possibly be suppressed by choosing the angles δ and β properly. Another perturbing issue can be that, initially, fanning and parasitic roundtrips are absent until a DPCM develops during successful holographic injection locking. The spectral changes of the light waves which arise from such locking can

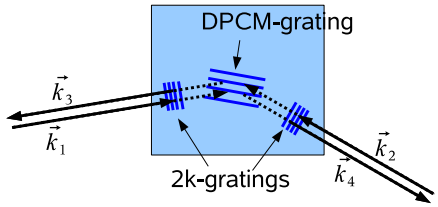

Figure 2.22: *Additional 2k-gratings can occur in a DPCM due to mutual coherence. The dotted lines indicate the reduced amount of light reading and writing the DCPM grating due to diffraction from the emerging 2k-gratings.*

then let the DCPM diffraction efficiency drop again, due fanning and parasitic gratings [77]. To more detail, this reduction of the diffraction efficiency works as follows. When the beam of a BAL and the Ti:Sa are successfully coupled in a DPCM, the BAL will be injection-locked by the Ti:Sa laser and this reduces the spectral linewidth of the BAL reduces to the linewidth of the Ti:Sa laser. While, initially, the two lasers were temporally incoherent with respect to each other (this is allowed because a grating is written between an incoming beam and its own refracted beam which are coherent), a narrow linewidth renders both mutually coherent, e.g. a temporally stable interference pattern can be observed, if the beam coming from the BAL and the beam coming from the Ti:Sa overlap. These interference patterns will arise between $\vec{k_1}$ and $\vec{k_3}$ and between $\vec{k_2}$ and $\vec{k_4}$, on the way to the DPCM grating (see figure 2.22) thereby writing a photorefractive gratings there. These so-called 2k-gratings are problematic because they Bragg-reflect the incoming beams (from the Ti:Sa laser and from the BAL) before they reach the DPCM grating. This undesired effect, which can perturb the proper working of a DPCM configuration, was first explained by De La Cruz et al. [78]

One way to suppress these 2k-gratings was presented by Iida et al. [79] and involves two in piezo-driven mirrors by which the ingoing beams are sent into the crystal. When the position of these mirrors was synchronously and periodically displaced with regard to the crystal, this was observed to remove the undesired 2k-gratings. The same approach has been adopted by us in order to realise the first stable, holographic mutual coherent injection locking of a BAL. It showed that the removal of 2k-gratings lead to a much

improved long-term stability of the locking via feedback from the DCPM (see section 3.2).

Despite these complicating factors, there are good reasons to use a DPCM setup instead of a FWM setup in a holographic injection locking experiment. Firstly, complications with beam fanning and parasitic roundtrips also emerge in other setups, including that based on FWM. A second reason favouring a DPCM over a FWM has been mentioned before, namely that a FWM requires initial temporal coherence between the incoming beams. The approach with a DPCM does not depend on such a requirement because, here, the incoming beams may be be mutually incoherent. Finally, an advantage of a DPCM over a FWM setup is the somewhat easier alignment. This is the case because only two, instead of three incoming beams are involved, and these two beams do not have to propagate in the opposite direction, as is required for the two pump beams in a FWM setup. As a conclusion from this comparison, we decided to generally work with the DCPM approach first. Only when we found this not to be successful, due to specific experimental boundary conditions, we decided to use a FWM setup, instead.

2.6 Summary

In this chapter we have recalled the optical properties of diode lasers, the properties of injection locking of diode lasers, phase conjugation and the photorefractive effect as required for a basic understanding of the experiments that we performed, as will be described in the chapters 3 and 4. Emphasis was put on essential differences between single spatial mode diode lasers and broad area diodes lasers (BAL's) in terms of their maximum achievable output power and their spectral and spatial beam quality. It was discussed how injection locking can change the spectral and spatial properties of, particularly, such BAL's.

We reviewed the basic physics of phase conjugation as the perfect mirror, by which a beam always travels back to its origin. This concept allows for an exact correction of arbitrary distortions in the wavefront of a beam.

We recalled the differences between photorefraction in inorganic crystals and organic polymers, by comparing the maximum modulation depth, the response time, and by comparing the phase angle between the illuminating

interference pattern and the resulting hologram. Further issues of practical importance were compared, such as the robustness of the material, the refractive index of the materials and its implications, memory effects and the limited degree of freedom concerning an appropriate shaping of the photorefractive material.

Finally, three basic setups, were presented. The first is two-beam gain (TBG) coupling of two incident beams as this is a important basic setup for understanding the spatial power flow imposed by the photorefractive effect and the origin of a number of parasitic effects. For the two next setups, four-wave mixing (FWM) and a double phase conjugate mirror (DPCM), their advantages and disadvantages with respect to using them as a configuration for holographic injection locking were discussed.

Chapter 3

Holographic locking via a photorefractive crystal

Abstract

This chapter presents our experiments on holographically locking a broad area laser diode (BAL) to a single-frequency TEM_{00} beam. The experiments were performed using a $BaTiO_3$ crystal in a double phase conjugate mirror (DPCM) configuration. The results show that locking was successful. We achieved and maintained single-frequency operation of the BAL in a regime in which the BAL and the single-frequency laser assume a mutual coherence. Furthermore, the DPCM also allows for a spatial conversion of the locked complex BAL mode pattern into a high-quality beam which resembles that of the injected TEM_{00} beam.

In our first experiment we used a cobalt-doped $BaTiO_3$ crystal in a double phase conjugated mirror (DPCM) configuration. First some practical issues involved in using a DPCM in a locking experiment will be discussed, including the configuration of beams with respect to the crystal and a practical solution to avoid parasitic 2k-gratings. Second, a number of setups, will be explained and the results evaluated.

Although other configurations are possible, we choose for a DPCM because it requires only a very weak initial coherence between the primary and

secondary laser. Furthermore like all holographic locking setups, a DPCM solves the spatial issues involved in injection locking a BAL. In our experiments we used a single-frequency Ti:Sapphire-laser, referred to as Ti:Sa-laser, as the primary laser. When the beams of the Ti:Sa and BAL are overlapped in the photorefractive crystal a hologram will be written. This hologram outlives many competing holograms because it diffracts the light from the BAL to the Ti:Sa and vice versa on *the same* grating. The light that is diffracted from the Ti:Sa to the BAL will injection lock the spectrum of the BAL while the spatial output of the BAL adjusts the grating until a stable pattern is achieved.

The use of DPCMs, or similar configurations, for injection locking of BALs has been reported before [26–34]. However, those setups could not provide stable coherent locking; the build-up of 2k-gratings once the two laser sources became mutually coherent (see section 2.5.7) reduced the light flow to and from the DPCM grating such that, locking could not be maintained. Therefore, mutual temporal coherence was avoided by using a primary laser with a short coherence length (in the order of centimetres to tens of centimetres), and maintaining the locking in the mutual *incoherent* regime (section 2.1.2).

The spatial properties of the DPCM can be exploited beyond the spectral locking because it diffracts the spatial output pattern of the BAL into the spatial pattern of the Ti:Sa. Since the latter emits a Gaussian TEM_{00}, this offers the possibility to injection-lock the high-power BAL to a single-frequency and to also convert this beam to a spatial TEM_{00}.

From an applications point of view, one would like to inject a small amount of light to lock a BAL at a very high output. However, the contrast in the hologram, and the diffraction efficiency are highest when the two beams carry equal power. Thus, when the amount of light spectrally locked is maximum, the conversion efficiency to convert this beam is reduced. This trade-off limits the amount of light one can lock and is a fundamental limitation of the setup.

As explained in paragraph 2.5.7 on page 47, the lack of a detailed model of a DPCM troubles the initial choice for a configuration. Our choice is depicted in figure 3.1 and appears similar to the setup used by Iida et al. [29,79] and of Ross and Eason [80]. An important difference is the fact that we use a 45^o-cut crystal, where the optical axis makes an angle of 45^o with the crystal faces (perpendicular to the plane of the paper), instead of the 0^o-cut crystal

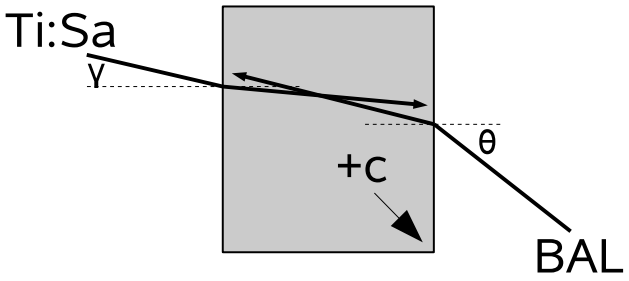

Figure 3.1: *The internal and external angles of the Ti:Sa laser and the BAL with respect to the crystal.*

used by Iida et al. The angles γ and θ are optimised for a low response time and minimal parasitic effects. Due to the orientation of the c-axis (figure 3.1), beam fanning of the Ti:Sa beam will occur in such a way, that the Ti:Sa beam is fanned into the direction of the beam from the BAL. This helps to establish the DPCM hologram desired to achieve injection locking. Figure 3.2 explains why the Ti:Sa beam is chosen close to the normal to avoid parasitic oscillations that rely on internal reflections and parasitic (TBG) gratings.

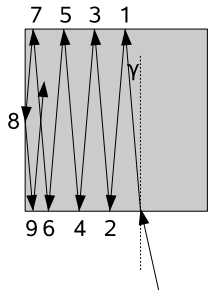

Figure 3.2: *Incoupling of the Ti:Sa beam close to the normal and not too close to a crystal edge. This introduces many internal reflections and thus high loss before the beam can cross itself.*

A BAL emits a complex multi-mode pattern along the slow axis and a much simpler single mode pattern along the fast axis. For different orientations of the BAL, the required DPCM hologram differs in its orientation with respect to the c-axis. Since the diffraction efficiency is a function of the angle with the respect to the c-axis, different orientations could show different behaviour. We investigated two orientations: with the fast axis aligned to the

plane of incidence and with the slow axis aligned to the plane of incidence. We paid particular attention to differences in locking stability.

Reproducibility in experiments is crucial and, unfortunately, $BaTiO_3$ is famous for a long memory so that residual holograms in the crystal cannot be fully suppressed which decreases the reproducibility of the experiments. The best reproducibility was observed between experiments that were done as the first experiment of the day so that the electrons had a full night to diffuse through the crystal back into their initial homogeneous distribution. To perform several experiments a day, a bright white light source (halogen spot of 50 W) or a green laser (532 nm, 100 mW) was used to erase holograms and provide the electrons in the crystal with extra energy to speed up the diffusion process. Despite these measures, measurements showed memory effects. Therefore, only first-of-the-day experiments are presented in this chapter.

We start with a single BAL as the secondary laser. In later experiments we replaced a single BAL with an array of BALs, of, in our case, 19 emitters. This was done to increase the achievable output power of the secondary laser. The output beam of a BAL-array is naturally even more complex than the output of a single BAL. Three series of experiments of increasingly stable locking will be discussed.

3.1 First locking of a BAL to a Titanium:Sapphire

The initial experiments explored the basic possibility of realising injection locking via a DPCM. Given the narrow linewidth of the Ti:Sa-laser (< 10 MHz) and the resulting long coherence length ($> 30\ m$) the Ti:Sa and the BAL are expected to lock in a mutually coherent way. Instabilities due to 2k gratings, once locking is achieved, are also expected (section 2.5.7). Since the Ti:Sa and the BAL are initially mutually incoherent and the time required to form holograms in the photorefractive material is in the order of minutes, we expect to initiate and observe locking. Furthermore, the formation of 2k-gratings, and the effects on the locking should also occur on an observable time scale.

Figure 3.3 depicts the setup. The beams from Ti:Sa and BAL overlap in the $BaTiO_3$-crystal (45^o-cut, width=6mm, depth=4mm, height=5mm). The respective angles at which the beams enter the crystal are $\gamma = 13^o \pm 2^o$ and

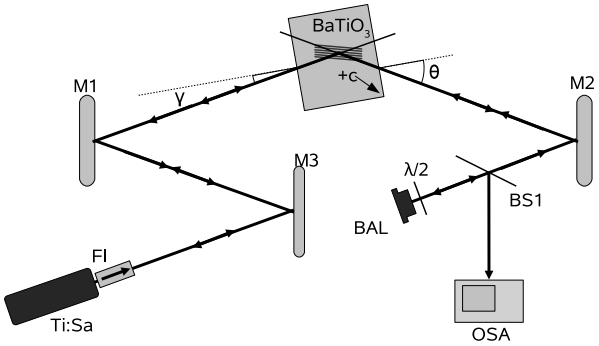

Figure 3.3: *Schematic of the setup. M1,M2,M3=high reflective mirrors, $BaTiO_3$=$BaTiO_3$-crystal, BS1=beamsplitter, Ti:Sa=Ti:Sapphire-laser, FI=Faraday isolator, BAL=broad area laser, $\lambda/2$=half wave plate, OSA=optical spectrum analyser,γ=angle between the Ti:Sa-beam and crystal face normal, θ=angle between BAL-beam and crystal face normal, +c=the direction of the positive optical axis.*

$\theta = 38^{o} \pm 2^{o}$. The beams are both focused into the crystal to a diameter of 3 mm inside the crystal. The BAL is oriented with the fast axis in the horizontal plane of the experiment and the polarisation of the BAL in the horizontal plane. The beamsplitter (BS1) reflects a few percent of the light emitted by the BAL to an optical spectrum analyser (OSA). The polarisation of the Ti:Sa is oriented in the horizontal plane as well. The wavelength of the Ti:Sa is set to be within the spectrum of the free-running BAL, i.e. the emission spectrum when no feedback is present for the BAL. The optical output power of the BAL is set to 180mW by adjusting the pump current. This is relatively close to the lasing threshold (80mW) which ensures that the BAL is susceptible to feedback avoids damage

Before an experiment both lasers are switched on and left to stabilise, without interaction via the DPCM for at least an hour. Once the lasers are stable, the beams path to the DPCM is opened and the spectrum of the BAL is monitored on the OSA. It takes between 5 and 12 minutes before a spectral response of the BAL is observed. From the response, snapshots are recorded and presented.

A selection of spectra can be seen in figure 3.4. Figure 3.4(a) shows the free running spectrum (spectrum without feedback). Figure 3.4(b) is recorded while the DPCM-grating is forming and the diffraction from the

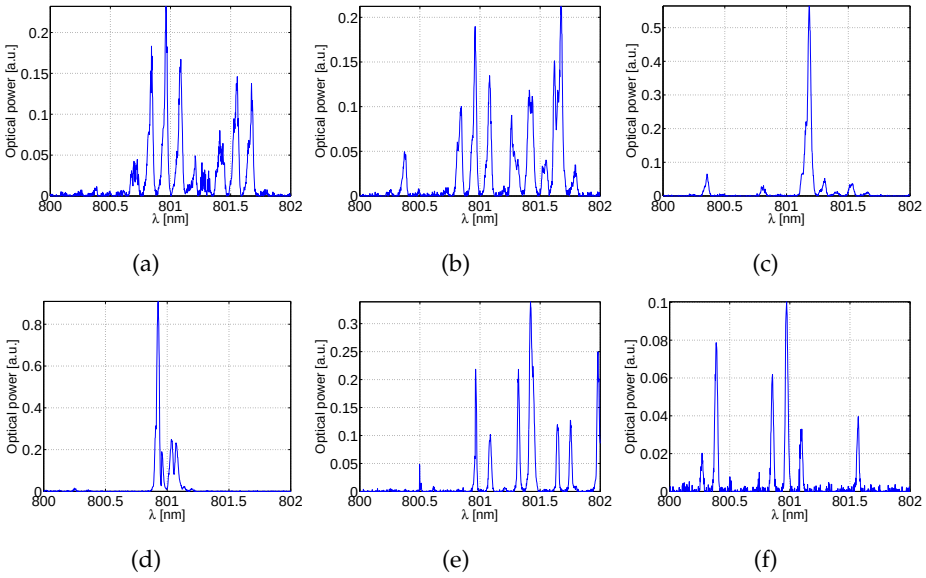

Figure 3.4: *First locking results.*

$BaTiO_3$ is insufficient to lock the BAL. These spectra are typically unstable, indicating that light from the Ti:Sa laser is fed into the BAL. Figure 3.4(c) and 3.4(d) show increased emission of a single wavelength (at the same wavelength as emitted from the Ti:Sa laser) after about 5-12 minutes, showing injection locking is indeed achieved. After locking is maintained for 1 to 5 minutes, as expected, a loss of the locking is observed (3.4(e) and 3.4(f)). We attribute this loss to the formation of parasitic 2k-gratings which degrade the DPCM grating. The complete cycle depicted here takes about 7-15 minutes: The initial locking from 3.4(a) to 3.4(c) is achieved within 5-12 minutes and the locking remains stable for 1-5 minutes (3.4(c) and 3.4(d)) before it degrades again (3.4(e) and 3.4(f)). After the initial locking the behaviour of the BAL was random and we did not observe subsequent cycles of locking.

The observed time intervals show that the time the 2k-gratings require to build up is much shorter than the build up of the initial DPCM-gratings. This is expected as the DPCM grating builds from random scattering and beam fanning processes (section 2.5.7), while the 2k-gratings are driven by the interference of two mutually coherent, single frequency beams at relatively high intensity.

3.2 Locking using piezo mirrors

To increase the duration of the locked interval, the 2k-gratings have to be suppressed. In literature, two methods are reported: A first possibility is, to increase the distance between the BAL and Ti:Sa laser. If this distance is longer than the coherence length of the Ti:Sa laser, the mutual coherence of the waves that create the 2k-gratings disappears. However, at an estimated coherence length >30 m (derived from the lasers <10 MHz spectral linewidth), this is not practical. A more compact and elegant solution, which we implemented, was demonstrated by Iida et al. [79]. In that experiment two, piezo mirrors, used to direct the beams into the crystal, were periodically moved in synchronism, in order to perturb the build-up of only the undesired gratings.

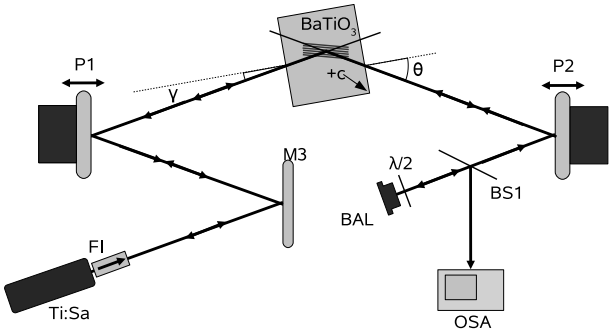

Figure 3.5: *The setup with piezo mirrors. P1,P2=piezo mirrors. M3=mirrors, $BaTiO_3$=$BaTiO_3$-crystal, BS1=beamsampler, Ti:Sa=Ti:Sapphire-laser, FI=Faraday isolator, BAL=broad area laser, $\lambda/2$=half wave plate, OSA=optical spectrum analyser,γ=angle between the Ti:Sa-beam and crystal face, θ=angle between BAL-beam and crystal face, +c=the direction of the positive optical axis.*

Figure 3.5 shows the setup with two piezo-mirrors (P1,P2). The mirrors are driven with an sinusoidal voltage (on top of a DC offset) in counterphase, so that in figure 3.5 the mirrors move synchronously to the left and right. The frequency of the mirror motion was set to 100Hz, much faster than the response time of the crystal, which is in the order of minutes. The amplitude of the vibration was chosen to be equal to an integer multiple of half the wavelength of the light. The effect of the mirror movement is that the po-

sitions of all standing wave patterns caused by *counterpropagating* waves are repeatedly swept through the crystal faster than its response time, so that the standing wave pattern does not cause the build-up of an index grating. The DPCM-grating is a transmission grating based on *co-propagating* waves and is not disturbed by the moving mirrors, as the relative phase between these beams is conserved.

Apart from the insertion of the piezo-mirrors, all parameters were kept the same.

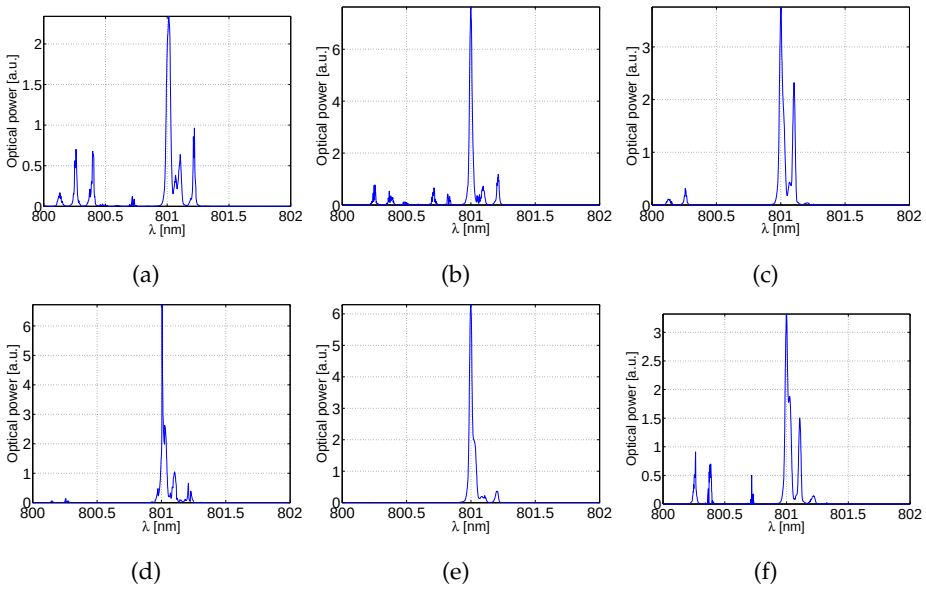

Figure 3.6: *Locking spectra with piezo mirrors*

The results are shown in figure 3.6. The spectra shown are taken after the initial start up time of 5-12 minutes. When compared to a free-running spectrum (figure 3.4(a)), the spectrum is significantly narrowed in all the figures. In some spectra, e.g. 3.6(b) , 3.6(d) and 3.6(e) , the energy at other frequencies seems completely suppressed, while in other spectra (3.6(a) , 3.6(c) and 3.6(f) more frequencies are present. The intensity in these unlocked frequencies is continuously changing, and every scan made by the OSA, which takes between 1 and 2 seconds is different. The complete time interval during which these measurements are taken is about 10 minutes, but the behaviour shown is continuous for at least an hour, after which the longest measurement is terminated.

Stable locking is not yet achieved, but, in contrast to the previous measurements, the fact that the spectra are narrow compared to the BAL free-running spectrum during the complete measurement indicates that the BAL sees feedback from the Ti:Sa laser all the time. This is in contrast with the first measurement series in which the BAL signal degraded after 1-5 minutes. The lack of correlation between two consecutive measurements indicates that the causes for the unstable behaviour are faster than the second-scale. These facts combined suggest that the piezo-mirrors are suppressing the 2k-gratings, but that the feedback is such that the BAL operates in an unstable injection locking regime.

3.3 Locking outside the spectrum

In the previous series of experiments the BAL appears locked in a chaotic regime rather than a stable regime [21, 22, 39–41] (section 2.1.2). Typically, operation in a chaotic regime indicates the feedback from the Ti:Sa laser to the BAL is too strong for stable operation. It seems straightforward to reduce the power of the Ti:Sa beam. However, here, the feedback is also determined by the diffraction efficiency of the hologram in the crystal which, in turn, depends on the locking of the BAL via that hologram. The effect of the feedback can also be reduced without affecting the diffraction efficiency, by shifting the feedback to a wavelength at which the gain is smaller; to spectrally detune the Ti:Sa laser with respect to the the free running spectrum of the BAL. Locking outside the free-running spectrum was demonstrated for standard single-mode diode lasers [26] and for BALs, although that was in a more complicated setup for holographic locking, involving two photorefractive crystals [33].

The locking for our system was investigated at several wavelengths for the Ti:Sa laser both on the long(red) side as and the short(blue) side of the spectrum. From these experiments we found that the most stable lock for the the BAL could be achieved at a wavelength of about 1 nm on the red side of the free running BAL spectrum. This is a wavelength close to the maximum offset at the red side at which locking could be achieved at all. Attempts to lock on the blue side proved to be hard and hardly show improvements in the stability of the spectrum.

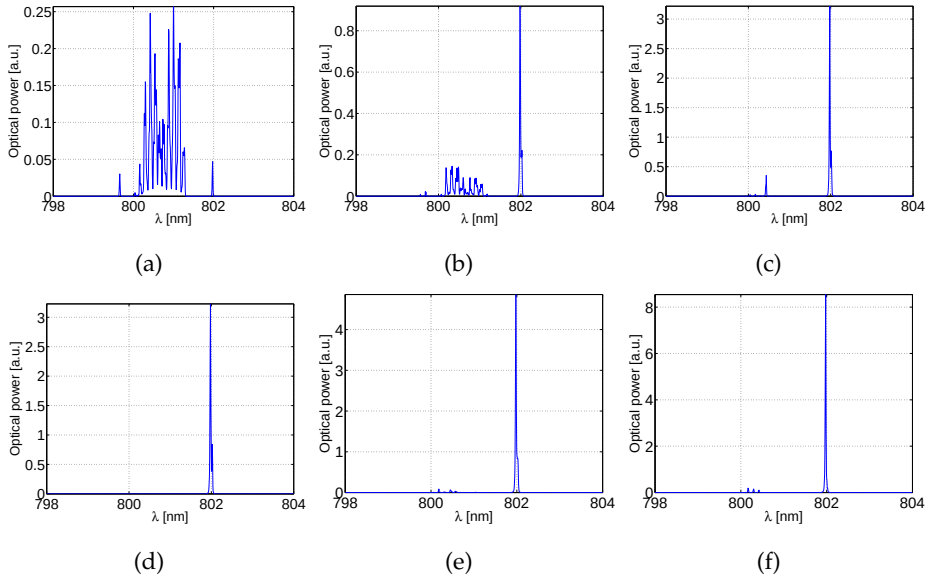

Figure 3.7: *Locking outside the spectrum*

In figure 3.7 typical spectra are shown for an injection wavelength 1 nm to the long-wavelength side of the free running BAL spectrum. In figure 3.7(a) , next to the broad irregular free running spectrum of the BAL, the single wavelength of the Ti:Sa can be seen on the right side. The coupling efficiencies into the optical spectrum analyser are different. In the figures 3.7(b) through 3.7(f) the spectrum of the BAL narrows to the linewidth of the Ti:Sa laser at the wavelength of the Ti:Sa laser and only small residual part of the original BAL spectrum remains unaffected. The linewidth of the locked BAL is below the resolution of the OSA (0.01 nm). We found the output power of the BAL to be the same before and after locking. The spectra shows stable locking in time and locking could be maintained for more than 30 minutes on average in a mutually coherent regime and the reflection efficiency of the DPCM is between 1-5 % during this interval.

In conclusion we demonstrated that it is possible to injection-lock a BAL to a single-frequency and maintain locking in a mutual coherent regime. With piezo-mirrors the 2k-gratings could be suppressed to avoid the loss of locking after 1-5 minutes as in figure 3.4. By detuning the Ti:Sa laser about 1 nm to the red side of the spectrum unstable locking behaviour as observed in figure 3.6 could be avoided. The wavelength of the Ti:Sa laser was scanned and locking

was to be found most stable at 1 nm to the red side, the maximum detuning within the locking range. Achieving locking on the blue side did not improve the stability for which we are unable to supply a reasons. In the experiment of Shimura [26], where a DPCM is used to lock to single-mode diodes, it is reported that locking outside the spectrum only works if light is injected at a wavelength fitting the cavity of the diode (e.g. an integer number multiplied by the FSR away from the (single-mode) free-running spectrum of the diode), but in our experiment, using the BAL and the Ti:Sa laser instead of the single-mode diodes, such a relation is not found.

A possible explanation for the loss of locking at large time intervals $>$30 minutes could be the particular type of motion of the piezo mirrors. We chose a simple sinusoidal motion, however, this means that the speed of the mirror during a vibration period is not constant. Especially near the two turning points of this motion the speed of the mirrors is close to zero such that, during these short time intervals, the interference pattern stands almost still as well, such that 2k-gratings might build up slowly. If this is what has limited our locking towards the long time scales ($>$30 minutes), then an improvement should, in principle be achievable by using a differently shaped drive function for the piezo-mirrors, e.g. a triangular (instead of a sinusoidal) shape. However, a problem in realising this is the finite response time of piezo-driven mirrors.

Once stable injection locking was achieved, other parameters in the experiment were investigated. All experiments presented so far were conducted while the fast axis of the BAL was oriented in the plane of the experiment. We repeated the experiments with the slow axis in the plane of the experiment to see whether this orientation influenced the results. We found that locking can be achieved along both axes, however locking is more stable with the fast axis in the plane of the experiment.

3.4 Spatial conversion

As discussed in chapter2, a spatial improvement of the output beam of the BAL is desirable as well as the spectral improvement. We use a holographic setup because in this way the spatial pattern of the Ti:Sa laser beam is diffracted into the spatial pattern of the BAL before it is injected into the BAL. When

locked, the BAL oscillates in a particular superposition of high-order transverse modes on the slow axis. As the photorefractive grating in the crystal is self-adjusting to any spatial phase front emitted by the BAL, it can be assumed that this way the grating adjusts to optimum feedback that spatially matches the BALs most efficient superposition of high-order modes. With a stable spectrum emitted by the BAL, we expect also a stable (but complex) spatial output pattern. When this pattern is diffracted by the hologram it is converted to the high quality spatial pattern of the Ti:Sa laser.

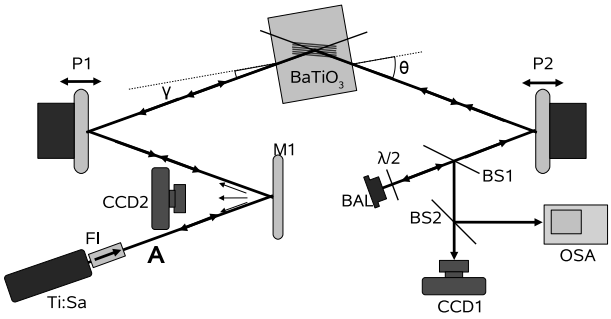

Figure 3.8: *The setup with piezo mirrors. P1,P2=piezo-mirrors, M3=mirror $BaTiO_3$=$BaTiO_3$-crystal, BS1,BS2=beamsampler, Ti:Sa=Ti:Sapphire-laser, FI=Faraday isolator, BAL=broad area laser, $\lambda/2$=half wave plate, OSA=optical spectrum analyser,γ=angle between the Ti:Sa-beam and crystal face, θ=angle between BAL-beam and crystal face, CCD1,CCD2=CCD-camera, A=point the Ti:Sa beam is shortly blocked to demonstrate spatial conversion.*

To measure the far field of the (unconverted) BAL, the setup is modified (figure 3.8) and beamsplitter BS2 and CCD camera CCD1 are introduced to measure the far field pattern emitted by the BAL.

In figure 3.9 two images captured on CCD1 are shown. The pattern on the left hand side is recorded while the BAL is injection locked. The slow axis is oriented horizontally, so only the vertical fringes relate to a multi-mode distribution along that axis. Fringes along the diagonal are an artifact from the optical components in the beam. The mode of the locked BAL is observed as a complex but temporally stable far field pattern, see figure 3.9(left). On the right hand side, the far field of the BAL is measured without feedback and the BAL shows a far field pattern with a continuous distribution of intensity

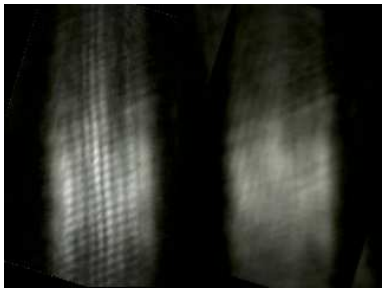

Figure 3.9: *Locked and free running far field pattern BAL compared. The slow axis is oriented horizontally.*

over the width of the beam as expected from a BAL that emits spectrally broadband multi-mode light.

With the stability of the spatial pattern of the BAL confirmed we can verify that the hologram that diffracts the light of the single spatial mode of the Ti:Sa into the complex mode of the BAL should also function in reverse: converting the mode of the BAL into the TEM_{00} mode of the Ti:Sa. The spatial shape of the light from the BAL after diffraction is recorded on CCD camera CCD2 (see figure 3.8). We use this camera to image the weak diffuse reflection of the diffracted beam on mirror M1, 1s after the Ti:Sa laser beam is blocked at the point denoted by '**A**'. After blocking the Ti:Sa beam, the hologram is no longer supported and will degrade, where the rate of degradation is dependent on the response time of the $BaTiO_3$-crystal. Since this response time is in the order of at least 10s of seconds we can safely do this and assume the degradation of the hologram in the crystal is negligible.

Figure 3.10: *The light of the BAL converted in the Gaussian TEM_{00} mode of the Ti:Sa*

The image of the diffracted light from the BAL beam is shown in figure 3.10. It can be seen that the beam is round and contains a single spatial

mode, closely resembling the TEM_{00} beam of the Ti:Sa laser. The size and position on the mirror are the same as the Ti:Sa laser beam. This shows that, with our experimental setup, it is possible to diffract the spatially complex beam of the locked BAL into a (near) diffraction limited good quality TEM_{00} beam.

3.5 Attempts to lock diode array

Given the success of locking a single broad area diode laser an attempted was made to lock a diode laser device of higher power specifications; an array consisting 19 elements, each element a BAL in itself. The beam of the array is even more complex than that of the single BAL. This increased complexity must be matched by the hologram required to achieve phase conjugation for all the BALs.

Two cylindrical lenses were used for the collimation of the output of the array along the slow and the fast axis (compared to a single aspherical lens used for the single BAL). Due to the strong divergence along the fast axis the first lens was only 12.5 mm away from the front of the diode array. Despite the anti-reflection coating of the lens, we observed light reflecting back into the direction of the array, spreading light from one element to the others. Tilting the first lens reduced the effect, but could not eliminate it. Locking requires that each element in the diode array, receives a much stronger injection from the Ti:Sa laser than from other elements. With additional feedback from back reflection, the threshold for locking increases. We did not achieve injection locking of the array to the single-frequency of the Ti:Sa. We expect that the self-injection from the reflection dominated and the feedback from the DPCM was not strong enough to lock the array.

3.6 Conclusions

In summary, we have shown the first coherent locking of a single broad area diode to the single frequency of a primary laser with a double phase conjugate mirror in the mutually coherent regime. Vibrating piezo-mirrors suppressed parasitic gratings. The highest long-term stability in locked operation is achieved with the Ti:Sa detuned about 1 nm to the red side of the free

running BAL spectrum, resulting in uninterrupted locking for longer than 30 minutes. The BAL could be locked with either the fast axis or the slow axis in the plane of the experiment, but the stability is slightly better on the fast axis. The measured diffraction efficiency was 1-5%.

In addition to these significant spectral improvements we realised a significant improvement of the spatial quality of the BAL. We observe that the diode is locked into its spatially self-preferred and thus most efficient superposition of higher order modes. This complex mode superposition, however, is accompanied by a complementary hologram. Complementary in the sense that the diffraction of the BAL's complex spatial mode superposition off that hologram yields a beam of high spatial quality. This diffraction was also observed for the first time. Diffraction of the BAL's complex mode superposition generated a TEM_{00}-like beam of high spatial quality, even when the Ti:Sa beam was blocked.

Chapter 4

Holographic locking via a photorefractive polymer

Abstract

In this chapter, experiments that use a photorefractive polymer in a thin-film device to achieve injection lockingare described. For such locking, photorefractive polymers offer a number of advantages over inorganic crystals. The most important ones are the improved and more controlled (nonlinear) properties of the material, allowing tailoring of a material for the experiment to increase the sensitivity of the material to light with a wavelength of 800 nm. Furthermore, due to their relative robustness, photorefractive polymers may also be applied outside a controlled environment. We demonstrate the first holographic injection locking of a laser via a photorefractive polymer.

In 1991, Ducharme et al. [57] demonstrated the first photorefractive polymers. Since then the field has advanced and new materials are being developed at a high rate [81–84]. This development of materials aims at applications like holographic data storage [50, 51], optical self-trapping of light [52], and (medical) imaging [53–56], but such polymers have never been investigated for injection locking of lasers. In this chapter, we collaborated with S. Tay and J. Thomas from the group of N. Peyghambarian from the College of

Optical Sciences from the University of Arizona to develop a photorefractive polymer suited for holographic injection locking of BALs.

4.1 Preparational experiments

The properties required for a photorefractive polymer to achieve holographic injection locking are different from the properties photorefractive polymers have for imaging or telecom-oriented applications, which are the kind of applications the group in Arizona has experience with. For these applications a short (order milliseconds or shorter) response time is most crucial, and often polymers will be optimised for response time at the cost of other properties. Instead of a low response time, we required a low absorption and a phase-shift of the photorefractive effect to provide two-beam gain (see section 2.5). The low absorption is needed because injection locking involves higher powers and high absorption might then destroy the photorefractive polymer. A phase-shift of 90^o would provide an optimum two-beam gain (TBG) (see section 2.5.3). In a liquid polymer, the holes are much more mobile than the electrons, but the electrons are still mobile, so the phase-shift is generally smaller than 90^o.

To improve a photorefractive polymer for a low absorption and a strong phase-shift, we can afford to increase the response time several orders of magnitude (from ms to seconds) and still be much faster than photorefractive crystals. A relationship between the response time and the phase shift and absorption exists via the ratio of deep and shallow charge traps (see section 2.5.4). The group in Arizona with whom we collaborated normally reduces response time by inducing as many shallow traps in the material as possible because charges are more easily excited from a shallow trap, while avoiding the deep traps. But charges can escape from a shallow trap due to thermal excitations, which means a charge trapped in a dark fringe can still migrate to the light fringes again, where it is likely to absorb at least one photon again before it diffuses back to a dark fringe. If many charges migrate back from the dark fringes into the light fringes per unit of time, the absorption increases. Also, charges trapped in shallow traps can support only a smaller value of the internal space-charge field generated by the photorefractive effect, and with this, the expected phase-shift is smaller than in a polymer

where deep traps dominate.

Several batches of samples were fabricated by the group in Arizona and tested by us before a composition was found that promised to work in an injection locking experiment. The samples were prepared for use in a photorefractive experiment. The liquid, a (usually red) polymer was sandwiched between two transparent ITO electrodes of about 2.5x2.5 cm^2 in a layer of 105 μm thickness. The polymer formed a round spot of about 1 to 1.5 cm in radius. We will refer to a thin film device (TFD) for a photorefractive polymer prepared in this way.

Besides identifying a suitable photorefractive polymer, several configurations also needed to be investigated, for two purposes, for a TBG-measurement and for a holographic locking setup. Because of the advantages of a DPCM over a FWM setup, once a potential successfull polymer is identified, we will first investigate possibilities for a DPCM configuration.

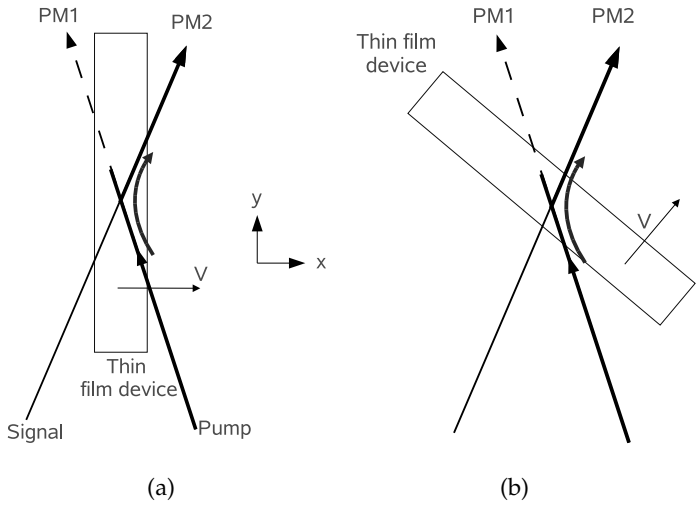

Figure 4.1: *Two configurations for a two-beam gain experiment. The curved arrow shows the direction of the gain. The positions PM1 an PM2 denote the postions a power meter is placed.*

When a TBG experiment is to be performed with the described TFDs, two orientations can be used, as is shown in figure 4.1. In figure 4.1(a) , the field, denoted by V, is oriented in the x-direction for maximum coupling and the beams enter the TFD from different sides. In figure 4.1(b) the TFD is rotated

by 45° to allow both beams to enter the sample from the same side. Both setups were investigated for the amount of achievable two-beam gain and the temporal stability of the TBG coupling between the beams. For the initial TBG experiments, only the Ti:Sa laser is used as a source and the beam is split to provide a pump beam (P=30 mW) and signal beam (P=3 mW). Both beams overlap on the TFD to a spot with a diameter of 0.5 cm. At PM1 or PM2 a power meter is positioned to measure the change in power due to TBG in the pump beam and in the signal beam. A voltage of 5 kV is applied over the TFD, in such a way the field is pointing in the direction indicated by 'V' in the figure.

Two different experiments are conducted with the TBG setups. Besides measuring the TBG, first the signal beam is blocked and the absorption of the light from the pump beam is measured, by positioning the optical powermeter (Ophir) at PM1 and comparing the transmitted optical power to the optical power before the sample. In successive batches the transmission went up from below 50%±2% to 70%±2%. Applying the external field increases the absorption because the now available free charges absorb light. The difference in transmission is within the tolerance of 2%.

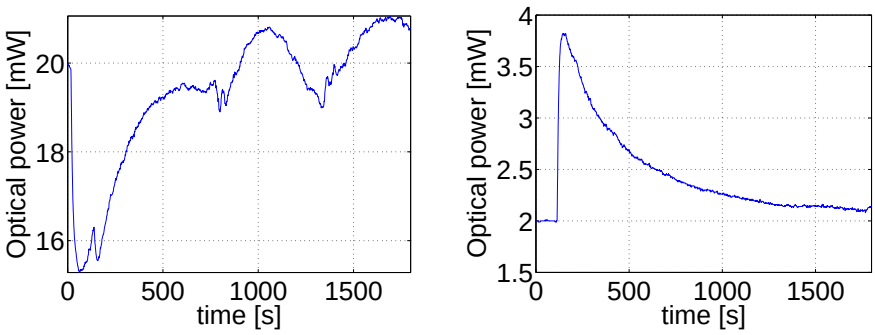

(a) (b)

Figure 4.2: *The dynamics of the pump beam(a) and the signal beam(b) in the unstable setup.*

In the second experiment the signal beam is introduced and the TBG is measured. This is done by measuring the evolution of the optical power of the pump beam at position PM1 as well as the evolution of the power of the signal beam at position PM2. Both powers are measured in consecutive

measurements. Initially, the voltage is switched off while the power meter records the power of pump or signal beam, in order to obtain a reference signal, which is required for determining the amount of gain due to TBG.

For configuration 4.1(a) , figure 4.2 shows the measured evolution of the pump(4.2(a)) and signal(4.2(b)) beam power over time during half an hour (1800 seconds), with the time on the x-axis and the measured optical power on the y-axis. When the voltage is applied shortly after starting the experiment, it can be seen that the power in the pump beam drops sharply and of the signal beam rises, thereby proving (two-beam) gain for the signal beam. After the pump has reached a minimum it slowly starts to rise again and in half an hour, it even overshoots the original level with 1 mW. Disturbances of the experiment at 800 and 1300 seconds show irregularities, but the overall trend of the rising signal is not disturbed. The reason for the (small) overshoot is not clear, either the optical power by the laser was not constant or the absorption of the TFD also has a (small) exposure-time dependent part. The optical power evolution at the signal beam is also shown to be unstable: it grows rapidly to a maximum, but starts to descent again until it has its (almost) original level again. We have no explanation for the unstable behaviour of the TBG. According to our Arizona collaborators it is highly unlikely that this instability is due to the chemical composition of the photorefractive polymer [62–64]. To gain more insight we tried a configuration more conventionally used for TBG experiments with TFD. Figure 4.1(b) shows such an arrangement where the grating vector is tilted with respect to the external field.

In figure 4.3 we show the same pump and signal measurements for the tilted arrangement. The measurements were again taken over half an hour and the measurement procedure is the same as the previous measurements. Now, after the voltage is applied, the pump-beam power drops and remains low except for two short disturbances. We attribute the disturbances in the pump-beam (at 900 and 1500 seconds) to mechanical vibrations of the table. The signal beam shows a continuous increase and is still rising after half an hour. This setup therefore seems a more reliable option to determine a value for the two-beam gain. The peak value for both configurations is close to 2.

Following the approach of our work on the photorefractive crystals, we investigated the possibility of injection locking a BAL using a DCPM-configuration.

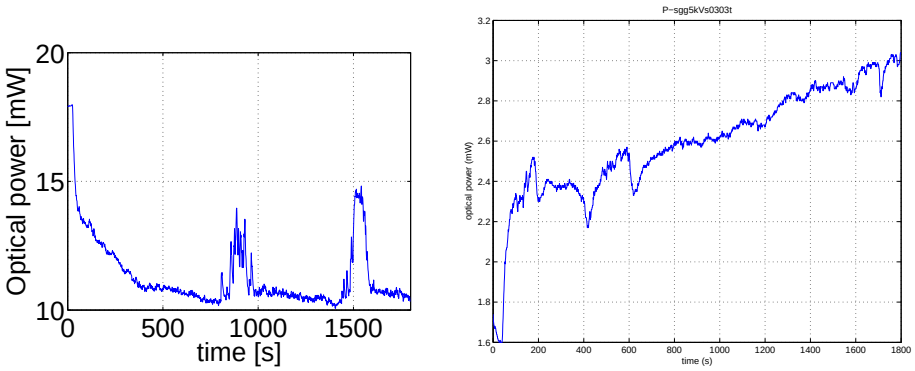

(a) (b)

Figure 4.3: *The stable setup with the pump beam(a) and the signal beam(b)*

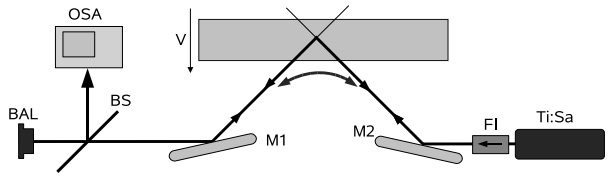

Figure 4.4: *DPCM setup using a TFD. BAL=Broad Area Laser Diode, Ti:Sa=Ti:Sapphire laser, FI=Faraday Isolator, (M1,M2)=Mirrors, OSA=Optical Spectrum analyser, BS=Beamsplitter. V denotes the direction of the electrical field.*

In figure 4.4 this setup is shown. Both lasers enter the TFD from the same side. The angle between the beams $\approx 90^o$ and between a beam and the sample $\approx 45^o$. Both the BAL and the Ti:Sa emit 100 mW. For all measurements the laser beams are put on the sample before the voltage is applied. The spectrum of the output of the BAL is measured using the OSA.

The spectral results are shown in figure 4.5. Figure 4.5(a) shows the spectrum without external feedback; i.e. before the voltage is applied and before the Ti:Sa beam enters the sample. Figures 4.5(b) to 4.5(e) show spectra with the voltage on the TFD. An increase of the emitted power at the injected wavelength is observed, but other wavelengths persist. Furthermore, the output spectrum was unstable. The photorefractive grating in the DPCM configuration has an orientation similar to the TBG grating that was previously found to be instable (figure 4.1(a)). These instabilities could originate

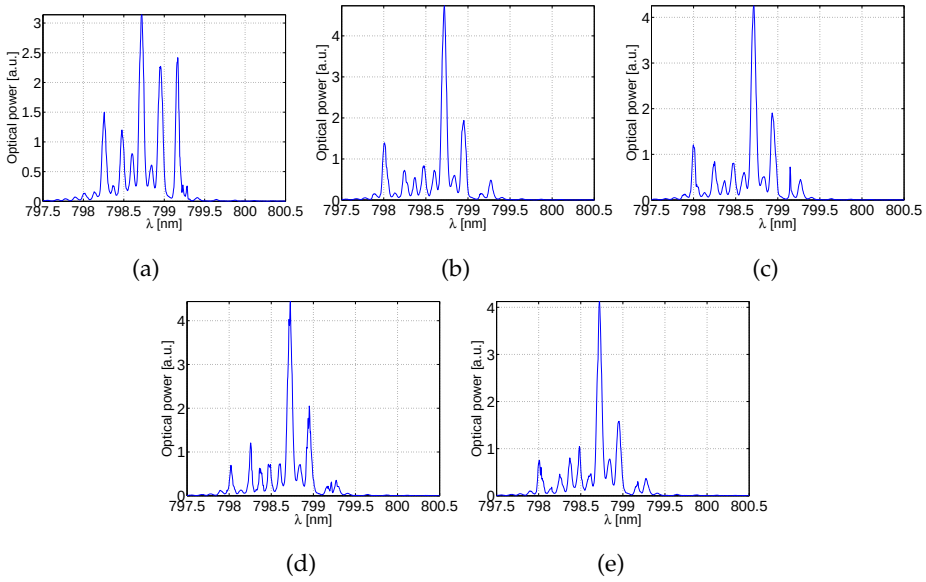

Figure 4.5: *Complete locking is not achievable.*

from a common cause and a different orientation of the grating could result in more stable behaviour. Due to the geometry of the mount of the TFD, mounting the TFD on both sides and having a thickness of 1 cm of its own, there was not much room for tilting the sample, to try an asymmetric setup. We could only decrease the angle between the sample and the Ti:Sa over about 10^o, and this did not change the observations.

4.2 FWM-setup

Another setup to generate a phaseconjugate signal is a degenerate fourwave mixing(FWM) configuration. This configuration has the advantage that the photorefractive gratings do not start from random fluctuation but from interference between incoming light beams. A disadvantage is that there is a more stringent requirement on phase stability; in a DPCM the holographic grating that couples the two sources (BAL and Ti:Sapphire) is maintained by both beams independently as they scatter in the grating. Stability of the grating in time requires only that the wavelengths of the sources do not drift outside the bandwidth of the grating. In a FWM geometry, the grating is maintained as an interference between incoming beams from both sources

which requires them to maintain a fixed phase relation. This is a much more stringent requirement than the bandwidth requirement of the DPCM. To find

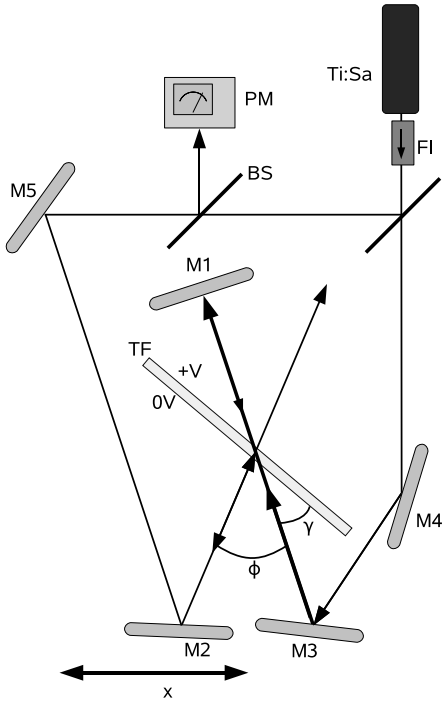

Figure 4.6: *Coherent experimental setup to optimise the angle-configuration. Mirror M2 is moved along the denoted x-axis while overlap of the beams is maintained at the sample by rotating M2 also, to vary the angle ϕ*

and optimise the angles ϕ and γ for which fourwave mixing occurs, the setup is first tested using only coherent beams from the Ti:Sa laser, see figure 4.6. The pump beam with an optical power of 70 mW is entering the sample from mirror M2 and retroreflected by M1 as probe beam. The signal beam (later to be replaced by the BAL) has an optical power of 26 mW and intersects the pump and probe beams after reflection of M2. Moving the mirror M2 along the x-axis, while making sure the beams remain intersected in the element by rotating mirror M2 and M5, varies the angle ϕ. Part of the generated phase-conjugate beam (of the probe beam) is reflected into the optical powermeter.

In figure 4.7 the optical power, as measured by the powermeter, is shown as a function of angle ϕ. From 14^o to 25^o the slope is almost zero and after 25^o

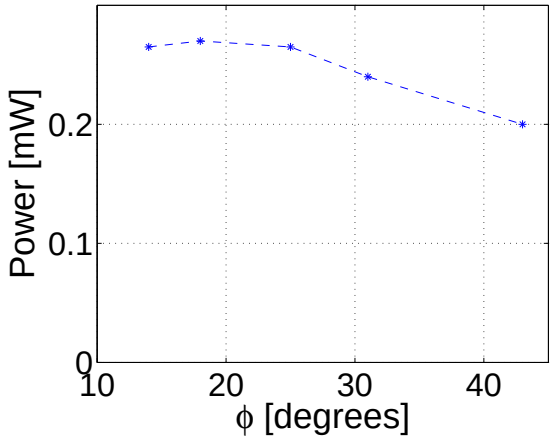

Figure 4.7:

the optical power decreases gently with the increasing angle. The optimum angle is not very critical but should be below 25°.

The angle γ can be varied by rotating the element. Varying γ from 15° to 25° did not result in a measurable difference in the phaseconjugated beam. In the following γ will be maintained at 20°.

Figure 4.8 shows the configuration for locking of the BAL to the Ti:Sa laser through a FWM configuration. The light from the continuous wave, single frequency, TEM_{00} Ti:Sa-laser (Ti:Sa, Coherent 899) is used as the pump and probe beam. The beam from the Ti:Sa laser and its retroreflected part, the probe beam, intersects in the 105 μm thick photorefractive TFD as a standing wave pattern. The photorefractive polymer composite selected is PATPD:7-DCST:APDC:TNFDM:ECZ (39.8:25:25:0.2:10 wt%). In this composite, PATPD is the hole transporting polymer backbone, 7-DCST and APDC are electro-optic chromophores, TNFDM is the sensitiser dye which absorbs light and injects holes to the photoconducting polymer, and ECZ is the plasticiser used to reduce the glass-transition temperature of the composite. The polymer is sandwiched between two ITO coated glass electrodes that are used to apply a DC bias of 4 kV to pole the electro-optic chromophores. The overall transmission of the photorefractive TFD is around 70%, due to small absorption of the polymer composite and Fresnel reflection losses at the glass-ITO electrodes. A passively cooled BAL (Sony SLD323V) generates the signal beam and is

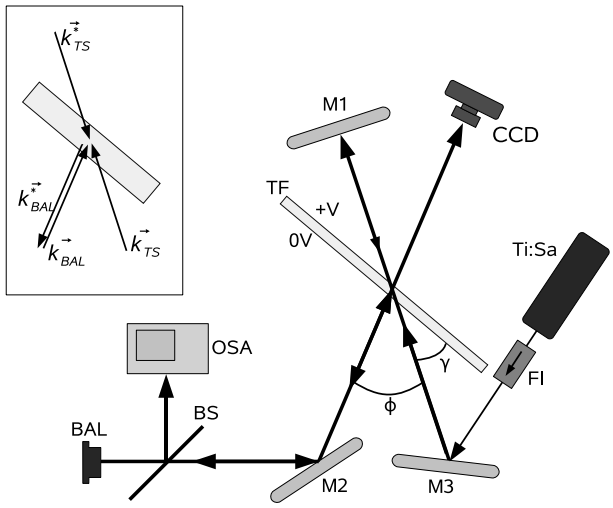

Figure 4.8: *Experimental setup. Insert: Schematic of the k-vectors involved in the four-wave mixing ($\vec{k_{TS1}}$, $\vec{k^*_{TS1}}$)=Incoming and phase-conjugated k-vectors from the Ti:Sa laser, ($\vec{k_{BAL}}$)=k-vector from the BAL, ($\vec{k^*_{BAL}}$)=The generated phaseconjugate k-vector form the BAL.*

overlapped with the light from the Ti:Sa in the TFD. The angles between the two beams, φ, and between the Ti:Sa beam and the TFD, γ, are $20^o \pm 2^o$ and $13^o \pm 2^o$, respectively, as indicated in figure 4.8. The optical power on the TFD from the Ti:Sa and the BAL are 50 mW and 100mW, respectively. The beamspot of the Ti:Sa-laser beams on the TFD is elliptical due to the angled incidence. The BAL beam just fits within this ellipse with a long axis of 5mm and a short axis of 3mm. The polarisation of the lasers and the fast axis of the diode laser lie in the plane of figure 4.8. The spectrum of the BAL is monitored by an optical spectrum analyser (OSA, Ando AQ6317) with a resolution of 0.01 nm. The far field beam profile of the BAL is measured on a CCD camera (CCD).

The Ti:Sa laser is tunable and can be coarsely tuned to a spectral mode of the BAL. To carry out the fine tuning, the current to the BAL is adjusted. Because the system is only passively cooled the operating temperature will rise slightly with an increasing current, and with a rising temperature the wavelength shifts to the red.

In the context of the fine-tuning it is relevant to know how close the wavelengths of the Ti:Sa laser ($\Delta\nu$=10 MHz rms) and the BAL have to match.

The matching bandwidth can be estimated from the response time of the polymer if we assume that the dynamic gratings can be written for a frequency mismatch that is smaller than the response time of the polymer. In our case, with a response time in the range of 10ms, this means $\Delta\lambda \leq 10^{-18}$ m$(10^{-9}$ nm$)$. The resolution of the OSA is limited to 0.01 nm. To achieve, and maintain locking, a very gentle fine tuning in the current of the BAL and a lot of patience was used.

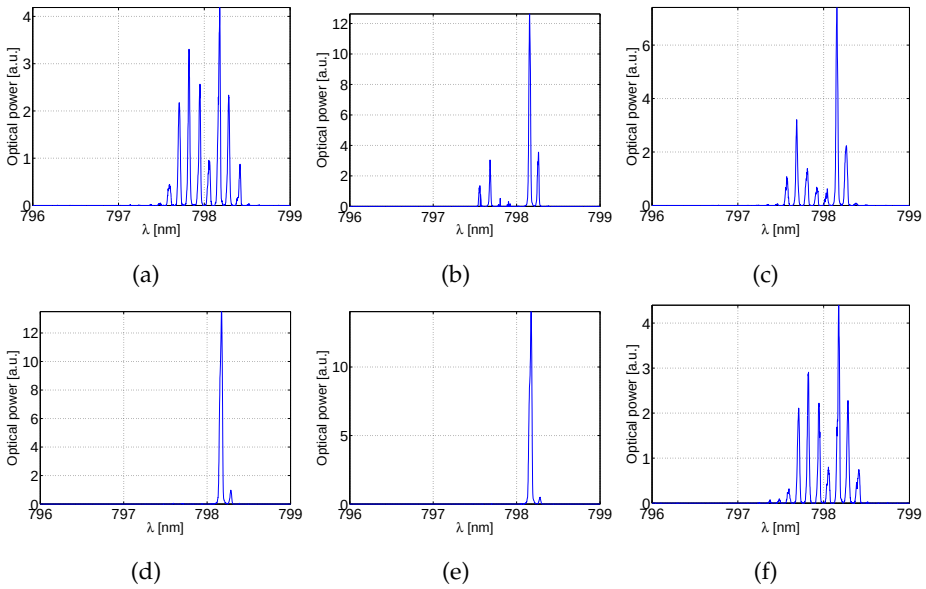

Figure 4.9: *Complete locking is achievable.*

Measurements of the BAL spectrum during the locking experiment can be seen in figure 4.9. In figure 4.9(a) the broad and irregular spectrum of the BAL without feedback can be seen. In figure 4.9(b) and 4.9(c) some locking can be observed when the wavelengths of the BAL and Ti:Sa laser beams partially overlap but is not yet perfect. In figures 4.9(d) and 4.9(e) full locking can be observed if the wavelengths fully overlap. Only a minor residual part of the light is still emitted at the original wavelengths of the BAL. The linewidth of the locked light is below the resolution of the spectum analyser. Due to temperature drift, locking is eventually lost in figure 4.9(f) . By careful tuning, locking can be maintained for time intervals up to 5 minutes, which is very long compared to the diode dynamics (order of the roundtrip time, ns) and long compared to the 10ms timescale at which gratings can be written

and erased. From these timescales we conclude that stable injection locking was achieved.

4.3 Spatial effects of the locking

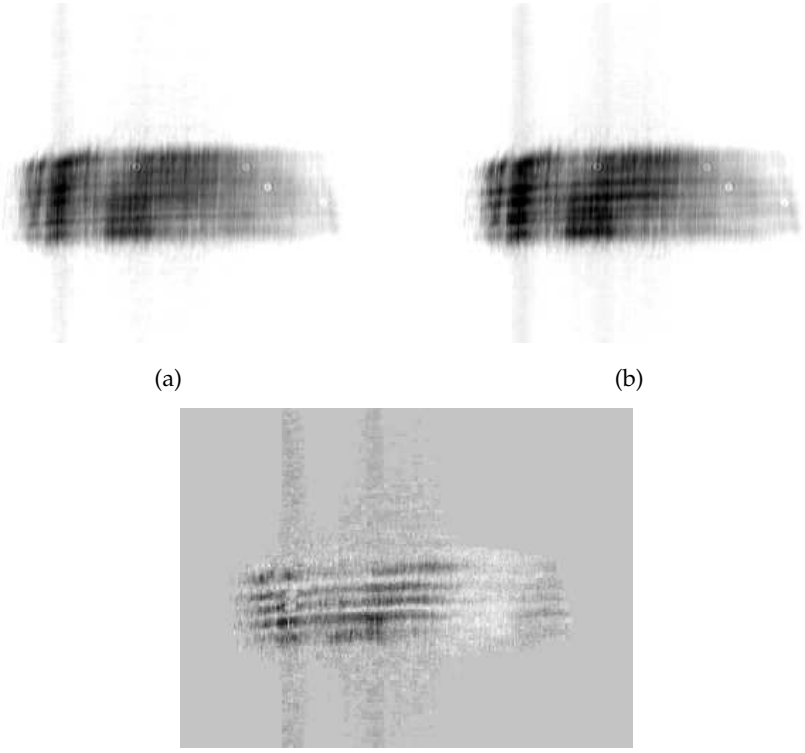

(a) (b)

(c)

Figure 4.10: *Compare the 'complete dynamic ugliness' (a) of the free running BAL to the 'static convertable ugliness' of the injection locked BAL (b). In (c) the figures from (a) and (b) are subtracted to emphasise the static regular fringes in the case of the locked BAL.*

To further characterise the injection locked BAL, the CCD camera in figure 4.8 is used to record the far field emission pattern of the BAL and compare the far field pattern during locking to the pattern without locking (the "free running" pattern). In figure 4.10 the recorded images are shown. In 4.10(a) the free running BAL pattern is depicted with the slow axis in the vertical direction. This is the multimode axis of the BAL, but, due to multi-wavelength

emission, higher-order modes are averaged out on the 1/30 second timescale at which the CCD records and only a slowly varying envelope can be observed along the vertical slow axis.

This behaviour is different from the injection locked case, depicted in figure 4.10(b) . Figure 4.10(c) displays the difference between 4.10(a) and 4.10(b) , to emphasise the changes. While the BAL is locked, a stable and distinct pattern can be observed along the slow axis. This pattern shows deep modulations characteristic of a high order mode. The stability of this pattern confirms the narrow linewidth of the locked BAL.

We can compare these results with section 3.4 on 63. There, the spatial effects of locking through the DPCM grating are explained, in a two-step process. First, the free running BAL is converted from a beam with almost no spatial structure to a superposition of high-order modes. This is, in principle, the same step as demonstrated here for the photorefractive polymer case. The locked far fields in figure 4.10 and figure 3.9 are similar. Based on the similarity of the result and similar principles on which the experiments are based, we can claim that the second step also applied to the FWM experiments and assume that the grating converts the spatial pattern of the BAL into a Gaussian TEM_{00} beam. By definition, the locked BAL beam is also then a near-diffraction limited beam (rather than limited by an incoherent addition of modes).

The current setup does not allow us to prove this directly by a measurement similar to section 3.4; blocking the beam of the Ti:Sa laser, cannot be used because of the improved response time of the photorefractive polymer. We have tried to monitor the light that is diffracted in either the direction of mirror M1 or M3 (see figure 4.8). Although mirror M1 and M3 are highly reflecting mirrors, a small amount of light will be transmitted. If a significant amount of BAL light is diffracted, the amount of light transmitted through M1 or M3 should increase. The measurements show fluctuations of few percent but these fluctuations are not correlated and a significant amount of BAL light could not be isolated from this fluctuations.

4.4 Discussion

In a FWM setup two orientations of the grating are possible [48, 49]. Normally, the grating with the preferred orientation with respect to the anisotropy of the material will be the only hologram that is observed.

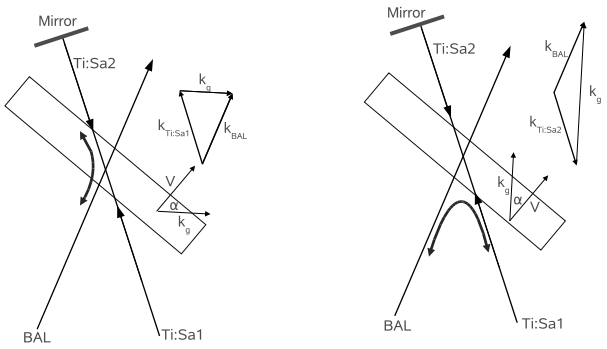

Figure 4.11: *Two possible gratings*

In our experiment however, neither of the gratings has a strong advantage. The configuration of the grating vectors is depicted in figure 4.11. The first possible grating vector $\vec{k_g}$ is constructed by subtracting $k_{\vec{BAL}}$ from $k_{\vec{Ti:Sa1}}$. For the second grating vector $k_{\vec{Ti:Sa1}}$ is replaced by $k_{\vec{Ti:Sa2}}$. The direction of the external electrical field in a photorefractive polymer can be compared to the optic c-axis in a photorefractive crystal. The angle α between the c-axis denoted by V and the k-vector of the grating, $\vec{k_g}$ determines the preferred grating. Although the precise optimum depends on a number of factors, for a FWM setup using a photorefractive polymer, approximately 45° should be good. In our scenario, one of the both angles α is 30° and the other 60°, so equally far of the optimum 45°. This means no grating is preferred, and it is possible both gratings exist in a superposition.

If both gratings coexist, light is diffracted along both directions depicted in figure 4.12 and only a significant net effect exists in the direction of the BAL. This might explain the occurrence of coupling despite our inability to detect any feedback behind the mirrors. However, the BAL is operated in the weakly coupled regime so that the maximum diffraction efficiency is unlikely to reach tens of percents.[1]

[1]In a conventional four-wave mixing setup, the polarisation of the probe beam is rotated

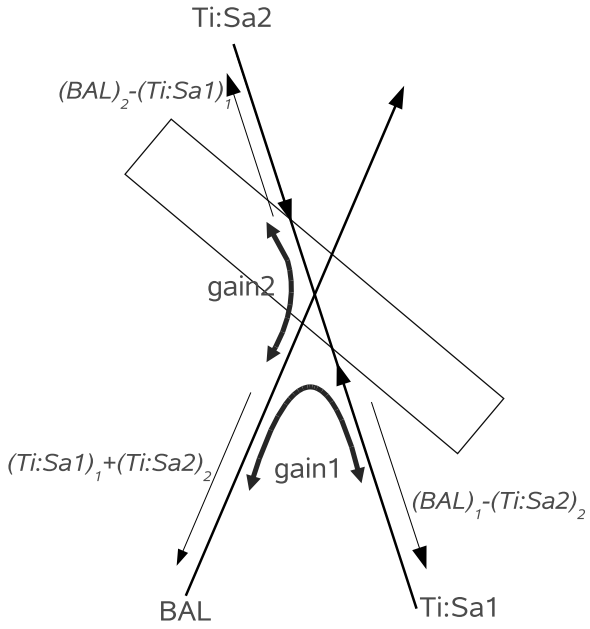

Figure 4.12: *The net gain changes in all directions due to the two gratings, denoted by the italic text next to the arrows. The subscription denotes the grating causing the light to diffract in the marked direction. If all the factors are approximately equal net gain only exists in the form of the phaseconjugate of the BAL beam.*

When the coherent FWM setup is recalled, it might even be likely both gratings exist in a superposition. From figure 4.12 can be seen the only effective coupling (both diffracted beams add) into the phase-conjugate of the incoming BAL beam, which was the signal beam in the coherent FWM setup. The maximum phase-conjugate signal is likely to be the phase-conjugate signal at which both gratings contribute.

For practical applications, the overall efficiency has to improve significantly to make photorefractive polymers a viable option for building lasers with a high power output and a good spectral and spatial beam quality.

90^o with respect to the writing beams [85]. In this way, it is always clear which grating will be written and the issue as described above does not emerge. If this technique is used, the phaseconjugated beam of the BAL would have the opposite polarisation of the emitted beam. This fact makes this technique not usable for us, because a polarisation rotated beam will not injection-lock the BAL.

Rapid developments in in the field of photorefractive polymeric materials can contribute to to finding new materials. We demonstrated holographic injection locking using photorefractive polymers as holographic medium is possible. By using photorefractive polymers the use of photorefractive crystals, with their inherent disadvantages in handling and experimenting can be avoided.

Chapter 5

Modelocking concept, setup and modelling

Abstract

A novel concept for a modelocked laser is explored in this chapter. An implementation is described based on a single mode diode array. Simulations to estimate the feasibility and constraints of the designed laser are presented.

The previous chapters described the holographic injection locking of a BAL. Without external feedback, such a BAL is characterised simultaneous oscillation of a large number of spatially different modes at multiple frequencies causing a low quality of the overall output beam shape. The goal in previous chapters was to use injection locking to restrict oscillation of these modes to the same, single-frequency, with temporally fixed, mutual phases, with minimal restriction to the spatial superposition of the different modes. In the final part of the thesis the aim is to achieve the mutual injection locking of up to 49 single-mode diode lasers in an array. The spatial properties of the array emission are restricted, due to the diffraction limited output of each of the single-mode emitters in the array. The goal is to spectro-temporally control the overall output of the array with feedback from a nonlinear optical element. Specifically this feedback aims to achieve oscillation of the single-mode emitters at equidistant frequencies and at fixed phases with respect to

each other, in order to generate a train of ultrashort pulses. Here we show that such a mode-locked array of single-mode lasers, which have not been realised or investigated before, will show some special properties that are quite different from a standard, mode-locked laser. For instance, very high repetition rates and a high average output power seem possible. This can be of interest for a number of applications, mainly in the field of nonlinear optics.

A comprehensive overview on the generation of ultrashort pulses via mode-locking can be found in standard textbooks on lasers [37, 43]. Briefly, mode-locking was predicted by Didomenco [86] in 1964 and was soon experimentally confirmed [87, 88]. In the first experiments active mode-locking was applied; the intracavity losses were modulated, with the period of the modulation matching the roundtrip time of light through the cavity (synchronous loss modulation). A year later, passive mode-locking was demonstrated for the first time [89, 90]. In a passively mode-locked laser the intracavity losses are higher for CW-light (with a low power) than for pulsed light (with a higher peak power). This differentiation can be achieved, for example with a saturable absorber. Such an absorber can be bleached (saturated) at elevated intensities for a short time interval. When the light is concentrated in a time interval smaller than this interval it experiences less loss. Under the right conditions this leads to a condensation of the intracavity power towards oscillation in the form of short pulses.

An alternative to such a description in the time domain can be given in the frequency domain, where the periodic generation of ultrashort pulses corresponds to multi-frequency laser oscillation at a set of equally spaced frequencies. When the saturable absorber is simultaneously irradiated with light at different frequencies, the nonlinear response of the absorber generates a set of spectral sidebands at the sum and difference frequencies of the incident light. If the light frequency of the sidebands is in sufficient proximity to the (incident) light frequencies of the laser and if they are injected back into the resonator, the sidebands cause injection locking. The onset of such self-injection locking of the laser, also called mode-locking, changes two properties of the output light field: The spectral power spectrum and the spectral phase.

The power spectrum of the laser initially consists of a spectrally non-equidistant superposition of modes with a strongly varying envelope and laser spectral gaps without emission (figure 5.1(a)). This spectrum changes

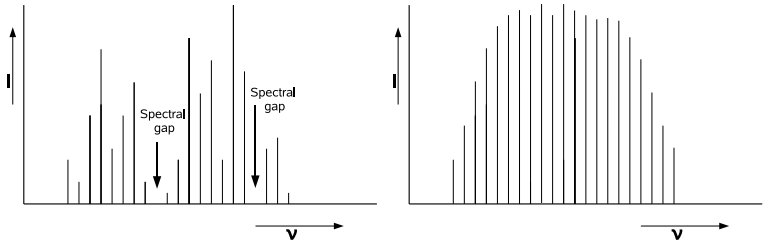

(a) (b)

Figure 5.1: *Comparing a free-running and a mode-locked spectrum, along the x-axis the frequency ν and along the y-axis the intensity I is put.*

into an array of equidistant modes with a smooth envelope (figure 5.1(b)). The reason is that the sideband generation initiates a transport of energy through the laser spectrum which tends to equalise the optical power of neighbouring modes.

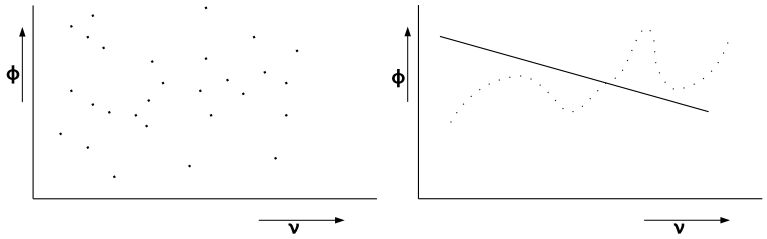

(a) (b)

Figure 5.2: *Comparing the phase distribution of a free-running and a mode-locked laser, along the x-axis the frequency ν and along the y-axis the phase ϕ can be seen. The solid line in (b) indicates the phase of a bandwidth-limited pulse, while the dotted line indicates the phase distribution in a mode-locked laser emitting a more complex intensity distribution in time.*

The second change, induced by self-injection locking, is a modified spectral phase of the oscillating modes, as depicted in figure 5.2. The initial phase distribution is a random distribution because the phases of the laser's free-running modes are determined by random spontaneous emission. Their start, and oscillation, and spontaneous emission, lets each phase diffuse ran-

domly during oscillation. In contrast, when self-injection locked, the phases of the modes try to adjust to each other to assume fixed relative values. This results in a temporally stable spectral phase distribution as shown in figure 5.2(b) . The shape of this distribution is given by additional phase-shifting effects, such as linear dispersion in the resonator, or, nonlinear effects, such as index-gain coupling in the amplifying medium (e.g. through the linewidth enhancement factor α [22]). If the phase is a linear function of frequency, the laser output in the time domain consists of bandwidth-limited pulses. If the phase spectrum contains a second-order parabola, the pulses are called linearly chirped [91]. This, and other types of output from a modelocked laser, also such as that given by the dashed trace in figure 5.2(b) , can be transformed into a bandwidth limited pulse by sending the output through materials or devices with a suitably chosen dispersion (e.g. grating compressor [92, 93].

Note that the description of mode-locking along with the figures 5.1 and 5.2, depicts two extreme cases: free running, a complete absence of mutual injection locking between the laser's modes or groups modes, and mode-locked, where all the modes participate in the mutual locking. These two extreme cases are almost never realised so distinctively. For instance, mode-locked lasers usually show a slow drift of their overall phase spectrum due to perturbing effects, such as spontaneous emission, thermal drift and acoustic vibrations of the optical alignment. Furthermore, towards the edges of the phase spectrum, one may expect an increasing amount of phase fluctuations because of the lower power of the generated sideband. Finally, it is well known that even a weak spectral variation of the roundtrip losses, such as residual reflections from intracavity surfaces, can suppress modelocking partially or fully. This is the case particularly in lasers with strong spectral mode competition due to a homogeneous broadening of the laser gain. Here, spectrally varying losses can suppress laser oscillation across large ranges of the gain spectrum such that gaps become visible in the laser output spectrum, as indicated in figure 5.1(a) . When such gaps remain, because the increased loss in a gap is not sufficiently compensated by the sideband-generation-induced energy transport into the gap, such a laser, although partially locked, may only show partial mode-locking across groups of modes which would result in a temporal output consisting of random spikes of elevated intensity

(above average power) and the lack of strictly periodic and well-separated light pulses.

In conclusion, the laser properties that promote mode-locking are: one, a nonlinear feedback element which provides strong sideband generation over wide spectral ranges. Two, a large number of oscillating modes and high overall (average) power which allows for a strong intensity modulation in the feedback element. Three, a reduction of intracavity losses to increase the intensity of the feedback element. Four, the removal of gain competition that should, via spectral varying of losses, lead to spectral gaps. Note that gain competition is suppressed to a maximum degree when using a laser gain medium that is inhomogeneously broadened, i.e., when stimulated emission into one laser mode does not reduce the gain experienced by any other laser mode.

5.1 Detection of mode-locking

When looking at the described physical processes and laser dynamics, two methods are generally applied in detecting mode-locking of lasers. The first approach, which is experimentally easy to implement, is to observe the lasers output spectrum with an optical spectrum analyser (OSA). When the spectrum of the laser changes to one with equally spaced emission lines with a smoothed spectral envelope, and where spectral gaps disappear, this indicates the transport of energy across the laser spectrum via successful sideband generation through the nonlinear feedback element (see figure 5.1.

The second method, is to monitor the changes in the phase spectrum as in figure 5.2 via time-domain techniques. These two methods are often applied together. Such techniques are based on temporal self or cross correlation, such as: intensity autocorrelation [91], interferometric auto-correlation [91], frequency resolved optical grating (FROG) [91], and, spectral phase interferometry for direct electric-field reconstruction (SPIDER) [94]. In the simplest of these techniques (intensity auto-correlation), the laser output is split into two beams which are overlapped in a second-order nonlinear crystal with an adjustable delay between the arms. The second harmonic generation from the crystal is recorded as a function of the delay time, which provides a so-called autocorrelation trace. When narrow and high peaks appear in this trace, this

indicates the emission of ultrashort pulses and thus the establishment of a phase-spectrum such as in figure 5.2(b) . In comparison, the absence of modelocking renders autocorrelation traces with only weakly pronounced peaks as expected from a randomly-phased superposition of the laser modes.

In our experiments, both techniques, the use of the OSA to measure the spectrum, and, the intensity autocorrelation, will be applied.

5.2 Limits of standard mode-locked lasers

Many different types of lasers have been mode-locked actively and passively, first gas lasers [95] then solid state lasers [96–98] and diode lasers [99–101]. Nowadays, passive modelocking is the main technique to create ultrashort pulses because it usually yields to shorter pulses than active mode-locking.

As will be explained in further detail below, three main difficulties have remained, despite the wide range of modelocked lasers. The first is that it remains difficult to realise a modelocked laser with a high average output power directly from the laser oscillator. Secondly, combining a high repetition rate with a short pulse duration is hard, and, finally shortening the pulse duration is limited by the gain bandwidth of the gain medium

The average output power and the temporal quality of the generated pulses are limited due to nonlinear effects and gain saturation in the gain medium. This is especially true, when high-power pulses have to be sustained by a single gain medium which has to amplify the entire spectrum of the pulse. The reason for this is that, while the gain medium is pumped continuously the depletion of the gain occurs during an extremely short time interval (the duration of the pulses to be generated), which generates an undesired reshaping of the pulse during amplification. This problem may be elevated, but not completely solved, by using lasers with an intracavity pulse stretcher and compressor [102, 103].

Work has been done to increase the repetition rate into the (tens of) GHz window [104–107] by decreasing the length of the cavity and thereby reducing the roundtrip time, however, the macroscopic physical dimension of many lasers imposes a limit for the repetition rate in the MHz range. Thus novel ways of generating extremely high repetition rates should be devised. A range of new applications would become feasible if the repetition

rate could be increased to the GHz range. Examples of such applications can be found in telecommunications [108, 109], optical clock distribution in optical processing [110, 111] or in very large scale integrated circuits [112]. Also high-speed electro-optic sampling techniques require pulse trains with short pulses and low timing-jitter with a repetition rate in the GHz window [113, 114].

In the current generation of modelocked lasers, a single gain medium is used to amplify the pulse, this requires that the single gain medium has to support the complete bandwidth of the pulse. For instance, the shortest pulses that have been generated so far rely mostly on Ti:Sapphire as the gain medium, which enables the generation of femtosecond pulses. In order to generate sub-femtosecond pulses directly from mode-locked lasers, novel approaches have to be identified that allow the employment of several gain media with the goal of providing a significantly broader gain spectrum. Examples of proposals that might enable mode-locked lasers in the attosecond regime are found in [115–118], but are achieved by modulating the polarisation of a femtosecond pulse and, after it, creating a higher-order harmonic with the pulse.

A novel approach needs to be identified where the gain of the laser becomes inhomogeneously broadened to a maximum extent. This could be addressed by employing several gain media in parallel so that each single frequency of the laser is amplified individually in its own gain medium. This way one could exclude undesired nonlinear effects during amplification, in particular, inherently-dependent and thus pulse-duration-dependent deformations of the pulse envelope. This novel approach should preferably decouple the pulse repetition rate from the physical length of the laser cavity. This would allow the realisation of ultra-high repetition rates without the need to provide a laser cavity of extremely short length, where average output powers become difficult to realise due to high spatial power densities.

5.3 Experimental setup for a SG-mode-locked laser

In the following a novel concept for mode-locked lasers is suggested and modelled. Although the generation of regular pulse trains in a corresponding experimental setup was not observed, preliminary characterisation of the

output (chapter 6) indicates first signs of mode-locking.

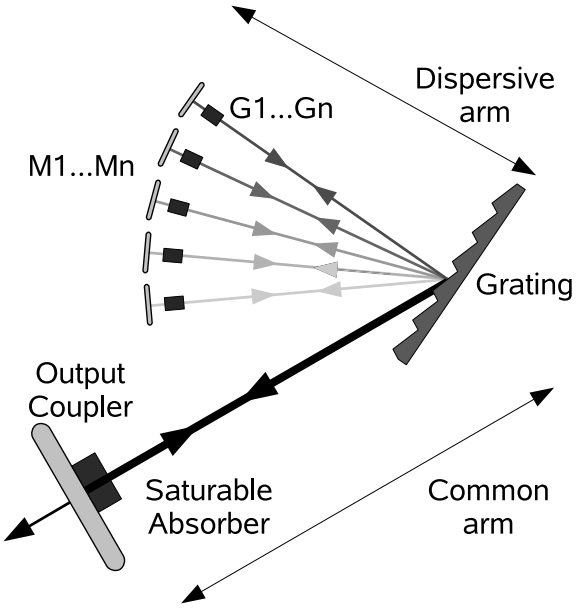

Figure 5.3: *Schematic of principle of inhomogeneously modelocked laser*

This concept is schematically depicted in figure 5.3. The central feature is that the laser gain is provided by a large number of physically separated, equally spaced gain elements, G1..GN, each of which is responsible for continuously amplifying a single frequency of the laser's multi-frequency spectrum. The multiple-beam emission from these elements is sent to a diffraction grating which combines the beams into a single beam. Thus, the laser essentially consists of a number (N) of individual, single-frequency, continuous-wave (CW) lasers which share one common arm of their laser cavities and a common output coupler. Without any further intracavity elements, the laser emission should resemble a spectrum of approximately equidistant frequencies, which are given by the grating dispersion, the location of the gain elements and the gain spectrum of each element. Temporally, one would expect a random mode beating due to the random relative phasing within the lasers multi-line spectrum. However, this should change when introducing a non-linear feedback element, as would be provided by a saturable absorber in the common arm, shown in figure 5.3. Depending on a number of physical pa-

rameters of the setup, shown in detail below, temporal intensity variations in the absorber, caused by the beating of the superimposed CW spectral components, should result in a sideband generation and, possibly, in the emission of ultrashort pulses. In the following these effects will be addressed by the term "separated-gain laser" and "separated-gain mode-locking", abbreviated to SG-lasers and SG-mode-locking, respectively.

By separating the modes into individual gain elements, cross gain saturation and similar nonlinear effects in the gain medium are avoided. The repetition rate is determined by the spectral separation of the modes which can be chosen independently of the cavity length. Since all of the spectral components of a pulse are amplified in a different gain medium, and different gain media can be used, the overall spectrum available can be increased as desired, e.g. in order to shorten the pulse duration to a value that is shorter than can be achieved in lasers with a single gain medium.

The concept of physical separation of the laser gain has been proposed and tested before [119], but only a separation into a few groups of many modes was considered, which effectively corresponds to a laser with some intracavity pulse stretching and amplification. In our approach with an SG-laser, the gain can be considered as completely inhomogeneously broadened since every mode is amplified in its own gain element. The grating and array combination was also explored for high power applications without any modelocking [120].

The remainder of this chapter is presented in three parts. The concept of SG-mode-locking is compared to standard mode-locking with a single gain medium in more detail. In the second part, specific design considerations are presented that were used in the experiment for SG-mode-locking of an array of single-mode diode lasers. Finally some results are presented of numerical modelling with the goal to identify suitable experimental parameters.

5.4 Review of standard mode-locking

For a comparison between standard mode-locking and SG-mode-locking, some general properties of standard mode-locking are reviewed. In the standard approach, all laser modes are amplified in a single gain medium. The gain is not shared among the modes in an inhomogeneous laser and every mode has

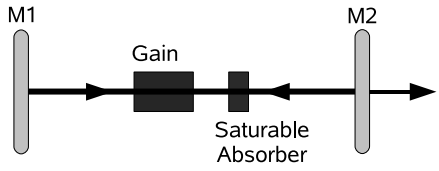

Figure 5.4: *Schematic of principle of homogeneously modelocked laser*

its own amplification. This is depicted in figure 5.4, where, in a single cavity, a single, broadband, gain medium and a saturable absorber are inserted. While the gain medium provides the light amplification, the saturable absorber, with its intensity-dependent transmission, forms an intensity-dependent feedback element that can lead to a condensation of the laser transmission into ultra-short pulses.

The output of a standard modelocked laser is described by a number of parameters. The first is the pulse duration τ_{pulse}, which is inversely proportional to the spectral bandwidth of the pulse, if the mode-locking results in a linear phase spectrum (see figure 5.2(b)). This spectral bandwidth is generally limited by the gain bandwidth of the gain medium, i.e. the broader the gain bandwidth of the medium is, the shorter the generated pulse will be.

The second key parameter is the repetition frequency ν_{rep}. The repetition frequency is usually equal to the free spectral range (FSR) of the cavity. Because of this, a standard modelocked laser can be considered in the time domain as a laser in which one pulse is making roundtrips through the cavity.

The concept of an SG-modelocked laser as was described above and depicted in figure 5.3, provides some essential differences. In this concept, the light travels in the shape of a pulse only in the common arm, while in the dispersive arm the various beams contain CW-light. It is the spatial overlapping of these spectral modes at the grating and their interference with each other that synthesises the pulses. The number of modes adding to the mode-locking is equal to the number of separated mirror-gain(Mn-Gn) elements. Due to the CW-light between the mirrors M1..Mn and the grating, the mode-locking dynamics of this laser does not follow the usual mode-locking behaviour. The gain saturation usually associated with the loss-modulation of the saturable absorber is only present in a standard modelocked laser. In an SG-mode-locked laser, each gain element will only see a single-frequency

which has its phase and precise spectral mode position modulated by the saturable absorber, but remains CW.

The key parameters like the pulse duration τ_{pulse} and the repetition frequency ν_{rep} are determined differently in a SG-mode-locked laser. The amount of dispersion introduced between the modes(In figure 5.3 determined by the line spacing of the grating and the angle between the modes) and the total number of modes (mirror-gain elements) define τ_{pulse} and ν_{rep}. In the separated part in figure 5.3 the frequencies are represented by ν1..νn. The repetition frequency is given by the difference between two consecutive modes.

$$\nu_{rep} = \nu(\mathrm{n}) - \nu(\mathrm{n}-1) \tag{5.1}$$

The total width of the spectrum is:

$$\nu_{total} = (\mathrm{N}-1)\nu_{rep} \tag{5.2}$$

From this τ_{pulse} can be calculated as:

$$\tau_{pulse} = \frac{1}{\nu_{total}} = \frac{1}{(\mathrm{N}-1)\nu_{rep}} \tag{5.3}$$

Therefore, the key parameters are not directly derived from the bandwidth of the gain medium and the cavity length, as in a standard mode-locked laser. The spectral width of the gain medium remains a boundary condition, but since several different kinds of gain media can be used, it is no longer the defining parameter of the achievable pulse width τ_{pulse}. And with ν_{rep} which is now given by the dispersion of the grating and the location of the separate gain elements, many pulses propagate in the cavity at the same time, so that the cavity length is not directly linked to repetition frequency.

5.5 Experimental setup

For an implementation of a SG-modelocked laser, all types of lasers may be suitable. However, here a diode array of single mode emitters is used. In previous work, the basic feasibility of operation as seen in figure 5.5 (without mode-locking) has been demonstrated [120]. In that experiment, every element in the used array received a slightly different frequency as feedback

and, in the common arm beams, these are spatially overlapped via the grating. The goal of that experiment was solely to increase the spatial brightness of the output, as compared to the free-running output. The spectrum consisted of a larger set of distinct frequencies, spanning a certain spectral range but the lines in the comb were not locked in phase with respect to each other so that the intensity showed random fluctuations as a function of time.

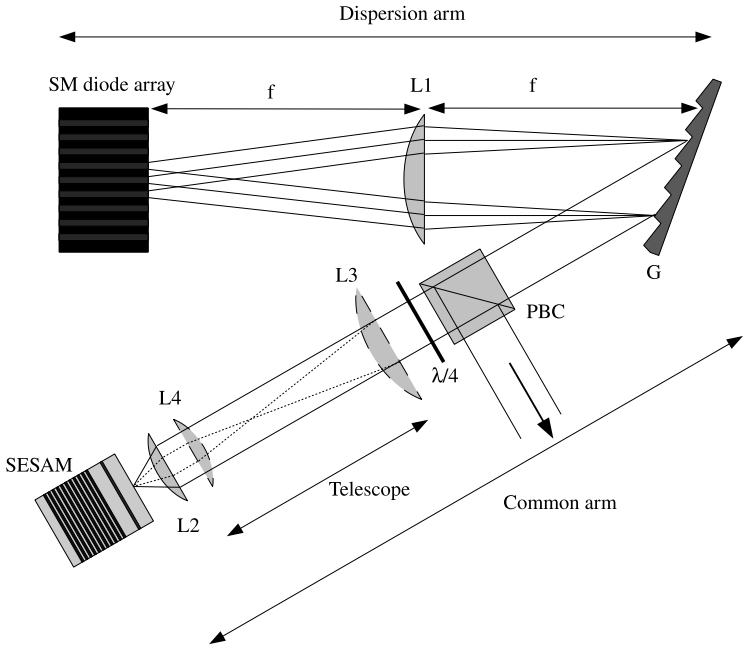

Figure 5.5: *The concept of the proposed modelocked laser that adds a saturable absorber the the common arm of a setup for wavelength combination.*

To enable mode-locking a saturable absorber is introduced in the common part of the cavity. The experimental setup is depicted in figure 5.5. The number of modes that take part in this locking is exactly the number of elements in the array. The array is a single mode array with 49 elements emitting at 980 nm provided by Bookham. This diode array, type SEAL-array, is anti-reflection-coated at the front facet (not standard). The lens L1 is a plano-convex lens with a diameter of 2 inches. The results from using two different focal distances in the configuration are presented below. The grating G has 1800 sinusoidal grooves per millimetre. In the common arm the light is

focused on the SESAM by lens L2. In the experimental part, various lenses were used for lens L2. By rotating the $\lambda/4$-plate and the polarising beam cube (PBC) a variable amount of light was coupled out from the SG-laser. The telescope formed by the lenses L3 and L4 was not present in every experiment hence the dotted lines, but was used in a part of the experiments described in chapter 6.

The remainder of this section will focus on calculating the pulse parameters for different configurations of the lens L1, and the potential geometric errors that can occur e.g. because the front facet of the diode array is flat and not curved as in figure 5.3. Different possible configurations for the common arm will be discussed in the next chapter (chapter 6)

5.5.1 Diffraction and pulse parameters

In order to calculate the pulse parameters, the difference in frequency between two elements is required. Because a grating maps the frequencies into real space, the distance between the elements in the array is a parameter which is required to calculate the difference in frequency between two elements. This number, and some other critical parameters of the SEAL-diode array from Bookham, is available from the datasheet in table 5.1. The parameters of the diode array are fixed and the most important things to determine are the focal length of the lens and the grating constant for the grating.

Table 5.1: *Critical parameters from the SEAL datasheet from Bookham*

Parameter	Symbol	Typical	Units
Centre wavelength	λ_{center}	980	nm
Spectral width	$\Delta\lambda$	10	nm
Beam divergence (hwhm)			
Parallel to junction	$\theta_{\parallel}$	7	degrees
Perpendicular to junction	$\theta_{\perp}$	22	degrees
Bar width	b	10	mm
Number of emitters	N	49	-
Emitter spacing	$\Delta l_{emitters}$	200	μm

The number of modes in the cavity is given by the number of elements

specified in the datasheet. The relation between the repetition period t_{rep} and the period of the pulses τ_{pulse} thus reads:

$$\frac{t_{rep}}{\tau_{pulse}} = N \tag{5.4}$$

The combination of focal length of the lens, the dispersion of the grating, and the distance between the elements $\Delta l_{emitters}$, determine the spectral range that is spread over the array. First calculations for practical (available) parameters show, that the dispersion needs to be high to spread the limited spectral bandwidth of the diode array over the physical width of the array within a reasonable distance. The grating formula, as can be found in paragraph 10.2.8 of [45] reads:

$$a(\sin\theta_m - \sin\theta_i) = m\lambda \tag{5.5}$$

m is the order of the diffraction, λ the wavelength, a is the grating constant, the distance between two grooves in meters. θ_i is the angle of the incoming beam and θ_m the angle of the diffracted beam corresponding to order m. λ is determined by the centre wavelength of the bar, λ_c=980nm. If m and a are known a curve for θ_m against θ_i can be drawn, to aid exploring possibilities. From a combination of calculations and catalogue investigation it can be found that gratings with 1800 grooves per millimetre are the most dispersive standard available gratings that can be used with 980 nm. With a at 1/1800*10^3=5.56*10^{-6} m, m is set to -1, because this is the only dispersive order that provides a solution for equation 5.5 with the chosen λ and a. In figure 5.6 the θ_i, θ_m curve is shown.

It is clear that both θ_i and θ_m have to be substantial. Using θ_i = 65^o yields θ_m = 47^o. Two scenarios will be calculated for the focal length of the lens: f=200 mm and f=300 mm. With these parameters fixed, the dispersion over the angle α is calculated and shown in figure 5.7. In this figure, e0 is the centre emitter and e1 is one emitter next to it. α_{center} is calculated as:

$$\alpha_{center} = \arctan(\frac{\Delta l_{emitters}}{f}) \tag{5.6}$$

Since the gain elements are not equally spaced along an arc, as in figure 5.3, but along a straight line at the diode array end-face, the angle α is slightly different at the outer elements. This estimation will introduce an error. To

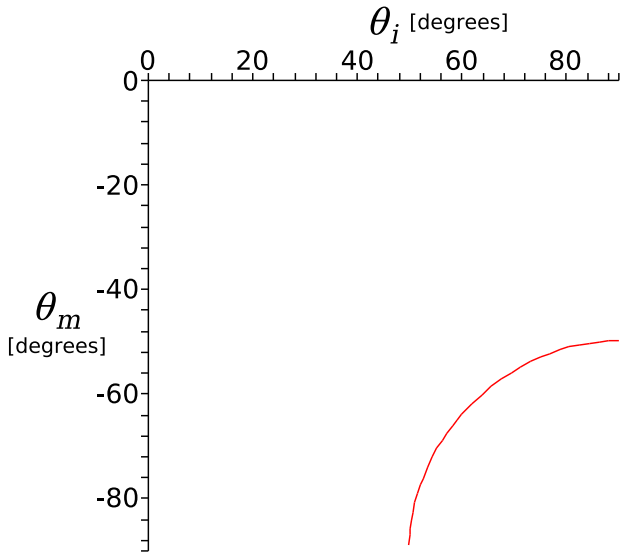

Figure 5.6: *A curve for θ_i (along the horizontal axis and θ_m along the vertical axis*

determine this error, α_{out}, the angle between the two outermost elements, e23 and e24 (49 elements, e0 is centre element, so (49-1)/2 is the outermost element) are calculated. In figure 5.8 the angle α_{out}, and its deviation from the ideal situation is shown.

α_{out} can be written as:

$$\alpha_{outer} = \arctan(\frac{b}{2f}) - \arctan(\frac{\frac{b}{2} - \Delta l_{emitters}}{f}) \tag{5.7}$$

Resulting in an error in α_{outer} compared to α_{center} of 0.2%. This error can potentially create an undesired shift in the frequency comb spectrum, which has very limited clearance on error.

From the emission data of the array, the spotsizes can be estimated to have a width $b_{emitter}$ ($\theta_{\parallel}$) of 4 μm and a height $h_{emitter}$ ($\theta_{\perp}$) of 1 μm. In the context of the error in α_{outer} compared to α_{center} the ratio of the width $b_{emitter}$ compared to the element spacing $\Delta l_{emitters}$, $b_{emitter}/\Delta l_{emitters}$=2%. This is the error in the wavelength because of the nonzero width of an element. This error is much larger than the error of 0.2% in the angles α. The width $b_{emitter}$ thus helps to eliminate the error in α. It should therefore be possible to lock all the

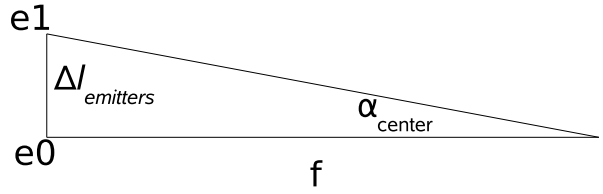

Figure 5.7: *Scheme of the calculation of the angle α_{center}, e0 is the centre emitter in the diode array and e1 is an element next to it. f is the focal length of the lens, an $\Delta l_{emitters}$ is the distance between two emitters.*

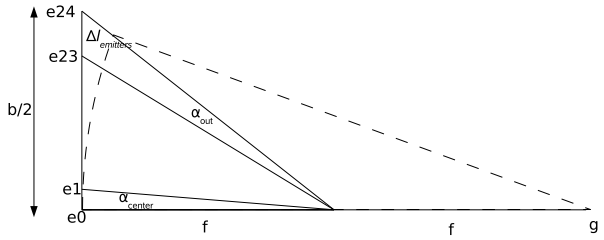

Figure 5.8: *Scheme of the calculation of the angle α_{outer}, e0 is the centre emitter in the diode array and e23 and e24 the outermost emitters. f is the focal length of the lens, $\Delta l_{emitters}$ is the distance between two emitters, b/2 the bar width divided by two and g the position of the grating. The dotted arc illustrates the ideal positions for e23 and e24.*

elements on a precisely spaced frequency comb.

With α_{center} known the grating equation has to be solved again, but this time with λ as a variable and θ_i replaced by $\theta_i - \alpha$. This will result in the difference in wavelength between two elements $\Delta\lambda_{emitter}$ and $\Delta\lambda_{total}$, λ_{min} and λ_{max} can be calculated.

$$\Delta\lambda_{total} = (N-1)\Delta\lambda_{emitter} \tag{5.8}$$

$$\lambda_{min} = \lambda_c - \frac{\Delta\lambda_{total}}{2} \tag{5.9}$$

$$\lambda_{max} = \lambda_c + \frac{\Delta\lambda_{total}}{2} \tag{5.10}$$

With the dispersion known, the frequency comb is characterised, and the duration of a single pulse, τ_{pulse} can be calculated by

$$\frac{1}{\tau_{pulse}} = \frac{c}{\lambda_{min}} - \frac{c}{\lambda_{max}} \tag{5.11}$$

with c the speed of light. By using equation 5.4 the repetition rate, $1/\tau_{rep}$ can also be calculated. All the pulsing properties are summarised in table 5.2.

Table 5.2: *Results if f=200 and f=300*

Parameter	Symbol	f=200	f=300	Units
Spectral width	$\Delta\lambda$	16	10.3	nm
Pulse duration	τ_{pulse}	200	300	fs
Repetition rate	ν_{rep}	100	68	GHz

5.5.2 Geometric parameters

In figure 5.9 the relevant angles, beam diameters and distances related to θ_i and θ_m are depicted. For the calculations, a few parameters are given in table

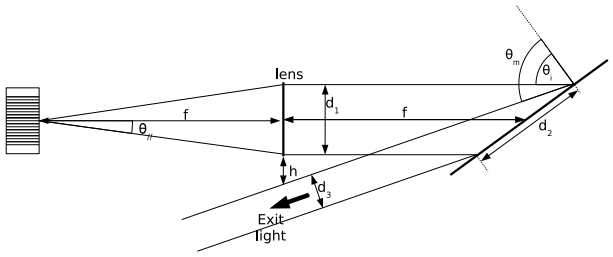

Figure 5.9: *The beampaths with the lens and grating included.*

5.3. The lens diameter puts a constraint on the maximum diameter of the beam at d_1. This size is given by the focal length and the $\theta_{||}$ of an element of the array. The grating size puts a limit on the diameter d_2, this may not exceed the grating size. The focal length and the lens+mount diameter determine the height h which should be larger than 0 in order to guarantee clean output coupling of the exit beam. With some geometry and the grating formula,

Table 5.3: *Given dimensions*

Parameter	Symbol	Value	Units
Lens diameter	d_{lens}	50.8	mm
Lens + mount diameter	d_{mount}	60	mm
Grating size	bxh	52x52	mm

all parameters can now be derived and calculated for any chosen θ_i and the given parameters.

$$d_1 = 2f\tan\theta_{\parallel} \qquad d_1 \leq 50.8\text{mm} \tag{5.12}$$

$$d_2 = \frac{d_1}{\cos\theta_i} \qquad d_2 \leq 52\text{mm} \tag{5.13}$$

$$d_3 = d_2\cos\theta_m \tag{5.14}$$

$$h = f\tan(\theta_m - \theta_i) - d_{mount} \tag{5.15}$$

All sizes that are restricted do not exceed the aperture of the lens or the size of the grating and the value of h also ensures a good clearance between the exit beam and the lens.

Table 5.4: *Calculated layout of the experiment*

Parameter	Symbol	f=200	f=300	Units
Incoming angle	θ_i	53.9		degrees
Refracted angle	θ_m	73		degrees
Entrance beam diameter	d_1	49.1	73.7	mm
Beam diameter on grating	d_2	83.4	86	mm
Exit beam diameter	d_3	15.2		mm
Clearing distance lens	h	9.3		mm

Some light is lost at the lens and the grating. The gain in the diode array will be sufficient to compensate for these losses. Compared to the losses in the waveguide in the diode the losses are small.

The fast axis with an opening angle $\theta_{\perp}$=22^{o} (half angle) is in the vertical plane. The first lens in the horizontal plane is 300mm away. This will introduce large losses in the vertical plane. To reduce losses, two extra cylindrical lenses are needed, as is depicted in figure 5.10. The first cylindrical lens, cl1 in the figure creates a parallel beam from the emitted light. The second lens, a convex lens, cl2 will diverge the beam again, but with a much reduced opening angle. The diode array will be in the focal plane of the second lens, seemingly making the light come from this focal plane. Because of this, the light will be parallel after the spherical lens which also has the diode array in the focal plane. This last lens is the same as the lens depicted in figure 5.9.

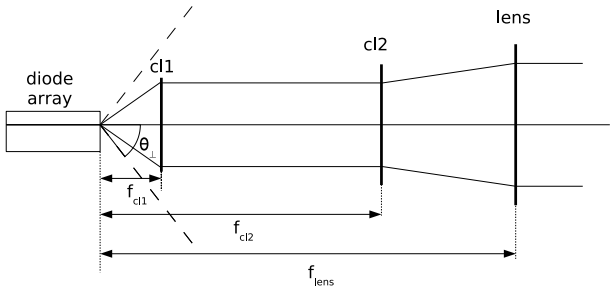

Figure 5.10: *The beampath of the light emitted in the vertical plane with a large opening angle $\theta_\perp$. cl1 is a positive cylindrical lens, cl2 is a negative cylindrical lens, lens is the spherical lens with f=300 also used in the horizontal plane.*

The required f/d needed for the cylindrical lens cl1 to collect all the light is:

$$\frac{f}{d} = \frac{1}{2\text{tan}\theta_\perp} \tag{5.16}$$

For a $\theta_\perp = 22^o$, f/d would need to be approximately 0.2. The minimum value of f/d of a plano-convex lens is 1. Putting two plano-convex lenses together will make a biconvex lens. If both plano-convex lenses used have an f/d of 1, the resulting biconvex lens has an $f/d = 0.5$. This is still not sufficient to collect all the light from the diode array. In our case the biconvex lens is made of an plano-convex lens with d=20mm and f=20mm and a plano-convex lens with f=30mm and d=20mm, resulting in an f/d=0.6 which is tolerable.

5.5.3 SESAM

To induce modelocking, a saturable absorber mechanism, reducing the loss for pulsed light compared to CW light, must be inserted in the cavity. In literature a number of mechanisms can be found; a reversible bleachable dye [89, 90, 98], self-focussing by Kerr-lensing in the gain medium [121–123] and intracavity frequency doubling [124–126].

In 1992 the semiconductor saturable absorber was introduced [127], improving the widely used reversible bleachable dye solutions as saturable absorbers. Because SESAMs can be designed and grown like common semiconductor materials, and have advantageous modelocking properties, the application of SESAMs has grown enormously since their introduction [107, 128].

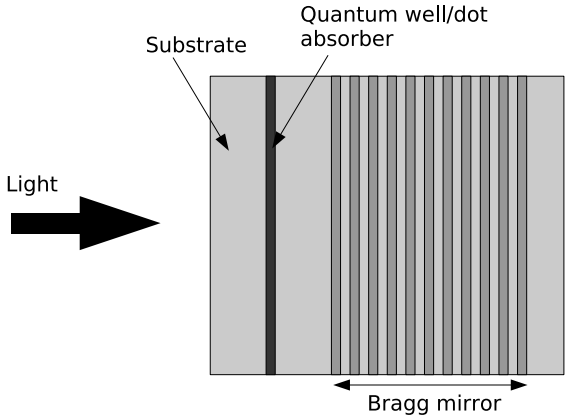

Figure 5.11: *Schematic of principle of homogeneously modelocked laser*

A (nonresonant) SESAM structure is shown in figure 5.11. The back is a dielectric mirror, while in front of the mirror a quantum well or a layer of quantum dots is positioned. This layer is about 10-20nm thick. The mirror is constructed to be a 100% reflector for the wavelength the SESAM is designed for. Before light can be reflected, it has to penetrate through the quantum well layer. The energy band of this layer is chosen in such a way that it absorbs the light, see figure 5.12. The excited electrons have to stay within the quantum well layer due to the energy gap between the conduction band of the quantum well and the surrounding substrate. As soon as half the electrons are in the upper state, absorption of new photons is balanced by spontaneous emission and the quantum well layer becomes transparent. For stable operation, all the electrons must be back in the valence band before the next pulse arrives, otherwise the SESAM will be driven to a state of permanent saturation if the nonlinear absorptance is not sufficient. This means the SESAM only has to keep up with the repetition rate, while the pulse duration can be much shorter.

Key parameters in a SESAM are the saturation fluence, the relaxation time, and the modulation depth of the mirror. For a GHz repetition rate, while Mhz is more common, one would expect to require a very high average power to achieve the same level of saturation. To reduce this, a lens with a short focal length can be used to reduce the spot size on the SESAM

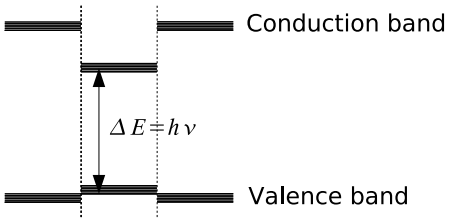

Figure 5.12: *Schematic of principle of homogeneously modelocked laser*

as much as possible. To calculate the fluence of the pulses θ_{pulse}, (assuming the beam is a Gaussian round beam), the average power $P_{average}$, the repetition frequency ν_{rep}, the beam diameter before the focussing lens d_{lens} and the focal distance f of the lens are needed:

$$\theta_{pulse} = \frac{E_{pulse}}{O} \tag{5.17}$$

$$E_{pulse} = \frac{P_{average}}{\nu_{rep}} \tag{5.18}$$

$$O = \frac{1}{4}\pi d_{focus}^2 \tag{5.19}$$

$$d_{focus} = \frac{\lambda f}{d_{lens}} \tag{5.20}$$

O is the surface of the spot of the beam on the SESAM and E_{pulse} the energy of a single pulse.

Modelocking has to start from fluctuations. The random fluctuations of the field (where you would expect excursion in the order of the square root of the number of modes) change into pulsed behaviour if there is enough differentiation in gain (and loss). For 50 competing modes, the pulsed output would vary between all 50 modes in phase (amplitude 50, intensity 2500) and all modes counter-phased (amplitude and intensity 0). The random case would vary around the average for incoherent addition (intensity added incoherently: 50) with fluctuation of seven coherent modes (amplitude 7 or intensity 49) so that you would expect a rage mostly between 0 and 100 over the duration of one repetition period. Thus, the saturation of the SESAM has to happen between twice the average output power (50) and the average output power plus the seven coherent modes (50+49≈100). When the SESAM saturates all modes will see a higher reflectivity from the common

part (e.g. say that the SESAM would be integrated somewhere before the output coupler) and therefore would see a slightly higher feedback for that value of the phase. The gain will stay almost the same (compensating for the total roundtrip losses), and the field amplitude and intensity will also stay the same (decrease a little because the decreased losses).

Table 5.5: *Parameters Batop SESAMs for 980 nm*

Parameter	Symbol	Value	Units
High reflection band (R>99%)	λ	960-1040	nm
Saturable absorptance SESAM 7	A_0	7	%
Saturable absorptance SESAM 18	A_0	18	%
Saturation fluence	θ_{sat}	50	$\mu J/cm^2$
Relaxation time constant	τ	$\leq$10	ps
Non saturable loss SESAM 7	A_{ns}	<0.5	%
Non saturable loss SESAM 18	A_{ns}	<3	%
Chip area		4x4	mm

In table 5.5 the parameters of the two SESAMs available to us for the experiments are shown. The main difference between the two SESAMS is the amount of nonlinear, or saturable absorptance A_0, resulting in different modulation depths. However, from the table, it can also be seen that SESAM 18, with the high A_0=18%, has a bit more loss, 3 %. This loss is relevant at high power (few watts) and might heat and eventually damage the SESAM.

One method to reduce the relaxation time and the fluence level of the SESAM is to apply a voltage over the SESAM, filling a part of the quantum well. This method has been proposed by Heck et. al. [119].

5.6 Numerical model

A model is implemented in Matlab to test the basic feasibility of the proposed SG-laser for modelocking, to explore the influence of certain physical parameters, and to identify promising choices for such parameters in a first experimental test.

5.6.1 Simulation description blocks

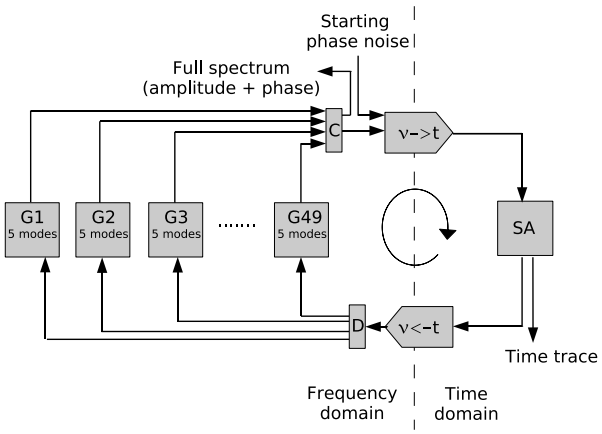

Figure 5.13: *The scheme for the roundtrips in the SG-laser for the numerical model, the gain elements (G1..G49) are modelled in the frequency domain and the saturable absorber is modelled in the time domain, ν-¿t and ν¡-t (inverse) Fourier transformation blocks*

The model is implemented according to the scheme depicted in figure 5.13, which shows the physical processes involved in the mode-locking of a SG-laser. Our model follows the more general lines as given in 119 but, is limited to those details which concern the actual implementation of the physical processes involved. When following the roundtrips through the SG-laser, there is light amplification in each of the lasers separate gain elements (G1..G49), the superposition of the light from the elements into a single beam (C), the temporal modification of the light intensity by a saturable absorber (SA) and, finally, the spectral decomposition of the light in the common arm by the grating dispersion (D). The symbols 'ν-¿t' and 'ν¡-t' indicates a (inverse) Fourier transform, to switch between the time and spectral domain descriptions of the field generated by the laser.

When looking at one cycle of the simulation, the calculations start from phase noise with a flat spectrum which is used here to model the random phase in spontaneous emission. Any intensity peak generated in superposition (C) experiences reduced losses at the saturable absorber. These losses depend on the saturation fluence and saturable absorptance of the absorber. Peaks above the fluence threshold in the time domain, after dispersion by

the grating (D), correspond to a modified amplitude and phase of the field envelopes which enter the gain elements. These field envelopes are then amplified and, after superposition, fed back to the saturable absorber. After a number of roundtrips with a suitable set of parameters, the output from the model corresponds to mode-locked pulses.

To model the overall spectrum of the laser per gain element, five frequencies were assumed to be relevant, briefly called modes. The broadening of the gain from a single element into these five modes is homogeneous, and, if internal competition among these modes is dominant, eventually only one mode will emit light. The spectral range between two adjacent elements was chosen to be 10 times the free spectral range between the modes. More details on the gain curve for the overall spectrum and per element can be found in figure 5.14.

The gain is modelled with three variable parameters, the overall gain profile (flat or parabolically curved like figure 5.14(a)), the number of side-modes (0 or 2, with 2 resulting in 5 modes per element), and the shape of the gain within an element (figure 5.14(c)). The last parameter is not always equal for all modes, due to the spatial mismatch effects discussed in section 5.5.1.

The saturable absorber is characterised by three parameters; the nonlinear absorptance (absorptivity), response time, and the fluence. A fluence is expressed in energy per pulse per square meter. The propagation of waves through the cavity is not simulated and therefore the area is not relevant in our simulation. The energy of a pulse can be approximated as the product of the pulse duration multiplied by the peak intensity (multiplied by a constant to take the shape of the pulse into account). The time duration for a pulse is fixed for pulsed operation, $1/49^{th}$ of a single period for a bandwidth-limited pulse. The peak intensity of a pulse with such a duration required to saturate the absorber will be referred to as fluence level, and defined as a multiple of the average power.

5.6.2 Reference case

In the following basic results are presented, obtained with the described numerical model. In order to demonstrate the basic working of the model and to put constraints on critical parameters involved in the description of the

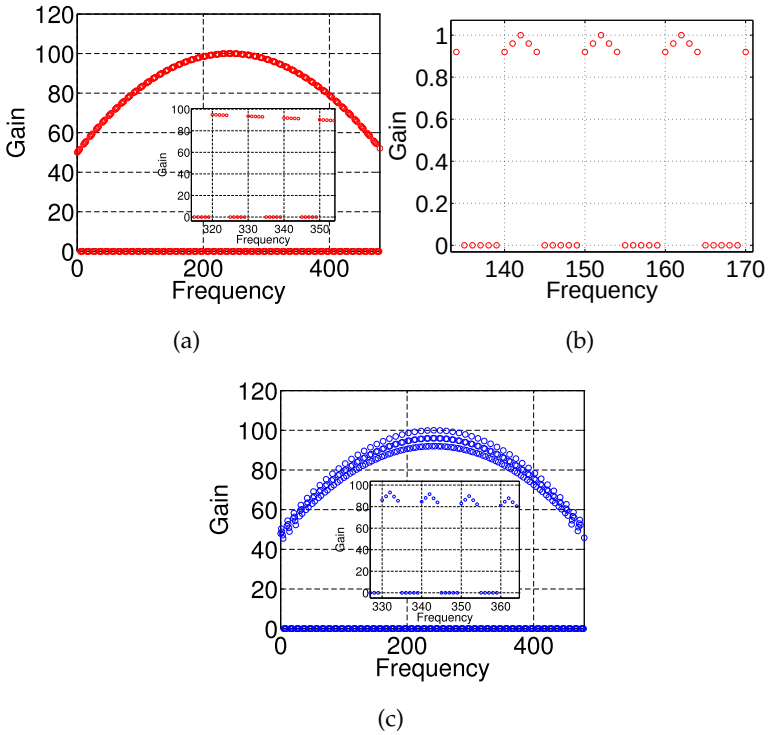

Figure 5.14: *Over the full array the gain is modelled parabolic, see figure (a), with a detail of the same graph in the inset. In figure (b) the gain profile within an element can be seen. Due to a spatial mismatch only the centre-mode perfectly fits the gain element and the adjacent side-modes suffer some loss. The total gain is calculated by multiplying the two curves (a) and (b) for all elements, as can be seen in (c).*

gain and the saturable absorber, calculations are presented with a certain set of model parameters, referred to as the reference simulation. Both for the gain and the absorber a set of the three most critical parameters have been extracted.

For the gain, the gain profile is chosen to be flat at 10^2. For all simulations the roundtrip loss is taken to be 90%. In the reference scenario one mode is amplified in a single gain element, so no gain competition is present.

For the absorber, the fluence level is chosen to be 1.5 times the CW-level. The relaxation time constant τ is defined as a fraction of the pulse period (which is $1/\nu_{rep}$) as $1/20^{th}$ of the pulse period. The nonlinear absorptance is

chosen to be 75%. All the used values for the variable parameters for the gain and the absorber are summarised in table 5.6.

To acquire results all simulations will be run three times. This is needed because they all start from noise and so different runs can give different results depending on the initial condition. In the result, a pulse is considered valid if the peak level is at least half of the maximum achievable peak power. This implies that the peak power should be 1200, since the CW-level is used for normalisation and the maximum peak power is 49^2=2401. When all three runs show pulses with peak powers above the level of 1200, the parameter set for this simulation is considered a pulsing laser.

Table 5.6: *Parameters used in the reference simulation*

Parameter	Value	Units
Gain		
Gain profile over all elements	100 flat	–
Modes per element	1	–
Gain per element	1	–
SESAM		
Fluence level	1.5	cw-level
Relaxation time constant τ	1/20	period time
Nonlinear absorptance	75%	

In a simulation, 1000 roundtrips are calculated in order to reach a steady-state solution. The results of the simulations are available in both the time- and frequency domain. In the frequency domain the resulting amplified spectrum will be shown, and in the time domain the corresponding figure of a pulse train will be presented. The latter can be used to determine pulse-to-pulse differences or pulse shapes.

The results for the reference simulation can be seen in figure 5.15. In figure 5.15(a) a pulse train, of identical pulses, can be observed. Along the y-axis the intensity is plotted in units of the average intensity. According to standard mode-locking theory [37, 43] the maximum peak power for bandwidth-limited pulses should be a factor n above the average power, where n is the number of oscillating modes. In this model the oscillation of 49 modes (see figure 5.13), and a relative peak power of $\approx$2400 is observed,

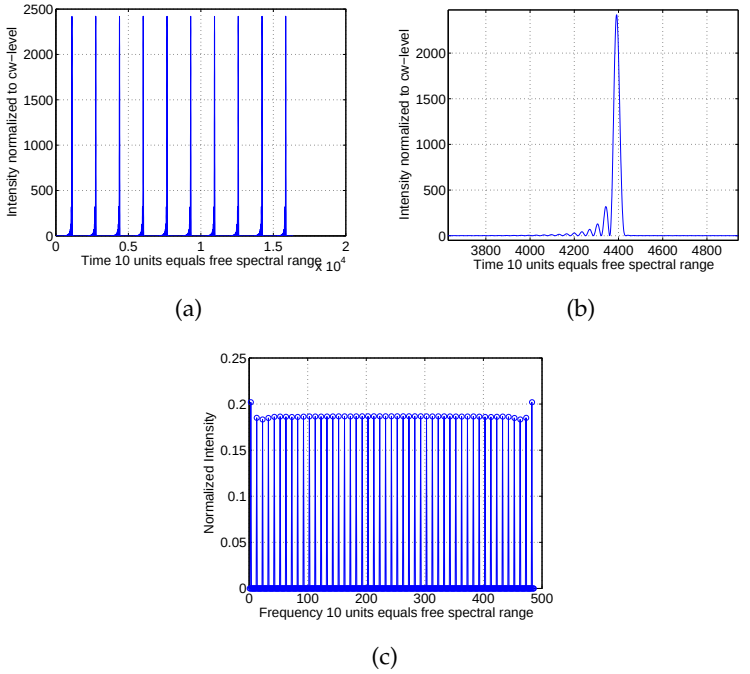

Figure 5.15: *The reference simulation. (a) Pulse train (propagating to the right); (b) A single pulse; (c) The resulting spectrum.*

which indicates that the model is in agreement with standard mode-locking theory. For closer inspection, figure 5.15(b) shows a single pulse. It can be seen that the leading edge of the pulse, on the rhs, is rather steep. This can be interpreted as being caused by the saturable absorber, because this absorbs the strongest at the leading edge of the pulse. In contrast, the falling flank of the pulse passes the absorber when it is partially saturated, which explains the less steep falling edge. Figure 5.15(c) , shows the spectrum associated with the pulse train. The normalisation is chosen to be 10 times the average power, and, indeed, when taking the spectral integral (49 modes with a power of 0.2 each), the simulation displays a power of ten.

From the results of the reference simulation it can be seen, that, if the parameters are suitably chosen, the SG-laser should show mode-locking, seen as an emission of a periodic pulse train and seen as an output spectrum that consists of an evenly spaced comb of single frequencies. It should be noticed, however, that in this reference simulation some parameters were cho-

sen optimistically, such as the flat gain profile, and a single mode per gain element, which leads to zero power in the side-modes in each gain element (see table 5.6). What also can be called an optimistic choice of parameters is a relatively strong value for the nonlinear absorptance and a relatively fast relaxation time for the saturable absorber. To more systematically investigate the influence of more realistic parameter choices, the gain and absorber parameters are varied to determine the sensitivity of the system to their value.

In the next two paragraphs, more realistic gain and absorber parameters are introduced independently. For example, the parameters for the gain section are changed while keeping the absorber parameters constant and vice verse. This shows what the most critical components are when trying to realise a SG-mode-locked laser.

5.6.3 Realistic Gain

A realistic modelling of the gain includes a curved overall spectral gain profile and gain elements in which more modes (not spaced precisely at the repetition frequency) are allowed to oscillate. The gain profile is approximated by a parabolic profile that amplifies the outermost modes with only half the gain (small signal gain 50) of the centre-mode gain (small signal gain 100).

The presence of multiple frequencies in one gain element is modelled through the introduction of side-modes. These side-modes represent modes that fit the long laser cavity (approx 1 m) but are not desired for modelocking. At the gain centre these side modes have a lower gain than the centre frequency as this mode is assumed to overlap best with the gain element. For the outer elements a different profile must be used for the side-modes due to geometrical considerations (see 5.5.1 on α_{center} and α_{outer}). Only two side-modes on each side of the centre-mode are considered, so that 5 modes are present in each the gain element. For the presented the closest side-mode is estimated to have a 96 % overlap with the gain medium, if the center-mode exactly overlaps the gain element. Correspondingly, the outer side-modes have a 92 % overlap. The same spatial side-mode for the overlap were found for each element (except the outermost, as will be explained below), and the side-mode pattern becomes: [0.92 0.96 1 0.96 0.92].

To model the difference in the angles α_{center} and α_{outer} (see section 5.5.1),

which had a relative fault of 0.2 %, the side-modes are modelled differently for the three outermost modes on the left and right side. In this case, the mode fully overlapping the gain element is shifted one mode outwards. The side-mode pattern for the left becomes: [0.96 1 0.96 0.92 0.88]. And for the right: [0.88 0.92 0.96 1 0.96]. Because the mode overlapping the gain element is not the center-mode, the spectral frequency spacing becomes irregular because in homogeneous gain competition the mode with the least loss will be the only emitting mode in a steady state. However, it is possible that the sidebands generated by the absorber can overcome this effect. The parameters of the complete gain section are summarised in table 5.7.

Table 5.7: *Parameters used in the reference simulation*

Parameter	Value	Units
Gain		
Gain profile over all elements	parabolic: 50-100-50	
Modes per element	5	
side-modes pattern left	0.96 1 0.96 0.92 0.88	
side-modes pattern centre	0.92 0.96 1 0.96 0.92	
side-modes pattern right	0.88 0.92 0.96 1 0.96	

The results of calculations with these more realistic gain settings are shown in figure 5.16. The pulse train in figure 5.16(a) and the figure of an individual pulse 5.16(b) show pulses of a good quality, e.g. all are above the chosen minimum peak power level of 1200. However, modulation over the pulses can be seen in figure 5.16(a) . This modulation can be considered less severe, because the individual pulses are of a good quality, with an achieved peak power close to the maximum. The modulation in the time domain shows up as unsuppressed side-modes on the left side of the spectrum. Except for these not fully suppressed side-modes the resulting spectrum shows, compared to the reference simulation, a slightly curved spectrum over the full range.

These results suggest that the different side-mode patterns for the outer-most modes, possible in a SG-laser with a geometry described in section 5.3, is not a severe effect that would inhibit the generation of ultrashort pulses.

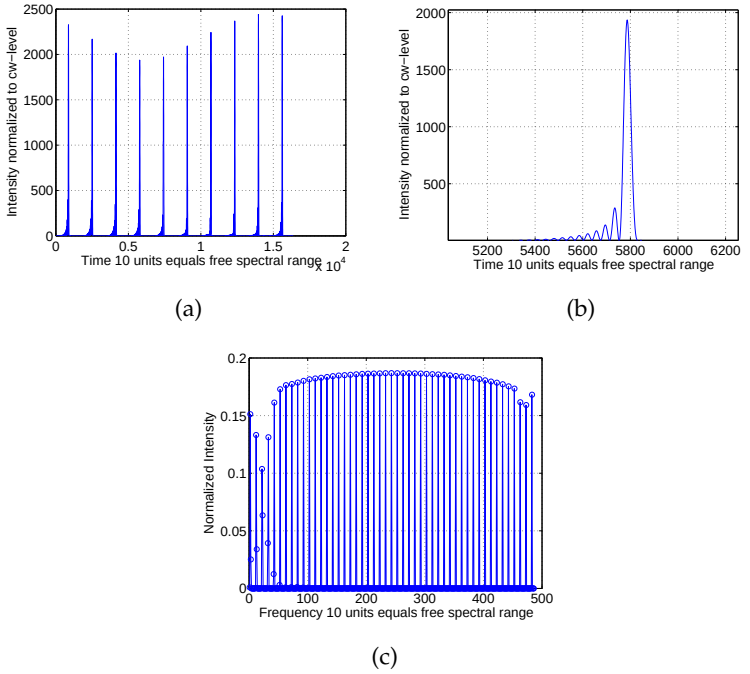

Figure 5.16: *Introducing realistic gain. (a) Pulse train (propagating to the right); (b) A single pulse; (c) The resulting spectrum.*

5.6.4 Restriction of parameters of the saturable absorber

Three parameters are included to model the absorber. First the influence of the relaxation time is investigated, then the nonlinear absorptance and, later, the influence of the saturation fluence.

To model a more realistic absorber with a slow relaxation time and low modulation depth compared to the reference simulation, a relaxation time of half the pulse period is introduced (instead of $1/20^{th}$) and for the modulation depth, 19% is used (instead of 75%). The results of the simulations with these parameters (while keeping the fluence level at 1.5 times the average level), are shown in figure 5.17. It is clear from this figure that the pulse train is severely deteriorated. The spectrum still appears rather smooth, but the time profile is shows that single pulses are not formed, but a number of smaller pulses are generated in a rather random way, each of them with a power that is much lower than the optimum peak power of the reference simulation. However, since all the smaller pulses are well above the fluence level of 1.5 this pulse

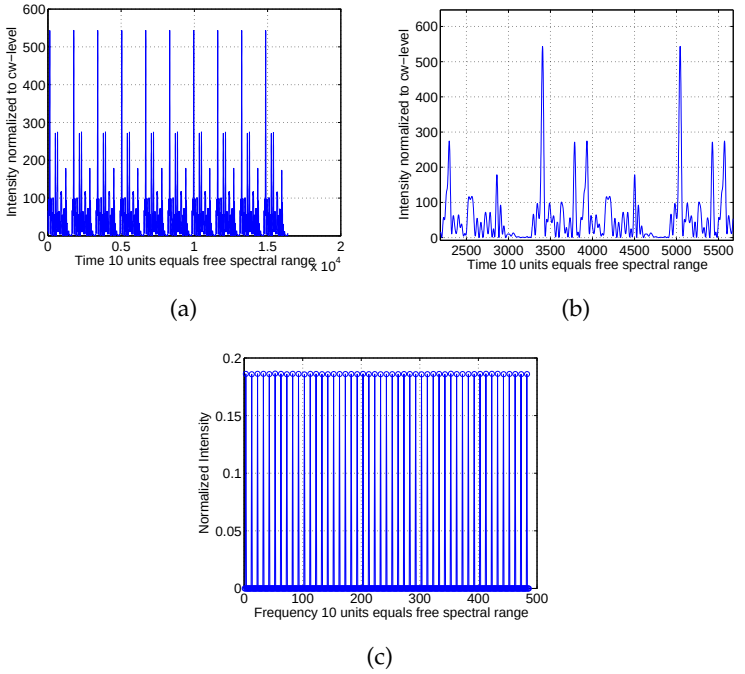

Figure 5.17: *Introducing the absorber. (a) Pulse train; (b) A single pulse; (c) The resulting spectrum.*

train shows long-time stability.

To investigate the effect of increasing the fluence on the peak power and stability of the pulse train, another simulation was done, with a fluence of 15, of which the results are shown in figure 5.18. It can be seen that, although, compared to the reference pulses, the pulse quality is decreased, the resulting pulses are clear and of a good quality, i.e. there are periodically appearing pulses well separated from each other and close to a peak power of 2000 compared to a maximum achievable peak power of 2400. It should be noted, however, that a high saturation fluence also introduces a stronger dependence on the initial conditions, which describes how reliably the laser dynamics would evolve to a mode-locked state. In the 5 runs made, the pulse shoulders varied and the peak intensity varied, between the maximum 2400 and a minimum of 1500. The fluence of 15 times the average energy seems feasible in our system.

In the next simulations, first the fluence level and the nonlinear absorp-

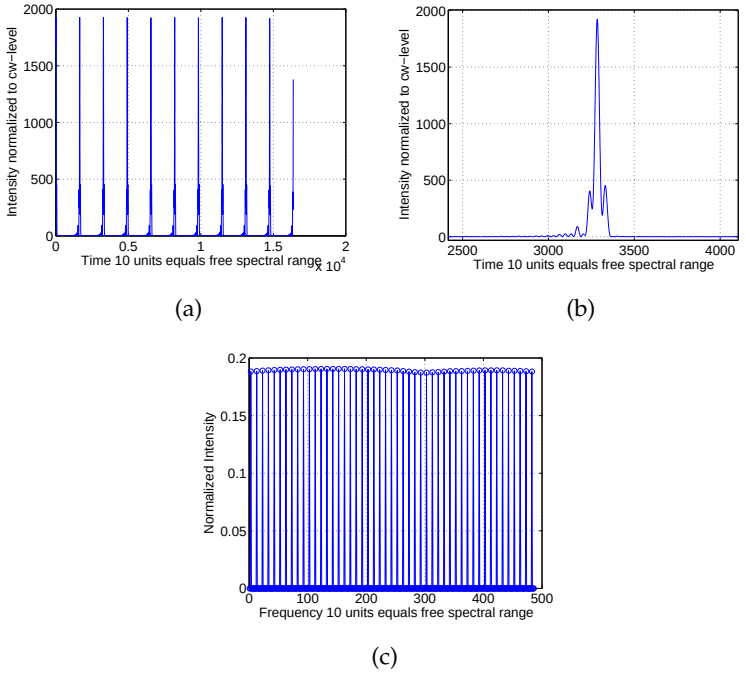

Figure 5.18: *Fluence level increased to 15. (a) Pulse train; (b) A single pulse; (c) The resulting spectrum.*

tance are varied to find pairs of parameter settings where the combination of the two produces pulses with a minimum peak power of 1200 in three simulations. The relaxation time is held fixed at 1/2 of the repetition period time. In the next step the nonlinear absorptance is kept constant at a level of 19% and the relaxation time and the fluence are varied, again to find ranges of parameters in which temporally stable pulses of high quality are produced.

An overview of the results from the first search of paired parameters is presented in figure 5.19, where for several combinations of fluence level and nonlinear absorptance the outcome of the simulation is evaluated. The evaluation was as follows: if in three consecutive simulations, the pulses in the time domain met the requirement of a peak power of at least half the optimal power compared to the reference simulation, the chosen pair of fluence-absorptance is counted as producing pulses of sufficiently quality. These pairs can be found within the grey block in figure 5.19. Below 19% (0.19 in the graph) no pulsing with sufficient quality is found. Above 36% (0.36) no

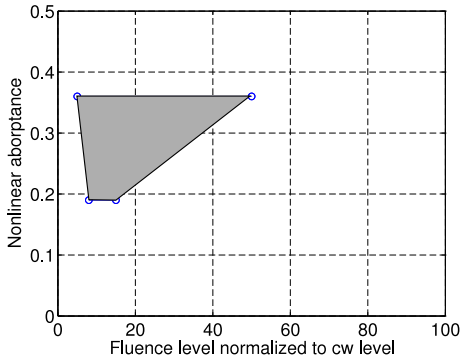

Figure 5.19: *To identify an area within which mode-locking is feasible, the saturation fluence level varied at several values for the nonlinear absorptance at a constant relaxation time of 1/2 the repetition time. The grey area indicates where modelocking is feasible.*

simulations were done, because it is not feasible to acquire an absorber with a fluence above 36% for the experimental setup.

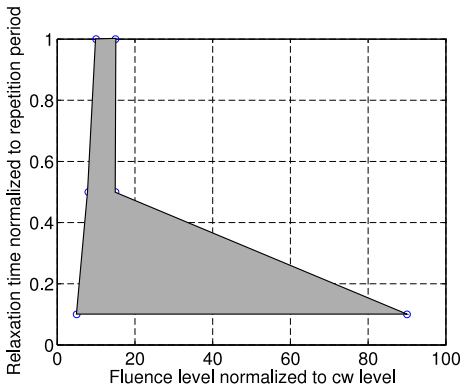

Figure 5.20: *The saturation fluence level was varied for several values of the relaxation time, at a constant nonlinear absorptance of 19%. The grey area indicates where, mode-locking seems feasible.*

Figure 5.20 shows the outcome of the second search for parameter pairs which enable mode-locking. If shorter values for the relaxation time are chosen, the fluence range in which pulses of sufficient quality can be found in simulations rapidly grows. Note that even with a rather slow absorber, when the relaxation time is equal to the repetition period, modelocking can be achieved. However, it can be seen that the fluence has to fall within a small

window of limit-values when an absorber with a long relaxation time is used.

5.6.5 SESAM and gain

To make a final assessment of the feasibility mode-locking in the proposed SG-laser, the more realistic assumption of the gain modelling and more realistic parameters for the saturable absorber are combined in one simulation. The goal of this simulation is to check whether or not new effects emerge as the result of an interplay between gain and absorber properties.

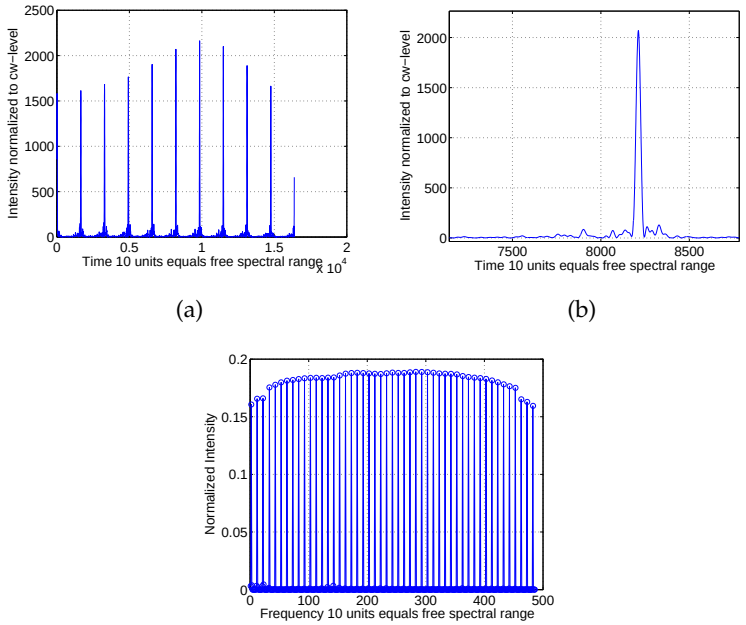

Figure 5.21: *Introducing realistic gain. (a) Pulse train (propagating to the right); (b) A single pulse; (c) The resulting spectrum.*

The results of this full implementation of gain and absorber properties are presented in figure 5.21. When compared to figure 5.16 (gain) and figure 5.18 (absorber), it can be seen that the results look like a linear superposition of gain and absorber-related effects. The modulation of the pulse train's overall envelope due to the side-mode mismatch can clearly be seen. The pulse peak intensity was decreased relative to the maximum achievable level (when compared to the reference simulation). In this figure, which shows

only one a single run of the simulation, the peak levels vary between 1600 and 2100, which results in a good pulse quality for all the pulses. However, the next four simulations showed that the peak power levels varied between 1600 and 400, i.e. this did not meet the requirement named above for successful mode-locking.

So, although it is still seems possible to achieve pulses with the currently available parameters, it is also clear that our experimental attempts with real components could fail or deliver pulses with severely reduced quality. For the gain, the most important parameter contributing to the degradation is the spectral mismatch between the modes in the centre elements and outermost elements. The SESAM however, is more critical. As can be seen in figures 5.19 and 5.20, the observation of mode-locking seems to be largely dependent on using an appropriate value for the nonlinear absorptance and, even more so, for the relaxation time.

5.7 Summary

In this chapter the concept of a separate gain (SG) modelocked laser was introduced and compared to a conventionally modelocked laser. It was explained that an SG-modelocked laser can be of special interest, namely in regimes in which a high repetition rate and a high average power is required.

To prepare a first demonstration of mode-locking an SG-laser, an implementation was designed. This design was based on an array of single-mode diode-laser to provide a large number(49) of separate gain elements and, on a suitable absorber. With this design, the influence of practical potential errors were evaluated, such as geometrical errors, such as the angle α which depends on the spatial position of the element and can introduce spectral mismatch. With these considerations, two potentially usable designs were identified, one with a repetition rate ν_{rep} of 100 GHz and a pulse duration τ_{pulse} of 200 fs, and one with ν_{rep}=67 GHz and τ_{pulse}=300 fs. These designs will form the starting point for experimental studies (chapter 6), and form the basis for further modifications.

In the last part, of the present chapter, the feasibility of mode-locking is investigated in such an SG-laser within a numerical model. The model predicts that mode-locking should be possible over a wide parameter range. Spectral

mismatch due to geometrical deviations were found to only lead to moderate deterioration of the mode-locking while the parameters for the saturable absorber proved critical. Decreasing the relaxation time τ rapidly increases the range for the fluence for which mode-locking is possible, as does an increase of the nonlinear absorptance but this effect is less strong.

Chapter 6

Modelocked diode array laser

Abstract

This chapter contains the experimental results from the operation of the grating-coupled diode array. Two different configurations of the dispersion arm, yielding different pulse durations and repetition rates are shown. Several configurations for the common arm are used, yielding different amounts of output coupling and different fluences on the SESAM. The fluence on the SESAM is the most critical (adjustable) factor to achieve pulsing. In the final results strong, unstable, dynamic behaviour is observed. However, the pulsing is not sufficiently stable to directly characterise the pulse. Improvements such as increasing the optical power in the cavity and reducing the relaxation time of the SESAM, are discussed.

The previous chapter describes two configurations for the dispersion arm, with different focal lengths of the spherical lens in this arm; one with f=200mm and one with f=300mm. The configurations support different pulse characteristics and both will be used in experimental setups.

The focus of this experimental chapter will be on different designs for the *common* part of the cavity. Different designs yield different fluences on the SESAM, which is critical to the nonlinear response of the SESAM. The simulations have already indicated that the SESAM is the most critical component in the setup. The relaxation time and nonlinear absorptance are fixed by the

design of the SESAM, leaving the fluence of the (potential) pulse as the variable parameter. We will start with a simple design with only a single lens in front of the SESAM. Later experiments involve a telescope to reduce losses and further increase the fluence level.

The laser spectrum, as measured by an OSA, is used as the primary indicator for the modelocking behaviour. When the spectrum shows indications of modelocking, an autocorrelator (Inrad model 5-14B) is used to analyse the temporal structure of the beam.

6.1 100 GHz system (f=200 mm)

In the first series of experiments, the f=200 mm spherical lens is used in the dispersion arm, supporting a 200 fs pulse at 100 GHz repetition rate, with a total spectral width of 16 nm. First the laser is built in the most basic configuration, omitting the SESAM and lens and using only a mirror to provide feedback, see figure 6.1. The diode array is water-cooled and driven at 12A. The quarter wave plate, used for output coupling, is a bit smaller than the standard 1“ from the mirror and is not put into the cavity, because it might introduce additional losses.

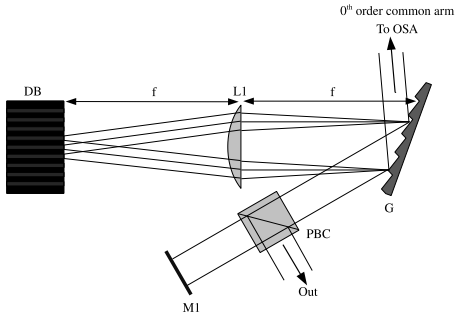

Figure 6.1: *Configuration of a basic common arm. DB=diode bar, L1=spherical lens with focal distance f, G=grating, PBC=polarising beam cube, M1=mirror. The cylindrical lenses in the fast axis of the diode bar are not drawn for simplicity.*

The free-running spectrum of the diode array is measured by blocking the beam between lens L1 and grating G and inserting the fibre leading to the OSA between the beam block and lens L1. All other spectra are measured

using the 0^{th} order reflection of the beam returning from the mirror on the grating G, see figure 6.1. In this beam all the spectral components overlap.

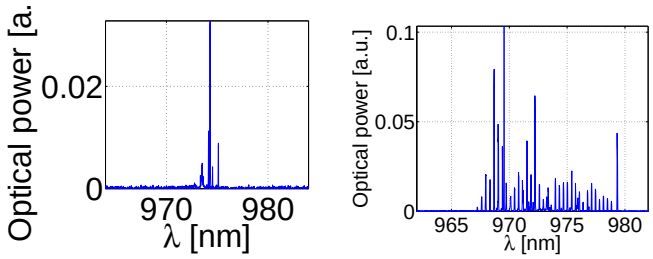

(a) (b)

Figure 6.2: *(a)The free-running spectrum; (b) Spectrum of grating-locked diode bar with only a mirror in the common arm.*

Figure 6.2 shows a measured spectrum for the basic configuration. The spectrum is 12 nm wide and contains 35 modes. The modespacing is 0.3 nm which fits with theory. Within the resolution of the OSA (0.01 nm), the spectrum is regularly spaced, except for some low intensity modes that can be seen close to 969 nm and 976 nm. Between the modes, no intensity is detected, indicating that the emission is dominated by the external cavity for each wavelength/element in the array. The mode intensities are neither equal nor regular indicating possible residual interferences.

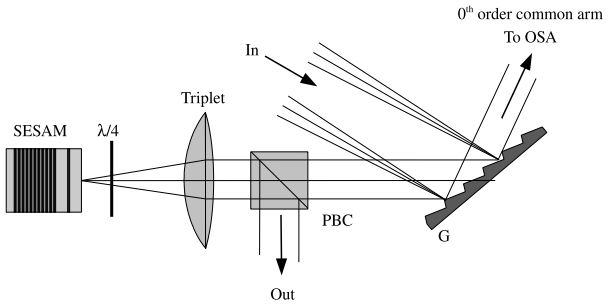

Figure 6.3: *The common arm with a triplet*

Next the SESAM and a lens are introduced. A triplet with a focal distance of 70 mm and a diameter of 60 mm is used because it creates a good quality focal spot and the large free aperture, avoids insertion losses, see figure 6.3. Two different SESAMs are used, SESAM 18 and SESAM 7, where the number

refers to the nonlinear absorptance: 18 % for SESAM 18 and 7 % for SESAM 7. More details about these two SESAMs can be found in table 5.5 on page 106. In general, a higher nonlinear absorbency is preferable to obtain modelocking but higher nonlinear absorption comes with a higher saturation fluence. This is not immediately clear from the table where the saturation fluence is specified only as "below 50 μJ/cm^2" for both. The diode array is powered with a 25 A current and the output coupling is set such that the output power is between 700 mW and 1 W.

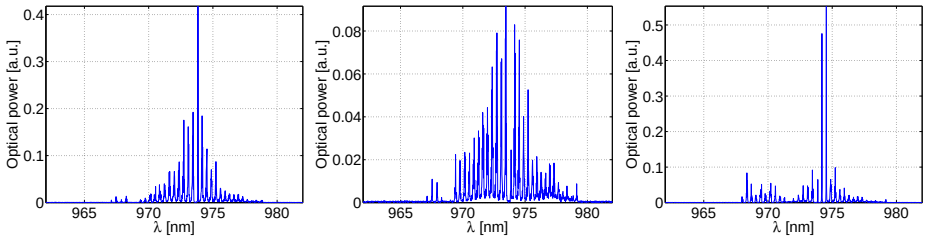

(a) (b) (c)

Figure 6.4: *Spectra measured with the triplet in the common arm and SESAM 18. The spectrum is shown to be unstable in time.*

In figures 6.4 and 6.5, measured spectra are shown for SESAM 18 and 7 respectively. In both cases the spectra were unstable in time and the spectra shown are snapshots. The changes take place on a speed exceeding the scanning speed of the OSA, which is on the second scale so that each scan is different. The intensity between the modes is clearly not zero at some postions in figure 6.4(b) , and even for large sections of the spectrum in figure 6.5(c) , indicating some lasing that is not dominated by the external cavity. Quite a few times the spectrum appears to be dominated by modes with intensities much higher than the rest (figure 6.4(c) ,6.5(b)).

A possible explanation for the unstable behaviour in time is the relaxation time constant for both SESAMs, specified to be $\leq$10 ps, which is rather high for a repetition rate of 100 GHz. To decrease the repetition rate, a different spherical lens is used in the dispersion part of the cavity, with an f=300 mm instead of 200 mm. This way a smaller spectral band is projected over the width of the diode array, decreasing the mode spacing and the repetition rate.

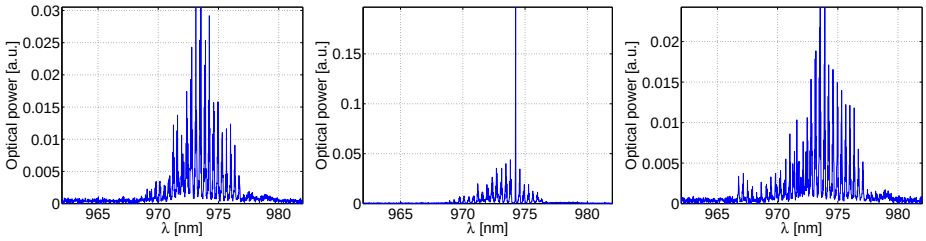

(a) (b) (c)

Figure 6.5: *Spectra measured with the triplet in the common arm and SESAM 7. The spectrum shows to be unstable in time.*

6.2 67 GHz system (f=300 mm)

All the following experiments were done with a 300 mm lens in the dispersion part of the cavity. The rest of the setup remained the same. SESAM 18 was used and the diode-current was 20 A. The output of the lase was sent to an autocorrelator to measure the time domain properties. In this autocorrelator two glass blocks with a thickness of 35 mm rotate in different arms of the autocorrelator, with a fixed angle between the blocks, to induce different time delays. The light from both arms was combined in a nonlinear crystal and a photomultiplier tube measures the light generated by second harmonic generation.

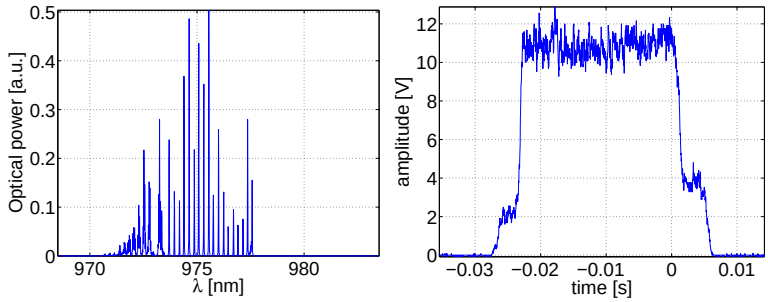

(a) (b)

Figure 6.6: *A spectrum and an autocorrelation trace measured with the triplet lens in the common arm.*

A spectrum and a timetrace are shown in figure 6.6. In the spectrum 20 modes appear to be lasing in an external cavity mode, emitting a single wave-

length with no detectable intensity between the modes. On the short wavelength side of the spectrum the modes are not regular and not well separated. The mode spacing is 0.2 nm as expected. The spectrum was stable in time

In figure 6.6(b) the corresponding autocorrelation trace is shown. Due to the rotating glass blocks the light reaches the detector only half the time, causing rectangular measurement windows. One rectangle represents a delay of 119 ps. If pulses shorter than this time are present in the signal, strong spikes on top of this block signal are expected. We would expect 8 pulses for a 68 GHz rate. In figure 6.6(b) , no spikes can be seen, indicating that the laser is not pulsing at a discernible repetition frequency.

Apparently the switch from 100 GHz to 68 GHz, because of the relaxation time of the SESAM, was not sufficient. However, for the remainder we keep this configuration because of the fluence; at the same average power, the energy per pulse is also higher for the 68 GHz repetition rate. This is because the pulse duration increases, while the peak intensity, the square of the number of modes and emitters, remains the same.

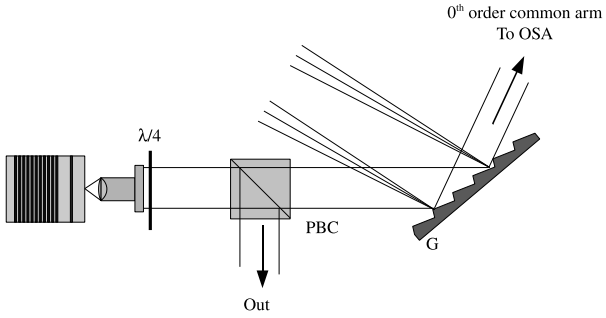

Figure 6.7: *The common arm with an objective*

The lack of any dynamic signature in the autocorrelator-trace makes it likely the fluence threshold of the SESAM is not yet met. To improve the saturation of the SESAM, the triplet lens is replaced by a microscope objective with a numerical aperture (NA) of 0.32, see figure 6.7. Reducing the focal length also reduces the size of the focal spot, which increases the fluence on the SESAM.

A spectrum and autocorrelate for a the common arm with the objective can be seen in figure 6.8. The autocorrelation in figure 6.8(b) , shows no puls-

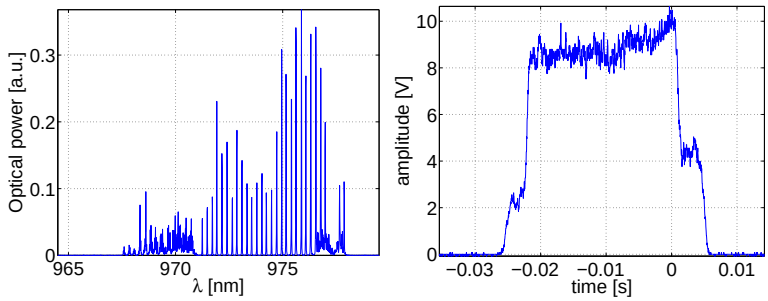

(a) (b)

Figure 6.8: *A spectrum and an autocorrelation trace for the common arm with the objective lens before the SESAM.*

ing. The spectrum appears dominated by the external cavity, with regularly spaced modes except at the outer edges.

6.3 Telescope system

To further improve the fluence on the SESAM, a telescope is introduced in the common arm of the laser, see figure 6.9. The telescope consists of a 2" spherical singlet with a focal distance of 200 mm and a 1" singlet with a focal distance of 50 mm. It reduces the beamsize by a factor 4, going from a beam diameter of 15 mm to 4 mm, to fit the complete beam into the aperture of the objective.

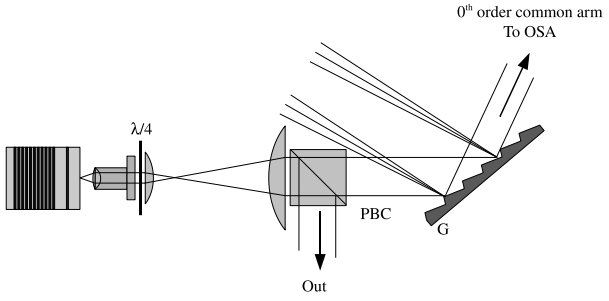

Figure 6.9: *The common arm with a telescope before the objective*

figure 6.10, shows the spectrum for the configuration with the telescope at an output power is 300 mW. In this configuration the maximum achievable

output power is improved from 1 W to 2 W, indicating reduced losses.

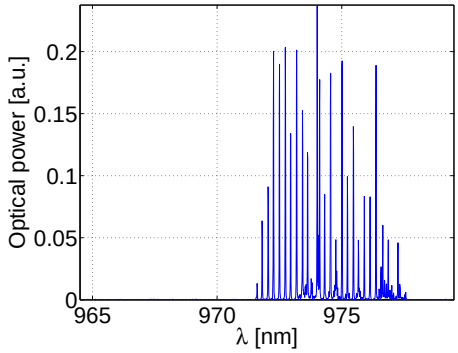

Figure 6.10: *Typical spectrum with the telescope in the common arm.*

An example of an autocorrelation trace can be found in figure 6.11, in which figure 6.11(b) is the rightmost part of the trace in figure 6.11(a) . These traces do not resemble a clean autocorrelation trace but they are far from featureless as the autocorrelation traces in figures 6.6 and 6.8. The peaks are too strong to be considered only noise and they appear often, indicating more dynamic behaviour than seen before.

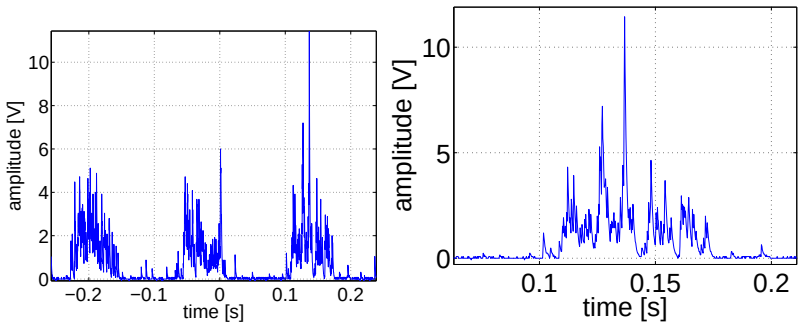

(a) (b)

Figure 6.11: *A spectrum and an autocorrelation trace for the common arm with the objective lens before the SESAM.*

6.4 Discussion

The autocorrelations presented suggest that the laser is pulsing for time intervals in the order of milliseconds, shorter than the time required to trace a full autocorrelator signal. It is likely that this is due to insufficient fluence. Based on measurements of the beam size and the optical power inside the cavity (while the laser was unlocked) we estimate the pulse energy to be between two and five times the nominally required fluence for the SESAM. Translating this to the simulation results in figure 5.19 (page 117) and 5.20 (page 117), this compares to a fluence level of 1200 for a factor 2 (2400*τ_{pulse}/2*τ_{pulse}) and for a factor 5, 480. Both values are indeed outside the stable pulsing window.

Tighter focusing is not practical and likely to suffer from chromatic abberations. However, the response of the SESAM can be improved by the introduction of a bias. This technique has only been demonstrated a few times but showed a reduction of the response time of the SESAM, by a factor 50-100. This would bring the setup well within the stable pulsing regime.

6.5 Summary

In this section two configurations of the dispersion arm have been examined. The configuration with a lens of f=300mm in the dispersion part of the cavity was found to perform better in terms of output power and dynamic behaviour, despite the increased losses due to the large beam size in the dispersion part. The energy in a pulse is expected to be superior in this configuration.

The key to modelocking is in the SESAM and the saturation fluence. Several configurations of the common arm have been tried to maximise the amount of fluence. A maximum fluence was found for the setup in which the telescope is applied, decreasing the beam size to a suitable size before the light is strongly focused onto the SESAM by an objective lens.

Two major possibilities for improvement are clear: the amount of energy in the cavity can be increased by reducing insertion losses. Much light is lost at the first cylindrical lens. A normal lens with an f/d smaller than the lens we currently use is not available but a microlens directly in front of the diode bar could be considered, however, backreflections must be avoided.

Another possibility is to apply a bias over the quantum well of the SESAM in order to reduce the relaxation time by a factor of 50-100. Despite the work still to be done, the preliminary experiments shown in this chapter show some distinct indications yet unstable mode-locking is measured, and with the still possible improvements the SG-modelocked laser is likely to be feasible.

Chapter 7

Summary and conclusions

In this thesis three experiments were presented. The aim in all of these experiments was to improve the beam quality of high-power diode lasers, using nonlinear-optical feedback. In the first two experiments, two different photorefractive materials were used for injection-locking of a high-power Broad Area Laser (BAL) diode via holographic feedback to the single frequency of an external laser source. In the last experiment, a saturable absorber mirror was used to obtain multi-frequency, modelocked operation of an array of single-stripe diode lasers for the generation of a train of ultrashort pulses.

In the first experiment, we employed the photorefractive response of a $BaTiO_3$ crystal to provide feedback from a double phase conjugated mirror (DPCM) for injection-locking the BAL to a primary laser, which is a continuous-wave, single-frequency Ti:Sa laser with a high-quality (near diffraction limited) output beam. With this we have shown what we believe to be the first locking of a BAL to the single-frequency spectrum of a primary laser using a DPCM. The locking remained stable for extended time intervals (>30 minutes) by suppressing parasitic gratings via a temporally periodic phase shift introduced by piezo-driven mirrors. The best stability was seen when the injected light was wavelength-detuned with regard to the spectrum of the free-running diode by about 1nm. Locking was observed with either the fast axis or the slow axis of the diode oriented in the plane formed by the propagation vector and the c-axis of the crystal, however the locking showed a higher temporal stability for the orientation along the fast axis. When looking at the complex spatial shape of the output beam from the BAL, the advantage of the

feedback from the DCPM is that it does not impose any particular beam shape on the diode emission. Thereby, although imposing single-frequency operation, the DCPM feedback allows that the diode oscillation self-organises into a preferred superposition of multiple-transverse modes such that the locked output power is maximised for the injected frequency. This is the case because, independent of the spatial mode pattern assumed by the diode, the hologram in the crystal adjusts such that the high-quality beam from the primary laser is diffracted into the same beam pattern (of high complexity) that is emitted by the diode, thereby providing an optimum spatial mode overlap for injection locking. Importantly, even when then the primary laser beam is blocked, the hologram established via prior locking should then maintain single-frequency operation in the same complex-shaped mode superposition selected by the diode. In this case the multi-mode output from the diode should be diffracted by the hologram into a near diffraction limited beam resembling that of the formerly injected primary laser. Indeed, in our experiments we observed a single-frequency, round beam of high spatial quality diffracted from the hologram, after the formerly injected primary laser was blocked, while the diode remained oscillating in its preferred, spatially complex mode superposition due to holographic feedback. The latter observation is currently limited to time intervals below the response time of the DCPM mirror, i.e., to the photorefractive response time of the used BaTiO3 crystal.

In the second experiment the photorefractive crystal was replaced by a polymer. The motivation for this is that polymeres are much less susceptible to mechanical stress and temperature changes, that a much faster response can be obtained, that the chemical composition can be varied for an optimisation, that a higher diffraction efficiency can be obtained, and that the fluid-state of the polymer allows for geometries that suppress undesired feedback paths. In our experiments we made use of the latter by using the polymer in the form of a thin-film device. With this geometry we investigated holographic injection-locking of the BAL in a somehat different arrangement based on Four Wave Mixing (FWM). In these experiments, we have shown what we believe to be the first holographic injection locking of a BAL using a photorefractive polymer. In contrast to the DPCM setup, in the FWM setup, a spectral matching between one of the modes of the BAL and that of the Ti:Sa laser was required to achieve locking. So far, locking was maintained for up

to 5 minutes but the experimental data suggest that an active stabilisation of the diode temperature (instead of passive cooling) can further extend the locking time.

In the last experiment, an array of 49 single-spatial-mode diode emitters (elements) fabricated on the same chip was used instead of a BAL. In the free-running case the output from the array can attain a high average power (30 Watt). However, the spatial quality of the output is low due to the large width over which the arrays emits (1 cm). The spectral quality is low as well because it is formed by the incoherent superposition of the emitters, each operating at a different wavelength, or set of wavelengths. In a first step, in order to obtain a high spatial quality we spatially superimpose the beams from the individual elements with a grating to form a common beam and by using a feedback mirror in the common beam. In this setup, which may be termed a separate gain (SG) multimode laser, a comb-like spectrum is generated, because each diode element in the array receives feedback at a wavelength that is slightly different from that of the neighbouring elements. Nevertheless, the spectral spacing and the overall spectral envelope in this comb remains somewhat random, while the random phasing of the individual emitters gives rise to the typical, random fluctuations found in multimode-lasers.

To increase the temporal quality as well, we introduce a saturable absorber into the common-beam feedback arm of the SG-laser, a SESAM (semiconductor saturable absorber mirror) in our case. The intended function of the absorber is to induce pulsed operation by passive modelocking which constitutes a novel concept for such separate gain lasers because it provides a number of advantages, as we explored in a numerical modelling of the laser dynamics. The repetition rate of the laser is no longer associated with the overall cavity length but it is determined by the dispersion of the grating and the physical spacing of the diode elements on the array. Thereby high (tens of GHz) repetition rates can be achieved Furthermore, the laser can be considered as operating with a inhomogeneously broadened gain. This should reduce perturbing nonlinear effects in the gain elements, such as the deterioration of ultrashort pulses due to gain saturation, because each single frequency in the comb-spectrum is separately amplified as in a continuous wave laser.

In the set of experiments hat we performed, first signs of modelocking

through the saturable absorber were observed, although the generation of a regular train of ultrahort pulses was not successful so far. Two signatures for the inset of partial modelocking were detected. The first is a smoothening of the overall envelope of the lasers power spectrum and the second, found in intensity-autocorrelation measurements, is the occurrence of sharp temporal spikes, above the fluctuating background expected from a non-modelocked laser. These experiments and our numerical modelling indicate that further improvements for generating a regular train of pulses (in this case with about 300fs duration and a repetition rate of about 70GHz) appears achievable. This would require to use absorbers with lower saturation fluence or faster response time, or by reducing the repetition rate via higher dispersion in the dispersion arm.

Bibliography

[1] A. Einstein. "Zur Quantentheorie der Strahlung". *Phys. Z.* **18**, 121–128 (1917).

[2] J.P. Gordon, J. Zeiger and C.H. Townes. "Molecular microwave oscillator and new hyperfine structure in the microwave spectrum of NH_3". *Phys. Rev.* **95**, 282–284 (1954).

[3] T.H. Maiman. "Stimulated Optical Radiation in Ruby". *Nature* **187**, 493–494 (1960).

[4] J. Lowen and R.H. Rediker. "Gallium-arsenide diffused dioded". *J. Electrochem. Soc.* **107**, 26–29 (1960).

[5] R.N. Hall, G.E. Fenner, J.D. Kingsley, T.J. Soltys and R.O. Carlson. "Coherent light emission from GaAs junctions". *Phys. Rev. Lett.* **9**, 366–369 (1962).

[6] D. Gabor. "A new microscopic principle". *Nature* **161**, 777–778 (1948).

[7] C. Huygens. "Oeuvres Complètes de Christiaan Huygens. Publiées par la Société Hollandaise des Sciences (22 vols.)". In *Vol. 5* pages 246–249. Den Haag: Martinus Nijhoff (1888-1950). Huygens to Moray, Feb 27 1665.

[8] K. Itaya, G. Hatakoshi, Y. Watanabe, M. Ishikawa and Y. Uematsu. "High-power cw operation of broad area InGaAIP visible light laser diodes". *Elect. Lett.* **26**, 214–215 (1990).

[9] "Thorlabs catalogue volume 19" (2008). www.thorlabs.com.

[10] T.Y. Fan. "Laser beam combining for high-power, high-radiance sources". *IEEE J. Sel. Top. in Quantum Electron.* **11**, 567–577 (2005).

[11] J.W. Crowe and W.E. Ahearn. "External cavity coupling and phase locking of gallium arsenide injection lasers". *IEEE J. Quantum Electron* **4**, 169–172 (1968).

[12] E.M. Phillip-Rutz. "Spatially coherent radiation from an array of GaAs lasers". *Appl. Phys. Lett.* **26**, 475–477 (1975).

[13] D.R. Scifres, R.D. Burnham and W. Steifer. "Phase-locked semiconductor laser array". *Appl. Phys. Lett.* **33**, 1015–1017 (1978).

[14] S. Sanders, R. Waarts, D. Nam, D. Welch, D. Scifres, J.C. Ehlert, W.J. Cassarly, J.M. Finlan and K.M. Flood. "High power coherent two-dimensional semiconductor laser array". *Appl. Phys. Lett.* **64**, 1478–1480 (1994).

[15] L. Shimshi A.A. Ishaaya, N. Davidson and A.A. Friesem. "Coherent addition of spatially incoherent light beams". *Opt. Expr.* **12**, 4929–4933 (2004).

[16] S. Kobayashi and T. Kimura. "Injection locking characteristics of an AlGaAs semiconductor laser". *IEEE J. Quantum Electron.* **16**, 915–917 (1980).

[17] G.L. Abbas, S. Yang, V.W.S. Chan and J.G. Fujimoto. "Injection behavior of high-power broad-area diode lasers". *Opt. Lett.* **12**, 605–607 (1987).

[18] M.W. Wright and J.G. McInerney. "Injection locking semiconductor lasers with phase conjugate feedback". *Opt. Comm.* **110**, 689–698 (1994).

[19] A. Jechow, V. Raab and R. Menzel. "High cw power using an external cavity for spectral beam combining of diode laser-bar emission". *Appl. Opt.* **45**, 3545–3547 (2006).

[20] S. Kobayashi, H. Nishmoto and R. Lang. "Experimental observation of asymmetric detuning characteristics in semiconductor laser injection locking". *Elect. Lett.* **18**, 54–56 (1981).

[21] R. Lang. "Injection locking properties of a semiconductor laser". *IEEE J. Quantum Electron.* **18**, 976–983 (1982).

[22] S. Wieczorek, B. Krauskopf, T.B. Simpson and D. Lenstra. "The dynamical complexity of optically injected semiconductor lasers". *Phys. Rep.* **416**, 1–128 (2005).

[23] C.J. Chang-Hasnain, J. Berger, D.R. Scifres, W. Sreifer, J.R. Whinery and A. Dienes. "High power with high efficiency in a narrow single-lobed beam from a diode laser array in an external cavity". *Appl. Phys. Lett.* **50**, 1465–1467 (1987).

[24] V. Raab and R. Menzel. "External resonator design for high-power lasers diodes that yields 400 mW of TEM_{00} power". *Opt. Lett.* **27**, 167–169 (2002).

[25] R.M.R. Pillai and E.M. Garmire. "Paraxial-misalignment insensitive external-cavity semiconductor-laer array emitting near-diffraction limited single-lobed beam". *IEEE J. Quantum Electron.* **32**, 996–1008 (1996).

[26] T. Shimura, M. Tamura and K. Kuroda. "Injection locking and mode switching of a diode laser with a double phase-conjugate mirror". *Opt. Lett.* **18**, 1645–1647 (1993).

[27] S. MacCormack, J. Feinberg and M.H. Garrett. "Injection locking a laser-diode array with a phase-conjugate beam". *Opt. Lett.* **19**, 120–122 (1994).

[28] H. Wang, N. Yoshikawa, S. Yoshikado and T. Aruga. "Mutually pumped phase conjugator with a rainbow configuration in $BaTiO_3$:Ce crystal using nanosecond pulses". *Opt. Lett.* **21**, 561–563 (1996).

[29] K. Iida, H. Horiuchi, O. Matoba, T. Omatsu, T. Shimura and K. Kuroda. "Injection locking of a broad-area diode laser through a double phase-conjugate mirror". *Opt. Commun.* **146**, 6–10 (1998).

[30] C.C. Chang. "Multiple beam coupling using a novel barium titanate mutually pumped phase conjugator". *Jpn. J. Appl. Phys.* **37**, L512–L515 (1998).

[31] H. Horiuchi, T. Shimura, T. Omatsu, O. Matoba and K. Kuroda. "Narrow bandwidth operation of high-power broad-area diode laser using cascaded phase-conjugate injection locking". *Appl. Phys. B* **68**, 1021–1025 (1999).

[32] C.C. Chang, Y.P. Tong, T.C. Chen, H.F. Yau and P.X. Ye. "Mutually pumped phase conjugator using a $BaTiO_3$ crystal having two inclined faces". *Appl. Phys. B* **71**, 47–50 (2000).

[33] F. Wang, A. Hermerschmidt, P. Pogany, S.X. Dou and H.J. Eichler. "Enhanced performance of a mutually pumped phase-conjugation setup using two photorefractive crystals". *Appl. Phys. B* **72**, 755–759 (2001).

[34] F. Wang, A. Hermerschmidt and H.J. Eichler. "High-power narrowed-bandwidth output of a broad-area multiple-stripe diode laser with photorefractive phase-conjugated injection". *Opt. Commun.* **209**, 391–395 (2002).

[35] J. Wilson and J. Hawkes. "Optoelectronics, an introduction". Prentice Hall Europe London (1998).

[36] T. Numai. "Fundamentals of Semiconductor Lasers". Springer New York (2004).

[37] A.E. Siegman. "Lasers". University Science Books Sausalito (1986).

[38] H.L. Stover and W. H. Steier. "Locking of laser oscillators by light injection". *Appl. Phys. Lett* **8**, 91–93 (1966).

[39] F. Mogensen, H. Olesen and G. Jacobsen. "Locking conditions and stability properties for a semiconductor laser with external light injection". *IEEE J. Quantum Electron.* **21**, 784–793 (1985).

[40] I. Petitbon, P. Gallion, G. Debarge and C. Chabran. "Locking bandwidth and relaxation oscillations of an injection-locked semiconductor laser". *IEEE J. Quantum Electron.* **24**, 148–154 (1988).

[41] C. Guignard and P. Besnard. "Experimental injection map of semiconductor laser submitted to filtered feedback". *Opt. and Quantum Electon.* **38**, 411–428 (2006).

[42] Y. Yamamoto. "Coherence, amplification and quantum effects in semiconductor lasers". Pure and applied optics. John Wiley & Sons Inc. New York (1991).

[43] O. Svelto. "Principles of Lasers" chapter 5. Plenum Press New York 4th edition (1998).

[44] B.Y. Zeldovich, V.I. Popovichev, V.V. Ragulskii and F.S. Faisullov. "Connection between the wave fronts of the reflected and exciting light in stimulated Mandel'shtam-Brillioun scattering". *Sov. Phys. JETP* **15**, 109 (1972).

[45] E. Hecht. "Optics". Addison-Wesley New York 4th edition (2002).

[46] F.A. Jenkins and H.E. White. "Fundamentals of ptics". McGraw-Hill Singapore 4th edition (1976).

[47] F.S. Chen. "A laser-induced inhomogeneity of refractive indices in KTN". *J. Appl. Phys.* **38**, 3418–3420 (1967).

[48] D.D. Nolte. "Photorefractive effects and materials". Kluwer Academic Publishers Boston (1995).

[49] P. Yeh. "Introduction to photorefractive nonlinear optics". John Wiley & Sons Inc. New York (1993).

[50] K. Buse, A. Adibi and D. Psaltis. "Non-volatile holographic storage in doubly doped crystals". *Nature* **393**, 665–668 (1998).

[51] D. Day, M. Gu and A. Smallridge. "Rewritable 3D bit optical data storage in a PMMA-based photorefractive polymer". *Adv. Mater.* **13**, 1005–1007 (2001).

[52] Z. Chen, M. Asparo, O. Ostroverkhova, W.F. Moerner, M. He and R.J. Twieg. "Self-trapping of light in an organic photorefractive glass". *Opt. Lett.* **28**, 2509–2511 (2003).

[53] P. Yu, M. Mustata, J.J Turek, P.M.W French, M.R. Melloch and D.D. Nolte. "Holographic optical coherence imaging of tumor spheroids". *Appl. Phys. Lett.* **83**, 575–577 (2003).

[54] P. Dean, M.R. Dickinson and D.P. West. "Depth-resolved holographic imaging through scattering media by use of a photorefractive polymer composite device in the near infrared". *Opt. Lett.* **30**, 1941–1943 (2005).

[55] K. Jeong, L. Peng, J.J. Turek, M.R. Melloch and D.D. Nolte. "Fourier-domain holographic optical coherence imaging of tumor spheroids and mouse eye". *Appl. Opt.* **44**, 1798–1805 (2005).

[56] M. Lesaffre, F. Jean, F. Ramaz and A.C. Boccara. "In situ monitoring of the photorefractive response time in a self-adaptive wavefront holography setup developed for accousto-optic imaging". *Opt. Expr.* **15**, 1030–1042 (2006).

[57] S. Ducharme, J.C. Scott, R.J. Twieg and W.E. Moerner. "Observation of the photorefractive effect in a polymer". *Phys. Rev. Lett.* **66**, 1846–1848 (1991).

[58] H.M. Smith, editor. "Holographic Recording Materials" volume 20 of *Topics in Applied Physics*. Springer-Verlag (1997).

[59] O. Ostroverkhova and M.E. Moerner. "Organic photorefractives: mechanisms, materials and applications". *Chem. Rev.* **104**, 3267–3314 (2004).

[60] W.E. Moerner and S.M. Silence. "Polymeric photorefractive materials". *Chem. Rev.* **84**, 127–155 (1994).

[61] A.Yariv. "Quantum Electronics" chapter 19. John Wiley & sons 3rd edition (1988).

[62] M.C.J.M. Donckers, S.M. Silence, C.A. Walsh, F. Hache, D.M. Burland, W.E. Moerner and R.J. Twieg. "Net two-beam-coupling gain in a polymeric photorefractive material". *Opt. Lett.* **18**, 1044–1046 (1993).

[63] M.E. Orczyk, B. Swedek, J. Zieba and P.N. Prasad. "Enhanced phtorefractive performance in a photorefractive polymeric composite". *J. Appl. Phys.* **76**, 4995–4998 (1994).

[64] A. Grunnet-Jepsen, C.L. Thompson, R.J. Twieg and W.E. Moerner. "High performance photorefractive polymer with improved stability". *Appl. Phys. Lett.* **70**, 1515–1517 (1997).

[65] W.E. Moerner, S.M. Silence adn F. Hache and G.C. Bjorklund. "Orientally enhanced photorefractive effect in polymers". *J. Opt. Soc. Am. B* **11**, 320–330 (1994).

[66] M.D. Ewbank. "Mechanism for photorefractive phase conjugation using incoherent beams". *Opt. Lett.* **13**, 47–49 (1988).

[67] P. Yeh, T.Y. Chang and M.D. Ewbank. "Model for mutually pumped phase conjugation". *J. Opt. Soc. Am. B* **8**, 1743–1749 (1988).

[68] D. Statman and B. Liby. "Two-beam cross coupling from mutually incoherent lasers". *J. Opt. Soc. Am. B* **6**, 1884–1983 (1988).

[69] Q.B. He, P. Yeh, C. Gu and R.R. Neurgaonkar. "Multigrading cometition effects in photorefractive mutually pumped phase conjugation". *J. Opt. Soc. Am. B* **9**, 114–120 (1992).

[70] M. Cronin-Golomb, B. Fischer, J.O. White and A. Yariv. "Theory and applications of four-wave mixing in photorefractive media". *IEEE J. Quantum Electron* **12**, 12–30 (1984).

[71] S. Sternklar, S. Weiss, M. Segev and B. Fischer. "Beam coupling and locking of lasers using photorefractive four-wave mixing". *Opt. Lett.* **11**, 528–530 (1986).

[72] S. Weiss, S Sternklar and B. Fischer. "Double phase-conjugate mirror: analysis, demonstration and applications". *Opt. Lett.* **12**, 114–116 (1987).

[73] R. Eason and A.M.C. Smout. "Bistability and noncommutative behavior of multiple-beam self-pulsing and self-pumping in $BaTiO_3$". *Opt. Lett.* **12**, 51–53 (1987).

[74] Y. Fainman, E Klancnik and S.H. Lee. "Optimal coherent image amplification by two-wave coupling in photorefractive $BaTiO_3$". *Opt. Eng.* **25**, 228–234 (1986).

[75] C. Mailhan, M. Goetz, N. Fressengeas and G. Kugel. "Insight into a new geometrical approach to beam fanning in $BaTiO_3$". *J. Opt. Soc. Am. B* **18**, 64–74 (2001).

[76] C. Mailhan, N. Fressengeas, M. Goetz and G. Kugel. "Stablilization of the photorefractive double phase-conjugate mirror in $BaTiO_3$". *Phys. Rev. A* 67 (2003).

[77] M.T. Gruneisen, E.D. Seeberger, J.F. Mileski and K. Koch. "Effects of laser coherence on coupling efficiency for the double phase-conjugate mirror". *Opt. Lett.* **16**, 596–598 (1991).

[78] S-C De La Cruz, S. MacCormack, J. Feinberg, Q.B. He, H.-K Liu and P. Yeh. "Effect of beam coherence on mutually pumped phase conjugators". *J. Opt. Soc.Am. B* **12**, 1363–1369 (1995).

[79] K. Iida, X. Tan, T. Shimura and K. Kuroda. "Stable injection locking of diode lasers through a phase-modulated double phase-conjugated mirror". *Appl. Opt.* **36**, 2491–2494 (1997).

[80] G.W. Ross and R.W. Eason. "Double phase-conjugate mirror with sixfold gain in photorefractive $BaTiO_3$ at near-infrared wavelengths". *Opt. Lett.* **18**, 571–573 (1993).

[81] S. Tay, J. Thomas, M. Eralp, G. Li, R.A. Norwood, A. Schülzgen, M. Yamamoto, S. Barlow, G.A. Walker, S.R. Marder and N. Peyghambarian. "High-performance photorefractive polymer operating at 1550 nm with near-video-rate response time". *Appl. Phys. Lett* **87**, 171105 (2005).

[82] G. Li, M. Eralp, J. Thomas, S. Tay, A. Schülzgen, R.A. Norwood and N. Peyghambarian. "All-optical dynamic correction of distorted communication signals using a photorefractive polymeric hologram". *Appl. Phys. Lett.* **86**, 161103 (2005).

[83] M. Eralp, J. Thomas, S. Tay, G. Li, G. Meredith, A. Schülzgen, N. Peyghambarian, G.A. Walker, S. Barlow and S.R. Marder. "High-performance photorefractive polymer operating at 975 nm". *App. Phys. Lett.* **85**, 1095–1097 (2004).

[84] M. Eralp, J. Thomas, G. Li, S. Tay, A. Schülzgen, R.A. Norwood, N. Peyghambarian and M. Yamamoto. "Photorefractive polymer device with video-rate response time operating at low voltages". *Opt. Lett.* **31**, 1408–1410 (2006).

[85] J.A. Herlocker, K.B. Ferrio, E. Hendrickx, B.D. Guenther, S. Mery, B. Kippelen and N. Peyghambarian. "Spectral dependence of the change in refractive index due to carrier injection". *Appl. Phys. Lett.* **76**, 2253–2255 (1999).

[86] M. Didomenco Jr. "Small-Signal Analysis of Internal (Coupling-Type) Modulation of Lasers". *J. Appl. Phys.* **35**, 2870–2876 (1964).

[87] L.E. Hargrove, R.L. Fork and M.A. Pollack. "Locking of He-Ne laser modes induced by synchronous intracavity modulation". *Appl. Phys. Lett.* **5**, 4–5 (1964).

[88] L. Curtis Forster, M.D. Ewy and C. Burton Crumly. "Laser mode locking by an external doppler cell". *Appl. Phys. Lett.* **6**, 6–8 (1965).

[89] H.W. Mocker and R.J. Collins. "Mode competition and self-locking effects in a Q-switched ruby laser". *Appl. Phys. Lett.* **7**, 270–273 (1965).

[90] A.J. DeMaria, D.A. Stetser and H. Heynau. "Self mode-locking of lasers with saturable absorbers". *Appl. Phys. Lett.* **8**, 174–176 (1966).

[91] R. Trebino. "Frequency-resolved optical grating: The measurement of ultrashort pulses". Kluwer Academic Publishers (2000).

[92] J.P. Heritage, R.N. Thurston, W.J. Tomlinson, A.M. Weiner and R.H. Stolen. "Spectral windowing of frequency-modulated optical pulses in a grating compressor". *Appl. Phys. Lett.* **47**, 87–89 (1985).

[93] R.N. Thurston, J.P. Heritage, A.M. Weiner and W.J. Tomlinson. "Analysis of picosecond pulse shape synthesis by spectral masking in a grating pulse compressor". *IEEE J. Quantum. Electron.* **22**, 682–696 (1986).

[94] C. Iaconis and I.A. Walmsley. "Self-referencing spectral interfermetry for measuring ultrashort optical pulses". *IEEE J. Quantum Electron.* **35**, 501–509 (1999).

[95] O.R. Wood and S.E. Schwartz. "Passive mode locking of a CO_2 laser". *Appl. Phys. Lett.* **12**, 263–165 (1968).

[96] M.Michon, J. Ernest and R. Auffret. "Stimulated Optical Radiation in Ruby". *IEEE J. Quantum Electron.* **5**, 125–126 (1969).

[97] A.R. Clobes and M.J.Brienza. "Passive mode locking of a pulsed Nd:YAG laser". *Appl. Phys. Lett.* **14**, 287–288 (1969).

[98] N. Sarukura, Y. Ishida and H. Nakano. "Generation of 50-fsec pulsesfrom a pulse-compressed, cw, passively modelocked Ti:sapphire laser". *Opt. Lett.* **16**, 153–155 (1991).

[99] Y.-K. Chen and M.C. Wu. "Monolithic Colliding-Pulse Mode-Locked Quantum-Well Lasers". *IEEE J. Quantum Electron.* **28**, 2176–2185 (1992).

[100] A. Rutz, V. Liverini, D.J.H.C. Maas, B. Rudin, A.-R. Bellancourt, S. Schön and U. Keller. "Passively modelocked GaInNAs VECSEL at centre wavelength around 1.3 μm". *Elect. Lett.* **6**, 926–927 (2006).

[101] W.K. Tan, H.Y. Wong, A.E. Kelly, M. Sorel, J.H. Marsh and A.C. Bryce. "Passive modelocking of InGaAsP/InP laser diode over wide operating temperature range". *Elect. Lett.* **41**, 1380–1381 (2005).

[102] S. Gee, G.A. Alphonse, J.C Connolly, C. Barty and P.J. Delfyett. "Ultrashort pulse genereration by intracavity spectral shaping and phase compensation of external-cavity modelocked semiconductor lasers". *IEEE J. Quantum Electron.* **36**, 1035–1040 (2000).

[103] B. Resan, L. Archundia and P.J. Delfyett. "FROG measured high-power 185-fs pulses generated by down-chirping of the dispersion managed breathing-mode semiconductor mode-locked laser". *IEEE Photon. Techn. Lett.* **17**, 1384–1386 (2005).

[104] S. Arahira and Y. Ogawa. "480-GHz subharmonic synchronous mode locking in a short-cavity colliding-pulse mode-locked laser diode". *IEEE Photon. Techn. Lett.* **14**, 537–539 (2002).

[105] U. Keller. "Recent developments in compact ultrafast lasers". *Nature* **424**, 831–838 (2003).

[106] R. Paschotta, L. Krainer, S. Lecomte, G.J. Spüler, S.C. Zeller, A. Aschwanden, D. Lorenser, H.J. Unold, K.J. Weingarten and U. Keller. "Picoscond pulse sources with multi-GHz repetition rates and high output power". *New J. of Phys.* **6**, 1–13 (2004).

[107] U. Keller and A.C. Tropper. "Passively modelocked surface-emitting semiconductor lasers". *Phys. Rep.* **429**, 67–120 (2006).

[108] L.F Mollenauer, P.V. Mamyshev, J. Gripp, M.J. Neubelt, N. Mamysheva, L. Grünter-Nielsen and T. Veng. "Demonstration of massive wavelength-division mulitplexing over transoceanic distances by use of dispersion-managed solitons". *Opt. Lett.* **25**, 704–706 (2000).

[109] X. Liu, D.M. Gill and S. Chandrasekhar. "Optical technologies and techniques for high bit rate fiber transmission". *Bell Labs Techn. J.* **11**, 83–104 (2006).

[110] D.A.B Miller. "Optical interconnects to silicon". *IEEE J. on Sel. Top. in Quantum Electron.* **6**, 1312–1317 (2000).

[111] P. Dong, S.F. Preble and M. Lipson. "All-optical compact silicon comb switch". *Opt. Expr.* **15**, 9600–9604 (2007).

[112] A.V. Krishnamoorthy and D.A.B Miller. "Scaling optoelectronic-VLSI circuits into the 21st century: a technology roadmap". *IEEE J. on Sel. Top. in Quantum Electron.* **2**, 55–76 (1996).

[113] J. A. Valdmanis and G. Mourou. "Subpicosecond electrooptic sampling: principles and applications". *IEEE J. Quantum Electron.* **22**, 69–77 (1986).

[114] K.J. Weingarten, M.J.W. Rodwell and D.M. Bloom. "Picosecond optical sampling of GaAs integrated circuits". *IEEE J. Quantum Electron.* **24**, 198–220 (1988).

[115] P. Antoine, A. L'Huillier and M. Lewenstein. "Attosecond pulse trains using high-order harmonics". *Phys. Rev. Lett.* **77**, 1234–1237 (1996).

[116] R. Kienberger, E. Goulielmakis, M. Uiberacker, A. Baltuska, V. Yakovlev, F. Bammer, A. Scrinzi, Th. Westerwalbesloh, U. Kleineberg, U. Heinzmann, M. Dreshcer and F. Krausz. "Atomic transient recorder". *Nature* **427**, 817–821 (2004).

[117] G. Sasone, E. Benedetti, F. Calegari, C. Vozzi, L. Avaldi, F. Flammini, L. Poletto, P. Villoresi, C. Altucci, R. Velotta, S. Stagira, S. De Silvestri and M. Nisoli. "Isolated single-cycle attosecond pulses". *Science* **314**, 443–446 (1991).

[118] M. Schultze, E. Goulielmakis, M. Uiberacker, M. Hofstetter, J. Kim, D. Kim, F. Krausz and U. Kleineberg. "Powerful 170-attosecond XUV pulses generated with few-cycle laser pulses and broadband multilayer optics". *New J. of Phys.* **9**, 243(11p.) (2007).

[119] M.J. Heck, E.A.J.M Bente, Y. Barbarin, D. Lenstra and M.K. Smit. "Simulation and desing of integrated femtosecond passively mode-locked semiconductor ring lasers including integrated passive pulse shaping components". *IEEE J. Sel. Top. in Quantum Electron.* **12**, 265–276 (2006).

[120] B. Chann, R.K. Huang, L.J. Missaggia, C.T. Harris, Z.L. Liau, A.K. Goyal, J.P. Donnelly, T.Y. Fan, A. Sanchez-Rubio and G.W. Turner. "Near-diffraction-limited diode laser arrays by wavelength beam combining". *Opt. Lett.* **30**, 2104–2106 (2006).

[121] O.E. Martinez, R.L. Fork and J.P Gordon. "Theory of passively mode-locked lasers including self-phase modulation and group-velocity dispersion". *Opt. Lett.* **9**, 156–158 (1984).

[122] G.P.A. Malcolm and A.I. Ferguson. "Self-mode locking of a diode-pumped Nd:YLF laser". *Opt. Lett.* **16**, 1967–1969 (1991).

[123] B. Proctor, E. Westwig and F. Wise. "Characterization of a Kerr-lens mode-locked Ti:sapphire laser with positive group-velocity dispersion". *Opt. Lett.* **18**, 1654–1656 (1993).

[124] T.R. Gurski. "Simultaneous mode-locking and second harmonic generation by the same nonlinear crystal". *Appl. Phys. Lett.* **5**, 5–6 (1969).

[125] C.B. Hitz and L.M. Osterink. "Simultaneous intracavity frequency doubling and mode locking in a Nd:YAG laser". *Appl. Phys. Lett.* **18**, 378–380 (1971).

[126] A.E. Siegman J.M. Heritier. "Analysis of mode-locked and intra-cavity frequency-doubled Nd-YAG laser". *IEEE J. Quantum Electron.* **16**, 324–335 (1980).

[127] U. Keller, D.A.B. Miller, G.D. Boyd, T.H. Chiu, J.F. Ferguson and M.T. Asom. "Solid-state low-loss intracavity saturable absorber for Nd:YLF lasers: An antiresonant semiconductor Farby-Perot saturable absorber". *Opt. Lett.* **17**, 505–507 (1992).

[128] U. Keller. "Ultrafast solid-state lasers". *Prog. in Opt.* **46**, 1–115 (2004).

Dankwoord

Na zo'n honderddertig bladzijden waarin het werk dat ik de afgelopen vier jaar heb uitgevoerd is samengevat, is het nu tijd voor het laatste stukje tekst in dit boekje in m'n moerstaal. Voor de meeste mensen had dit boekje waarschijnlijk evengoed uit alleen deze bladzijden en de nederlandse samenvatting kunnen bestaan.

Natuurlijk wil ik eerst mijn promotor Klaus Boller en begeleider Herman Offerhaus bedanken. Dankzij hen heb ik iets meer dan vier jaar geleden de, na het afronden van het hbo en een paar jaar werkervaring, niet geheel reguliere stap om te gaan promoveren kunnen maken. Gelukkig bleek mijn vermoeden waar dat er, naast de natuurkunde die ik inmiddels kende na mijn opleiding, nog veel leuke interessante en fascinerende natuurkunde te ontdekken was, waar. En dankzij de begeleiding van Herman en Klaus heb ik daar de afgelopen vier jaar een klein stukje van gezien.

Verder wil ik natuurlijk ook hier de commissieleden, Rob Eason, Cornelia Denz, Jennifer Herek en Markus Pollnau bedanken voor het plaatsnemen in mijn promotiecommissie. Ook wil ik Donna bedanken voor het proeflezen en corrigeren van de tekst.

Natuurlijk wil ik hierbij ook mijn (oud-)kamergenoten en collega's bedanken, ten eerste mister Liviu, voor wie 2008 ook het jaar van de 'golden bullet' moet worden, en nog 2 maanden voor de boeg heeft. Met het motto "Pain is only temporary, glory is forever", moet het hem ook wel gaan lukken. Maar natuurlijk ook Balaji, Denny, Dennis, Anton, Lars, Isabelle, Arie, Thijs, Marten, Rolf, Willem, Ab, Bert, Roel, Leon, Martijn, Mark, Fred, Arsen, Petra, Ian, Chris, Peter, Piet, Fred, Gerard, Jacob en natuurlijk Ruud, die in september verder is gegaan met het project.

Mijn familie kan ik natuurlijk ook niet overslaan, dankzij de gastvrijheid

van m'n zus Loes en Barry bijvoorbeeld was mijn overgang naar Enschede toch duidelijk een stuk makkelijker geweest, bijvoorbeeld. Verder natuurlijk m'n moeder, m'n vader, die mij op de middelbare school veel heeft geholpen met de grondbeginselen van de wiskunde, m'n andere zusje Hanneke en m'n zwager Mark, oma, grootmoeder, en hoewel hij er helaas niet meer is, grootvader, van wie ik de vele verhalen die hij vertelde niet snel zal vergeten.

En dan is er nog een groep mensen die de afgelopen maanden onder mijn gedrag heeft geleden. Zwaar hebben ze moeten lijden, en dan heb ik het over Marc, Reginald, Peter, Gerard, Marije, Gerbrand, Marjet, Marc, Rianne, Johan, Dick, Nicole, en hoewel ze het goudgele nat niet op waarde kan schatten, Jamila. Allen trof het tragische lot, omdat ondergetekende regelmatig weigerde, meer bier hebben moeten nuttigen. Ik ben voornemens mijn leven weer te beteren en mijn verantwoordelijkheid als het nodig is, weer zelf te nemen.

Dan zijn er natuurlijk nog heel veel andere mensen die het leven in Enschede of daarbuiten aangenaam hebben gemaakt en nog niet genoemd zijn, zoals bijvoorbeeld Wouter of Jurjen, maar er zijn er veel meer, ook deze dan ook bedankt!

Goed, tot zover het grote bedanken, dan sluit ik af met wat inmiddels wel een lijfspreuk is geworden,

Nunc est bibendum!

Peter